V-Band IMPATT Power Amplifier

S.W. Schell

TRW Electronic Systems Group
One Space Park
Redondo Beach, CA 90278

SEPTEMBER 1985

FINAL REPORT

Contract No. NAS5-27331

Prepared for

National Aeronautics and Space Administration

Goddard Space Flight Center
Greenbelt Road
Greenbelt, Maryland 90771

TABLE OF CONTENTS

LIST OF ILLUSTRATIONS

LIST OF ILLUSTRATIONS (CONTINUED)

LIST OF ILLUSTRATIONS (CONTINUED)

LIST OF TABLES

1. INTRODUCTION

This program is the result of the continuing demand and future requirement for a high data rate 60-GHz communications link. A reliable solid-state transmitter which delivers the necessary power over a wide bandwidth using present IMPATT diode technology required the development of new combining techniques. This final report details the development of a 60-GHz IMPATT power combiner amplifier. The results of this program form a basis from which future wideband, high-power IMPATT amplifiers may be developed. As a result of this program, several state-of-the-art advancements in millimeter-wave components technology have been achieved. Specific achievements necessary for the amplifier integration were:

- Development of a nonresonant divider/combiner circuit
- Reproducible multiple junction circulator assemblies
- Reliable high power 60-GHz IMPATT diodes.

The original approach to meeting these goals was based on developing a conical line power combiner capable of a minimum of 2.5-GHz RF bandwidth centered at 60.25 GHz. Four V-band single-diode stable IMPATT amplifier modules would be combined to yield the 1-W amplifier power output. Three single diode driver amplifier stages were to be fabricated to provide the required 17 dB gain. A six-junction circulator would be used to integrate the amplifier modules into a compact assembly.

The extensive studies performed on this conical line power combiner approach indicated an insurmountable problem in developing a conical line network having adequate isolation between the ports on which the IMPATT amplifier modules were mounted. This conical line combiner approach was subsequently abandoned in favor of a configuration of a pair of radial line 16-way divider/combiner networks. In this configuration, isolation is achieved by means of ferrite components external to the radial line. The geometry of the radial line network is a much simpler and more workable one.

The organization of the final report is as follows. Section 2 describes the program objectives, specifications, and requirements. Section 3 contains a detailed description of the amplifier, and discusses the various design approaches and tradeoffs which lead to the final amplifier configuration. Section 4, which presents a detailed circuit design for the various amplifier components, discusses the conical line combiner, radial line com-

biner, and circulator development. Also included will be achievements of TRW's silicon IMPATT diode development at 60 GHz. Section 5 presents the performance of the amplifier. Section 6 discusses the overall achievement of the program, implications of the results, and an assessment of future development needs and recommendations.

2. PROGRAM OBJECTIVE

The objective of this program was to develop a 60-GHz solid state power combining amplifier with the following RF performance goals:

Power output	1 W (minimum)
Dynamic RF band	59 to 61.5 GHz
RF gain	17 dB
Device junction temperature	250°C (maximum)

It was not the intent of this program to further develop IMPATT diode device capabilities, but rather to develop a power combining technique using the present diode technology.

3. SYSTEM DESIGN

The key elements of the amplifier development are the power combiner configuration, driver design, power modules, and IMPATT diodes. The individual capabilities and limitations of each key element play a major role in the configuration of the final amplifier. This section will present the evolution of this 60-GHz solid-state amplifier from its proposed design through the delivered hardware. It is important to review and understand this evolution so that one can better comprehend the final amplifier design.

3.1 BASIC DESIGN SELECTION

There are two basic methods to accomplish power accumulation from multiple devices in a small size transmitter:

- Resonant cavity combiner
- Nonresonant combiner.

3.1.1 Resonant Cavity Combiner

In this type of combiner, power accumulation takes place in a resonant cavity designed at the operating frequency. The resonator is an important element in the combiner operation; the high unloaded Q is the key element for high combining efficiency and coherent output. A high Q cavity is required to achieve high isolation from the diode to the external load and from diode-to-diode through the resonant modes of the cavity. Therefore, a basic bandwidth limitation exists in this type of combiner due to the highly resonant properties of the cavity.

Because of this relatively narrow bandwidth, resonant combiners are typically used in high gain, narrowband, injection-locked modes of operation. The locking bandwidth, as shown in Figure 3.1-1, can be plotted as a function of locking gain and the amplifier normalized locking bandwidth, as shown in Figure 3.1-2. For a given amplifier, the loaded Q (or Q_{ext}) defines the gain bandwidth relationship of the amplifier.

Typical resonant combiner performance is plotted in Figure 3.1-3 with a Q_{ext} = 25, which corresponds to a bandwidth of 1.2 percent at 10 dB gain. An overdriven amplifier with injection-locking gain significantly less than 10 dB generally produces undesirable nonlinear effects, such as spurious outputs caused by the large-signal effects of the device. A Q_{ext} less than 25, on the other hand, is extremely difficult to accomplish in a resonant

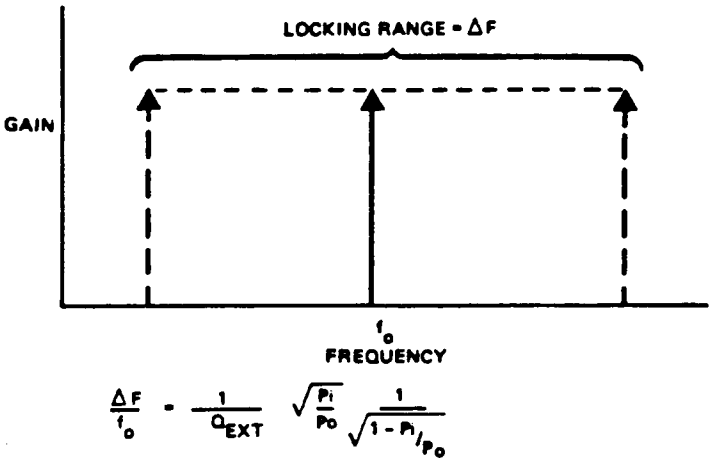

Figure 3.1-1. Voltage-gain bandwidth relationship.

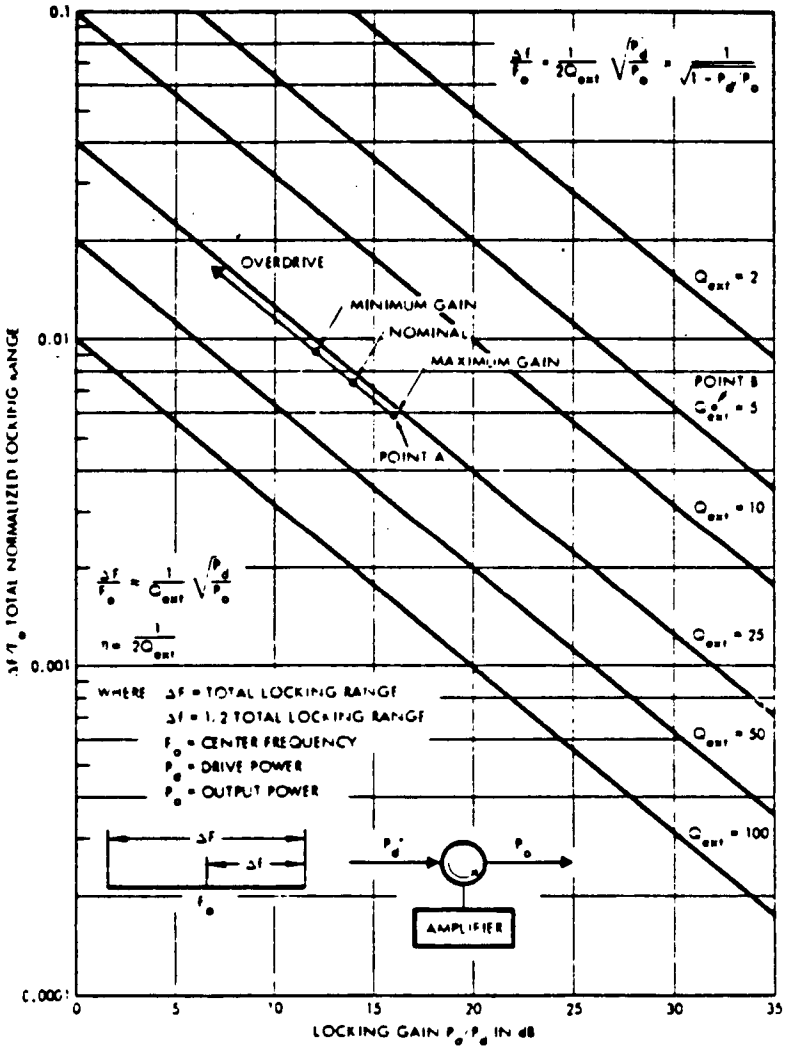

Figure 3.1-2. Injection-locking characteristics.

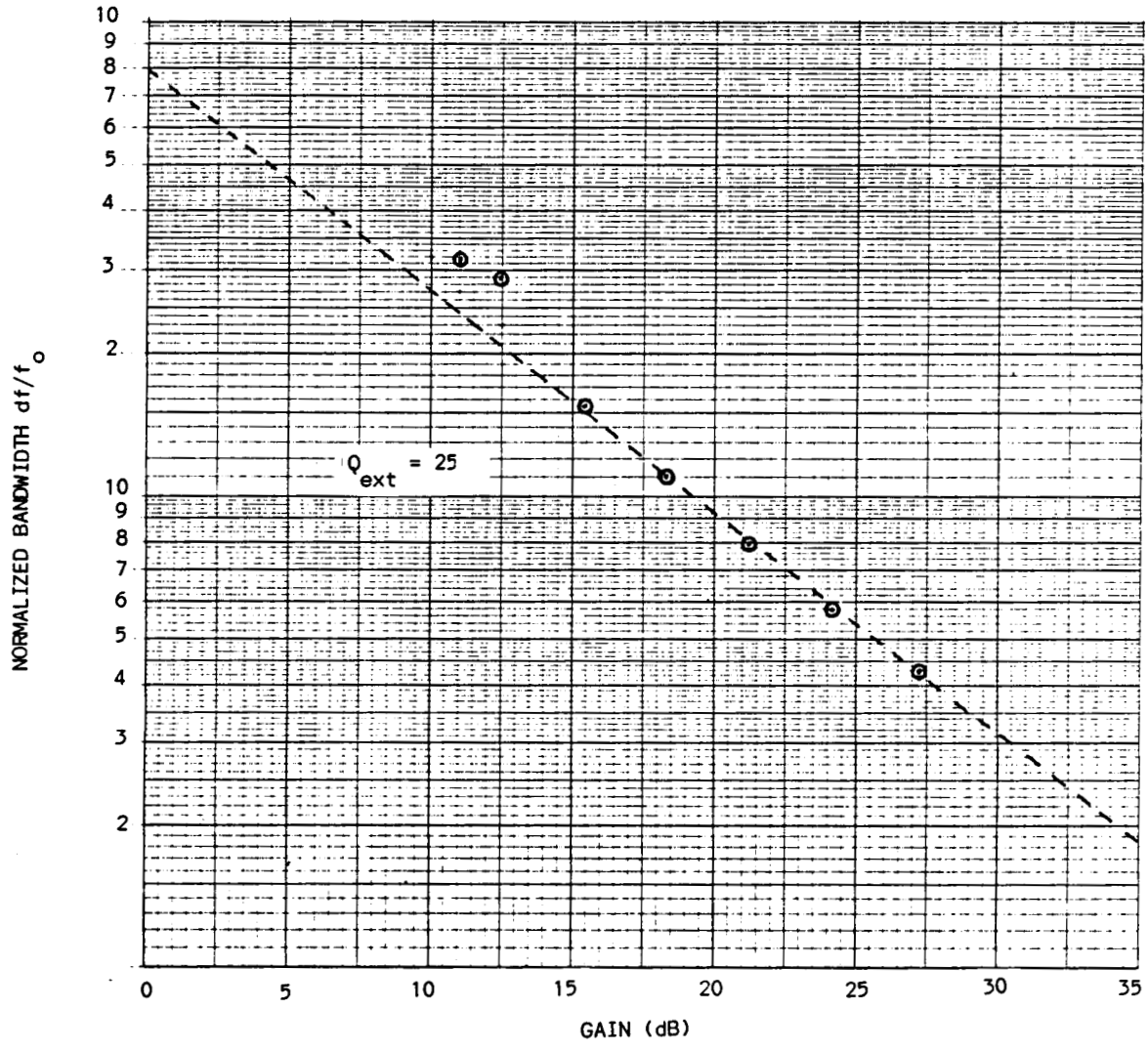

Figure 3.1-3. Typical bandwidth vs gain performance of an injection-locked oscillator.

cavity combiner; therefore, an injection-locked bandwidth of 2 percent is generally considered as the upper limit of a resonant cavity combiner. It was apparent that the resonant cavity combiner approach could not meet the required 2.5 GHz (~4 percent) bandwidth.

3.1.2 Nonresonant Combiner

To achieve the required bandwidth, a nonresonant type power combiner must be employed. This type of combining scheme usually consists of a number of identical independent amplifier modules mounted to a passive microwave combining network. The RF output from each amplifier module is added by the combiner network, and the resulting power emerges from one port of the microwave network. Figure 3.1-4 represents a general flowchart of a module nonresonant power combiner assembly.

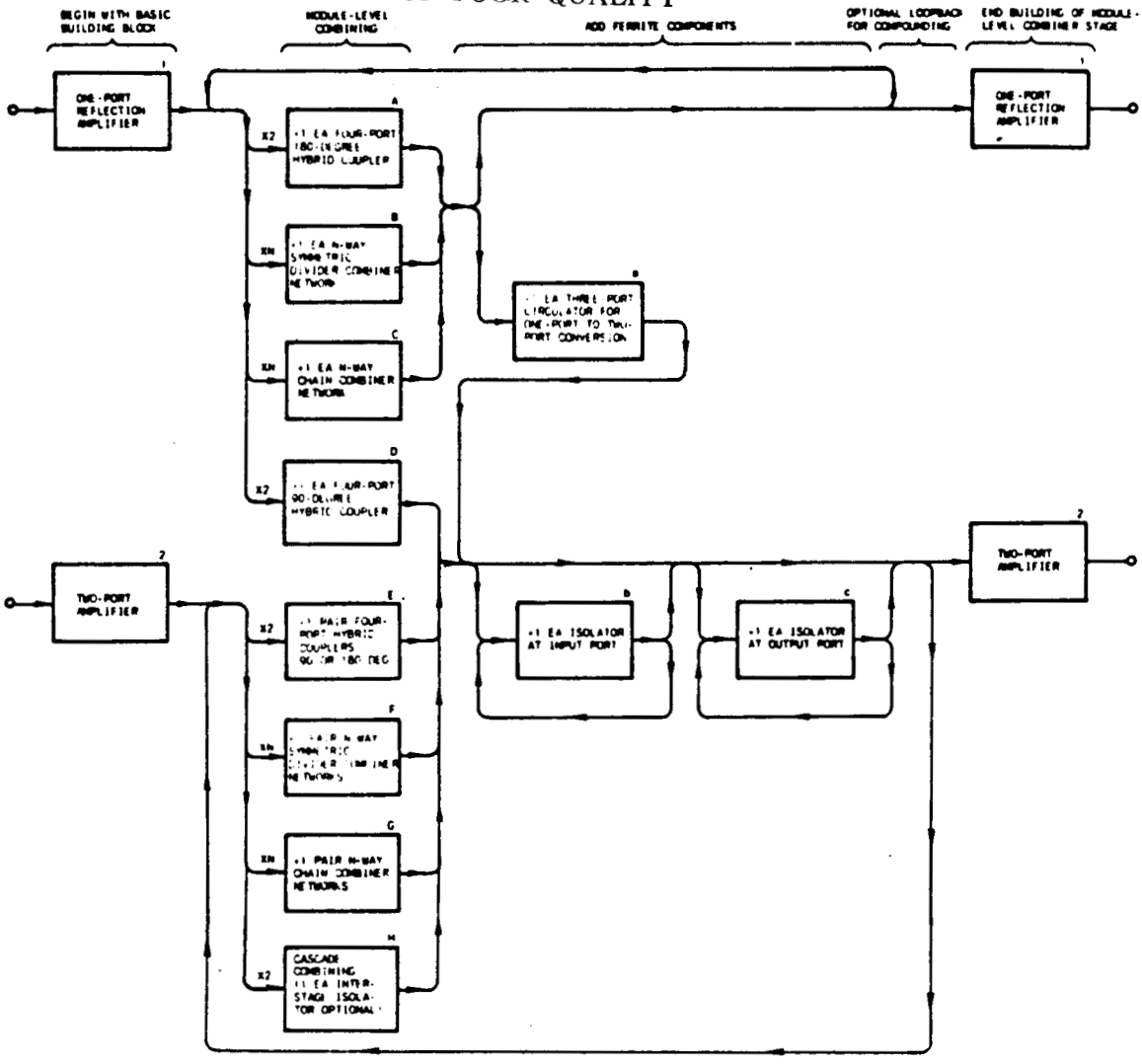

Figure 3.1-4. Flowchart for generalized module-level power combiner assembly.

The flowchart in Figure 3.1-4 considers both one-port and two-port reflection amplifiers; paths 1 and 2, respectively. IMPATT amplifiers are typically of the reflection type; and by adding a circulator, the one-port amplifier is transformed into a two-port amplifier. Beginning with the basic amplifier (one-port or two-port), the flowchart allows for one of four types of power level combining techniques. After power combining, the circuit designer has the option of adding ferrite devices to convert the one-port to a two-port amplifier; for the two-port amplifier, ferrite isolators

may be added at its input and/or output ports. If further combining is desired, a loopback path is available. A description of the basic cells of the flowchart in Figure 3.1-4 is as follows:

1) Basic Building Block

The chart allows module-level power combining of either one-port or two-port modules. Hence, there are two starting points. Concerning IMPATT amplifier modules, a basic configuration for a two-port amplifier is a one-port reflection IMPATT amplifier coupled to a three-port circulator.

2) Module-Level Combining

For each of the two types of modules shown at the starting point, a set of four power combiner paths is indicated. The combiner configurations indicated on each path are further described in this section. Note that three of the four paths which can be taken for a one-port building block module result in a one-port amplifier, while one of these four results in a two-port amplifier. All four paths from a two-port building block module result in a two-port amplifier.

3) Ferrite Components

Ferrite components, namely three-port circulators and two-port isolators, generally play an important role in building up a module-level power combiner stage. For the three paths of combining which result in a one-port module, a circulator can be added to the combiner to convert it to a two-port amplifier as the diagram indicates. Also shown, for two-port module-level power combiner amplifiers, any number of isolators may be added to the input and output ports of the resulting combiner. This is generally necessary in a module-level power combiner, as it is with a single-diode amplifier stage, to obtain adequate input and/or output isolation.

If the resulting combiner is to be used as a building block module (See 4, Optional Loopback for Compounding) for a subsequent module-level power combining step, the additional input and output isolators are generally required to obtain the necessary module-to-module isolation.

4) Optional Loopback for Compounding

After ferrite components have been added to build up the module-level power combiner stage, a number of identical module-level combiners may then be used as building blocks for a subsequent module-level power combining operation. On the flowchart, this option is represented by the paths back to the module-level power combining blocks. When one or more such loopbacks are taken, the resulting combiner will be termed a compound module-level power combiner. Note the separate loopback paths for one-port and two-port module-level combiners.

5) End Building Module-Level Combining Stage

When the optional loopback path is not taken, the buildup of the module-level power combiner stage is complete. Note that the resulting combiner stage can be either a one-port or two-port amplifier. However, for most practical applications, only two-port amplifier stages are useful.

A number of microwave networks and arrangements of the networks can be used for power combining. Some examples of networks available for power combining are:

- 90-degree, 3-dB hybrid couplers
- 180-degree, 3-dB hybrid couplers
- Symmetric N-way divider/combiner.

Each network can be assembled using either a one-port reflection amplifier module or two-port amplifier module. Configurations of each of these aforementioned combiner networks are presented in Figures 3.1-5 through 3.1-8.

The symmetric N-way divider/combiner has the advantage of combining N-matched amplifier modules using one or two similar combiner networks. In practice, most networks of this type do not have the minimum required port-to-port isolation necessary for the single-layered configuration. Using external ferrite devices, the one-port amplifier modules can be converted to two-port amplifiers, each with the required port-to-port isolation as necessary for the two-layered approach. The single- and double-layered designs are shown in Figures 3.1-7 and 3.1-8, respectively.

Each of the 90- and 180-degree hybrid coupler circuits shown in Figures 3.1-5 and 3.1-6 can fan out to combine any amplifier modules. For the configuration shown in Figure 3.1-9, each amplifier on the coupler is composed of identical hybrid coupler circuits. The amplifier port to each second-level coupler is either an amplifier module or additional identical hybrid coupler circuit. This configuration combines two amplifier modules where N is the number of division levels. For example, N = 3 in Figure 3.1-9. In addition, this configuration requires either 2^N-1 or 2^N combiner circuits, depending on the one- or two-layer approach. It should be noted that loss of the combining circuit increases (efficiency decreases) with increasing N. The loss per coupler imposes a limit on the quantity of stages that can be practically combined using this technique.

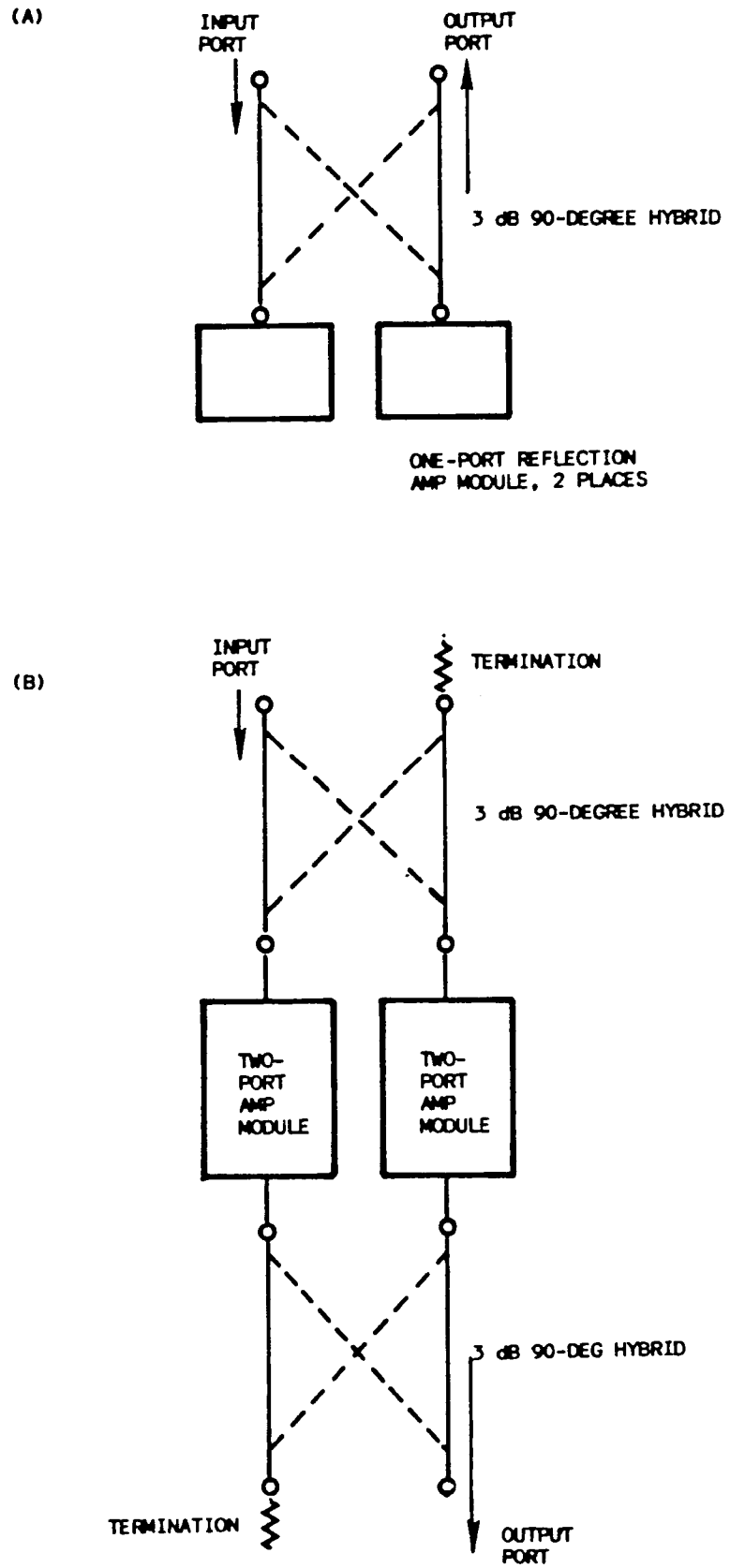

Figure 3.1-5. (a) Module-level power combining of a pair of one-port amplifier modules by a single 90-degree hybrid coupler. (b) Module-level power combining of a pair of two-port amplifier modules by a pair of 90-degree hybrid coupler.

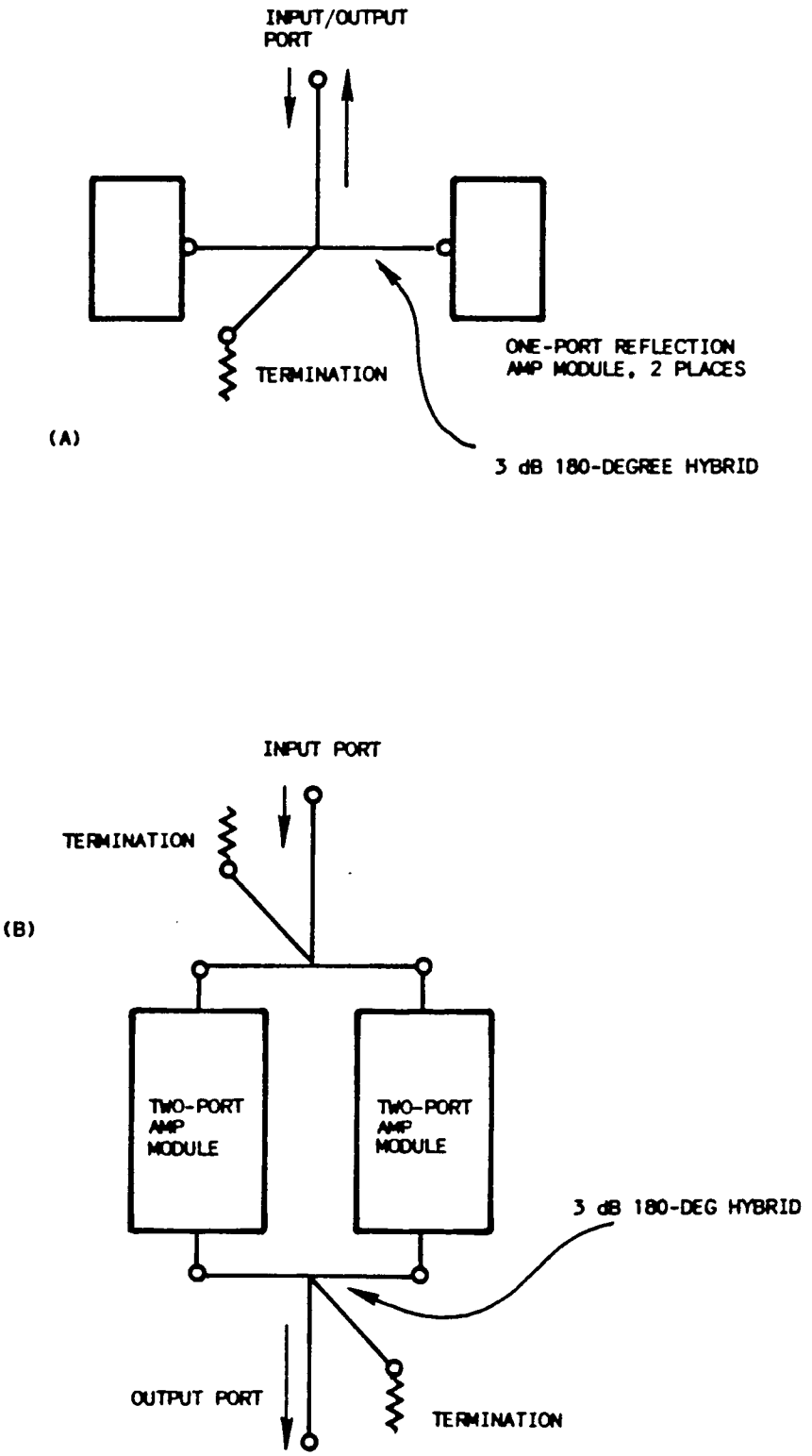

Figure 3.1-6. (a) Module-level power combining of a pair of one-port amplifier modules by a single 180-degree hybrid coupler. (b) Module-level power combining of a pair of two-port amplifier modules by a pair of 180-degree hybrid couplers.

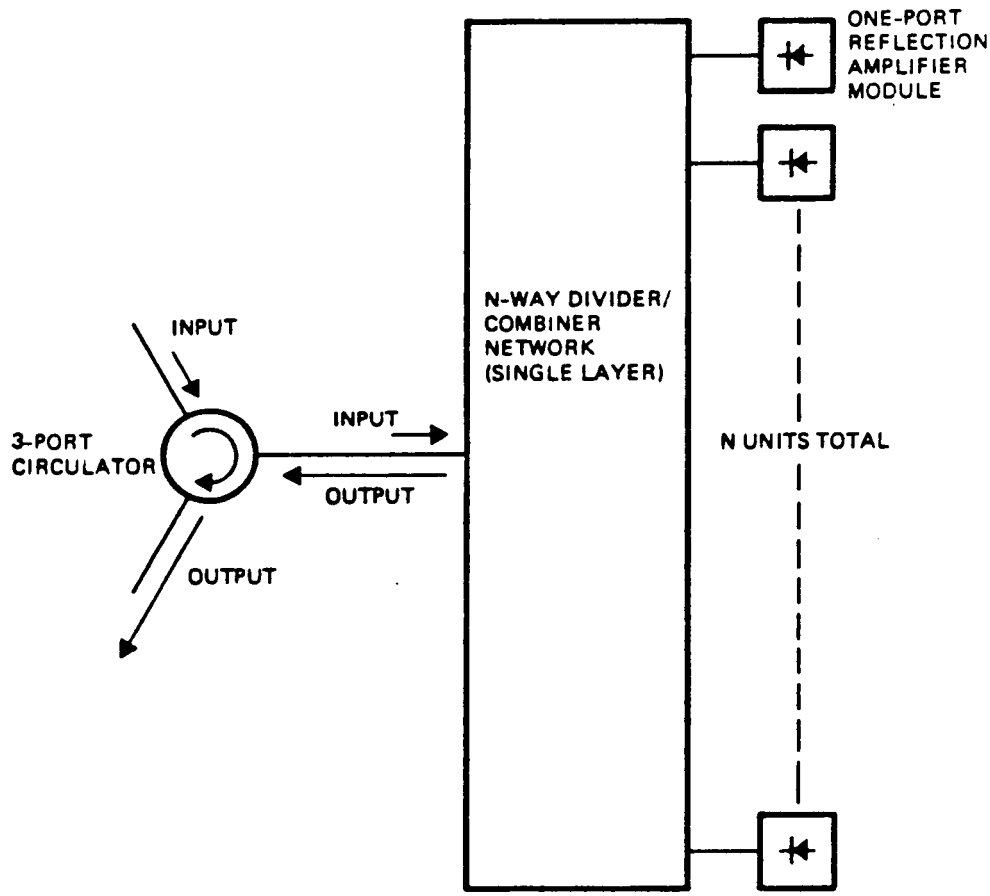

Figure 3.1-7. Configuration for single-layer module-level power combining of one-port amplifier modules by a single N-way divider/ combiner network.

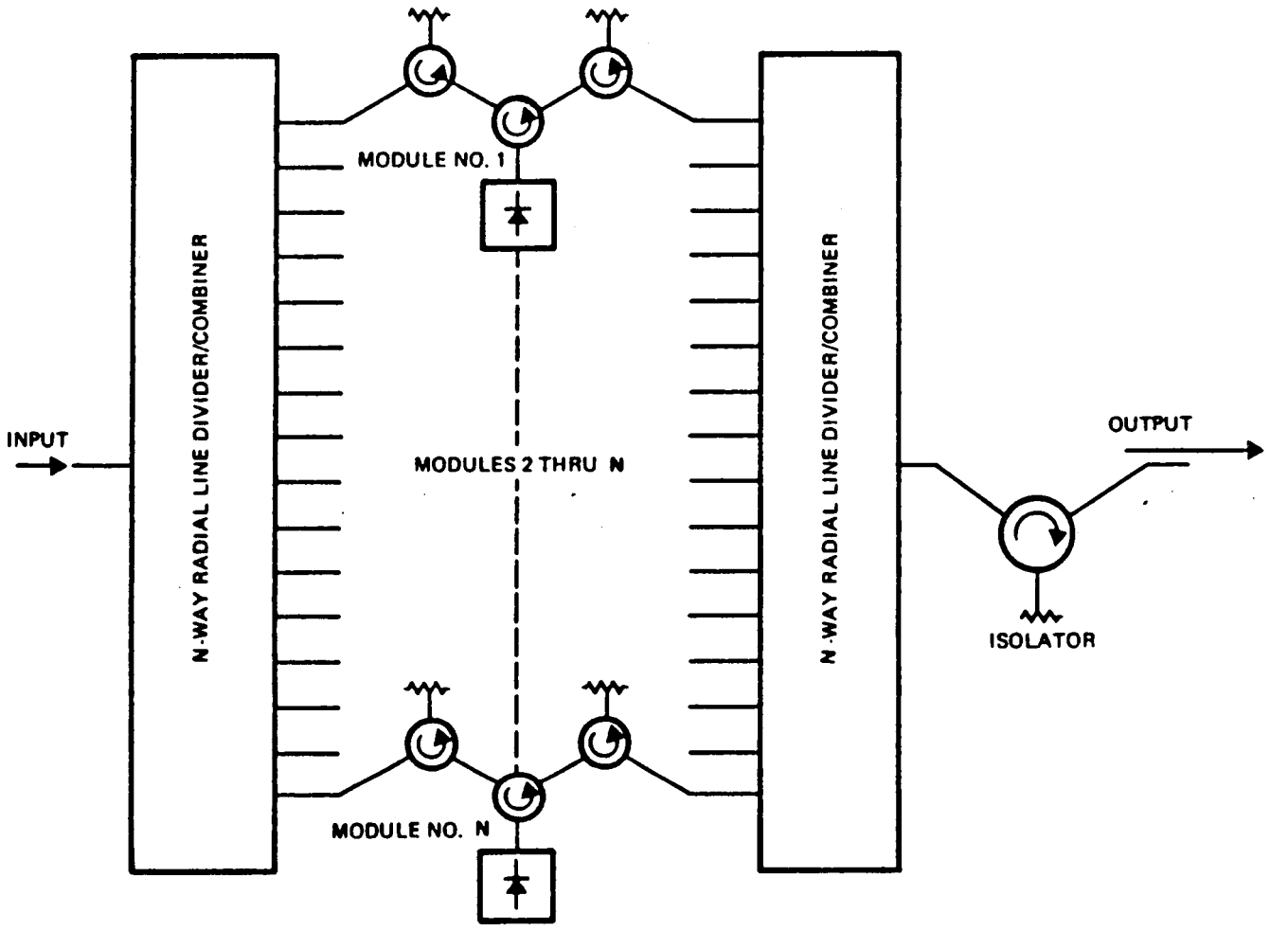

Figure 3.1-8. Configuration for two-layer module-level power combining of two-port amplifier modules by a pair of N-way divider/combiner networks.

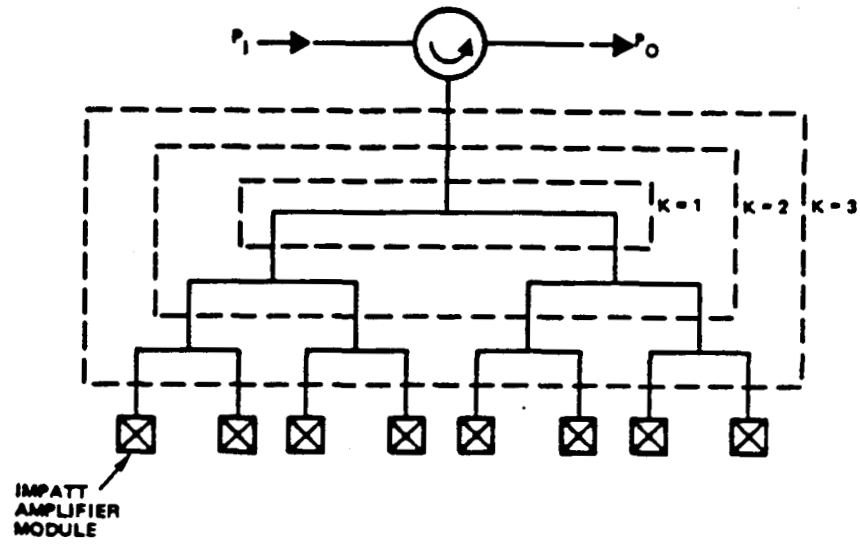

Figure 3.1-9. 3-stage combiner amplifier.

3.2 INITIAL DESIGN APPROACH

Our initial design approach was based on a four-diode conical line combiner used on the output stage of the amplifier. Successful power combining was first demonstrated by Quine, McMullen, and Khandewal*, in which eight IMPATT diodes were combined to achieve 18 W total output power at 14.6 GHz. Although wideband performance was not demonstrated in their pioneering work, we believed that the conical line combiner was capable of more than 10 percent bandwidth because of its nonresonant nature. This was substantiated by the preliminary experimental data to be presented.

The schematic representation of our baseline approach is presented in Figure 3.2-1 along with a detailed power budget for the amplifier. This initial design was the proposed approach using a three-module driver stage and the conical line structure combining four single-diode modules as the power stage.

The first three modules used in the driver stage are single-diode stable amplifiers cascaded via circulator junctions. The circulators used would be assembled in one compact assembly with each amplifier module mounted directly to its respective circulator junction.

The combining technique for the initial amplifier configuration uses a single layered conical line combiner. Operationally, power enters the

*"Ku-band IMPATT Amplifier and Power Combiners," Catalog No. 786H1355-7 MTT, IEEE MTT-S, pp. 346-348.

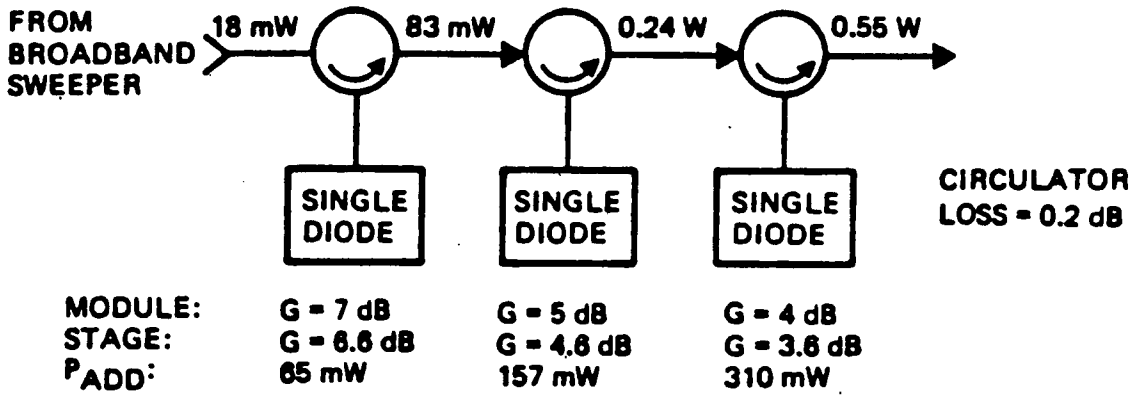

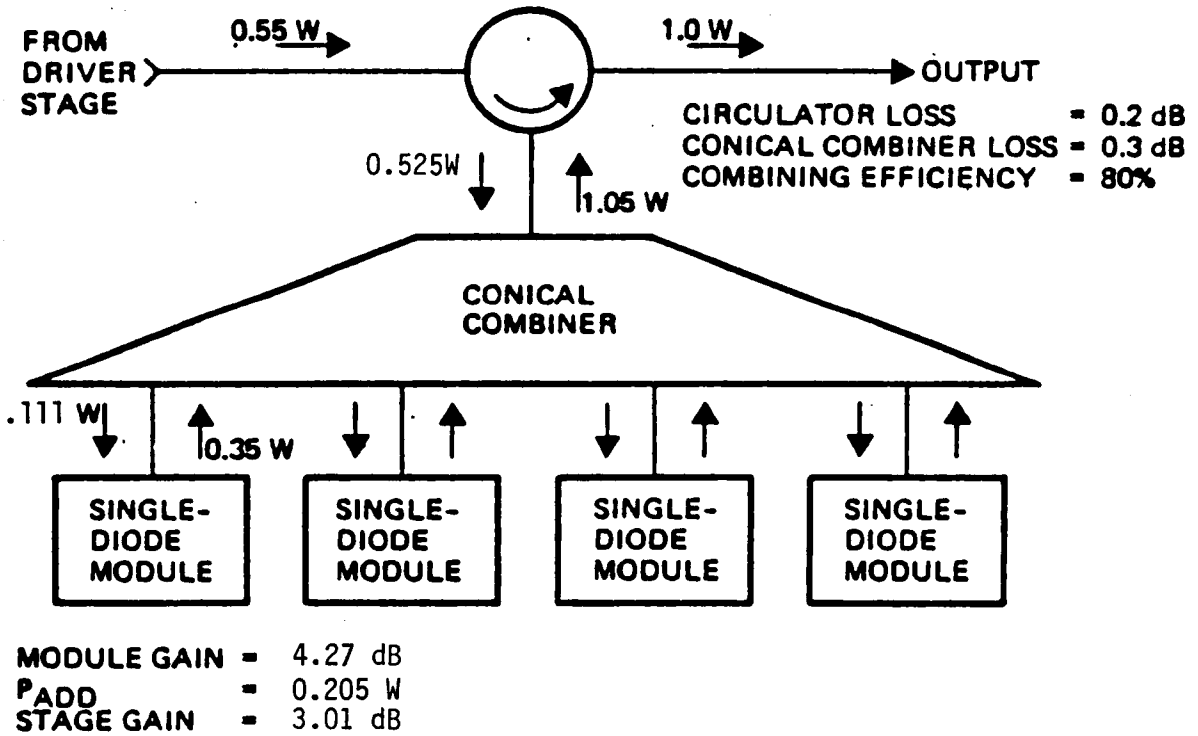

Figure 3.2-1. Baseline amplifier approach.

conical line at its input port via a circulator. It is then equally divided four ways within the combiner and exits the four output ports at the base of the conical line. Reflection-type stable amplifiers at each of the four ports amplifies this signal, which is then recombined within the conical line combiner. The amplified signal is directed to the output by the circulator at the apex of the conical line.

Development of the conical line combiner, detailed later in Section 4, required a transition from waveguide to coaxial line, coaxial line to conical line, and, finally, conical line to waveguide. The transition from waveguide to coaxial line and coaxial line to conical line had low loss and wideband performance. The transition from the conical line back to waveguide at the base of the combiner appeared to excite higher-order space harmonics. Lossy material introduced to suppress modes other than the predominant TEM mode within the conical line was used, but the result was an additional 1- to 2-dB loss; this is further detailed in Section 4. Mode conversion from a TEM mode with the conical line to a TE_{10} mode within rectangular waveguide proved to be inefficient. A qualitative explanation of how these space harmonics are generated follows: the incident RF is delivered to the conical structure via the input waveguide. The incident wave is traveling in the TE_{10} mode. The propagation is converted to the TEM mode by the waveguide-to-coaxial line to conical-line transition. The TEM wave travels along the conical line until it reaches the conical line-module-port interface. At the interface, the TEM wave is divided into quadrants with the RF energy in each quadrant becoming a TE_{10} wave exciting a module port. It is the abrupt change from a TEM wave to four TE_{10} waves (or vice versa) at the interface that higher-order space harmonics are generated so that the boundary conditions at the interface are satisfied. The problem is, therefore, to identify the higher-order space harmonics (to find their wave functions), calculate the RF energy contained in each of these harmonics, and efficiently convert them to the desired mode.

After extensive analysis and experimentation, it was determined that it would be very difficult, or even impossible, to develop a one-layer conical line combiner with low reflection at both input and output ports, minimal loss from the central input port to each of the four module output ports, and high isolation between output ports.

3.3 FIRST DESIGN REVISION

As the development effort proceeded, it was determined that the single-layer conical line combiner approach was unrealizable. A scheme to eliminate the need for high isolation between the output ports and low reflection requirements at these ports was devised. This new approach was the two-layered conical line combiner which required the addition of one more conical line structure and four circulator/isolator networks. Figure 3.3-1 shows the schematic representation of this design with only the final power combining stage and its four stable amplifier modules. The driver stage for this is identical to that used in the single-layer combining technique.

In this scheme, two conical structures are used: the first is for power division and the second, power combining. The input signal is fed into the first conical structure. The reflected wave due to the "imperfection" of the structure is dissipated in the termination via Circulator 1. The transmitted wave is divided into four waves and fed into the IMPATT module via Circulators 2 through 5. The same circulators convey the amplified signals to the second conical structure. Again, any reflected waves due to the imperfection of the structures are dissipated in RF terminations via the circulators. Thus, as far as the IMPATT modules are concerned, the "imperfect" conical structures are indistinguishable from "perfect" ones; the reflected waves never reach the IMPATT module. The transmitted waves in the second conical structure are combined into one signal and appear at the output port. A drawback to this design is the significant increase in the number of components necessary. It is important to note that all the added hardware is identical. That is, they are of the same configuration, have the same input power, and should produce identical output power. This modular type construction is typically easier to construct and facilitate for mass production. Further drawbacks to this back-to-back, two-layered construction are the additional room required and dissipation of heat from the four suspended modules.

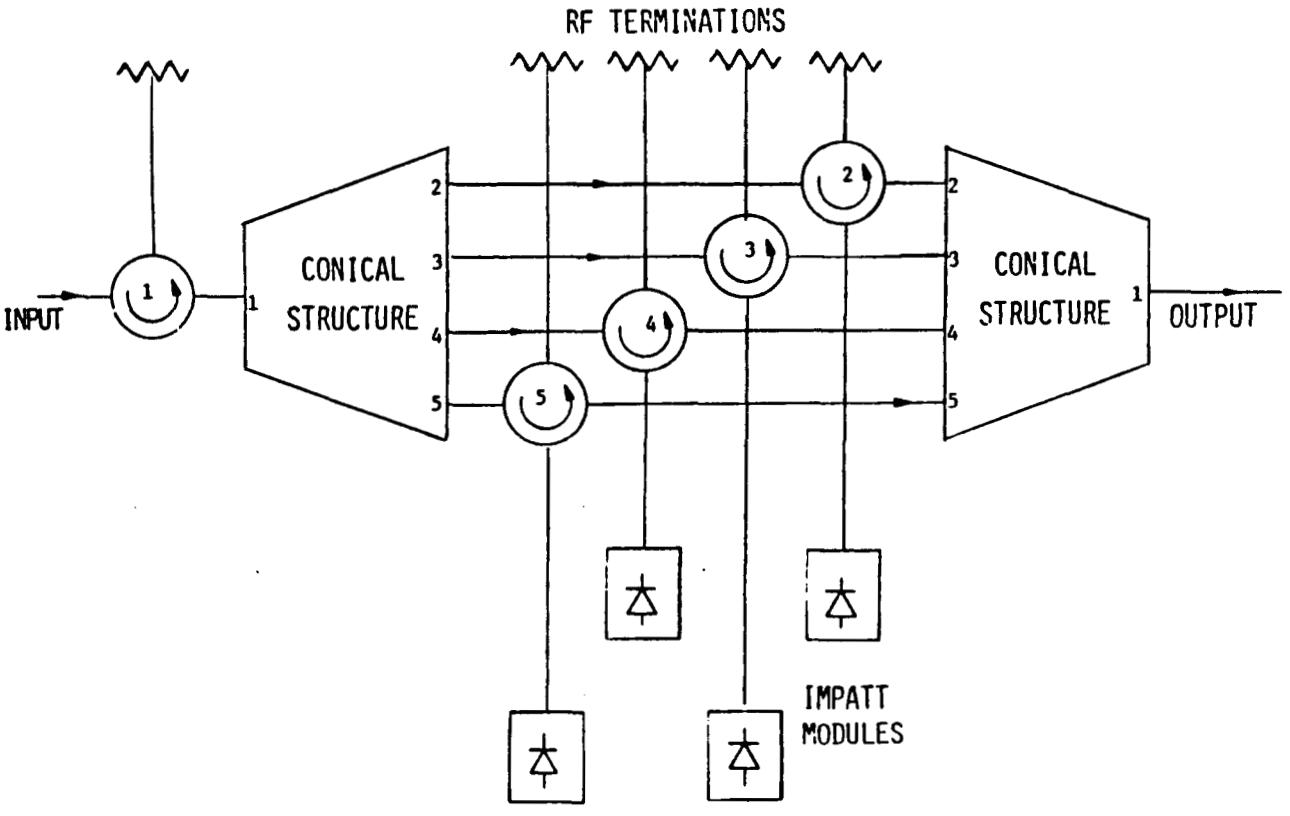

Figure 3.3-1. System configuration with "imperfect" conical structures.

It was decided that attempting to pursue an efficient method to eliminate the spacial harmonics could become very involved and ineffective. The conical line combiner/divider also proved to be a very difficult geometry to fabricate and tune. Due to its three-dimensional construction, great care must be taken when assembling to ensure that all parts are precisely positioned.

3.4 RADIAL LINE COMBINER

A simpler construction similar to the conical line was proposed. This new structure, the radial line combiner, is a two-dimensional assembly (Figure 3.4-1). This type of construction also requires transitions from waveguide to coaxial line, coaxial line to radial line, and radial line to waveguide; machining and assembly is much simpler due to its planar geometry. Similar to the conical line, the radial line also propagates a TEM-type mode which must be converted to the rectangular waveguide dominant TE_{10} mode. Like the conical line, this is expected to excite higher-order spatial harmonics at the waveguide interface. Therefore, the back-to-back two-layered construction will again be employed.

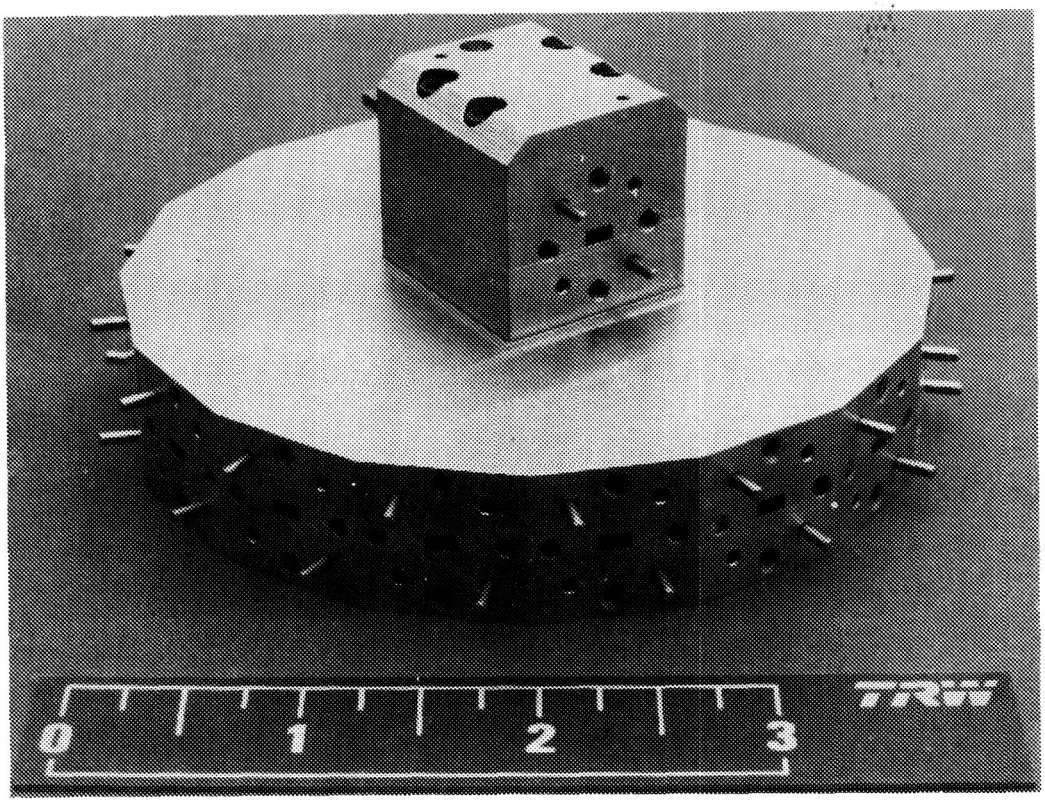

Figure 3.4-1. 16-way V-band radial line divider/combiner network - assembled.

Figure 3.4-2 is a detailed sketch of the radial line combiner for four output ports. This construction could be used just as the four-port conical line combiner could be used. An obvious problem with this design is that the radial line region, formed by the intersection of the four waveguides is not well defined. Referring to Figure 3.4-2, the distance from the center, input port to the nearest wall, R_1, is only one-half a wavelength for a radial wave at 60 GHz. In addition, the large abrupt corners formed by the four waveguides are sure to produce spacial harmonics and poor mode conversion.

To better define the radial line region, a cavity could be machined as shown in Figure 3.4-3. To help eliminate the generation of spatial harmonics, tapered transitions from the radial cavity to the waveguide interface could be incorporated.

Because this is a technology program and keeping in view future applications, we chose to construct a 16-port radial waveguide divider/combiner network. A photo of a disassembled 16-port radial line combiner is presented in Figure 3.4-4. Note that this construction yields both a well defined radial

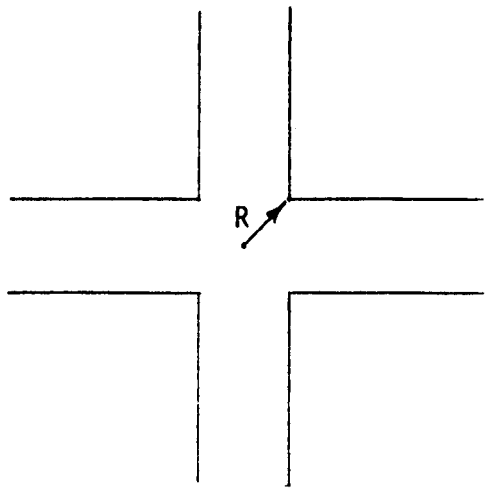

Figure 3.4-2. Radial line combiner formed by the intersection of four waveguides.

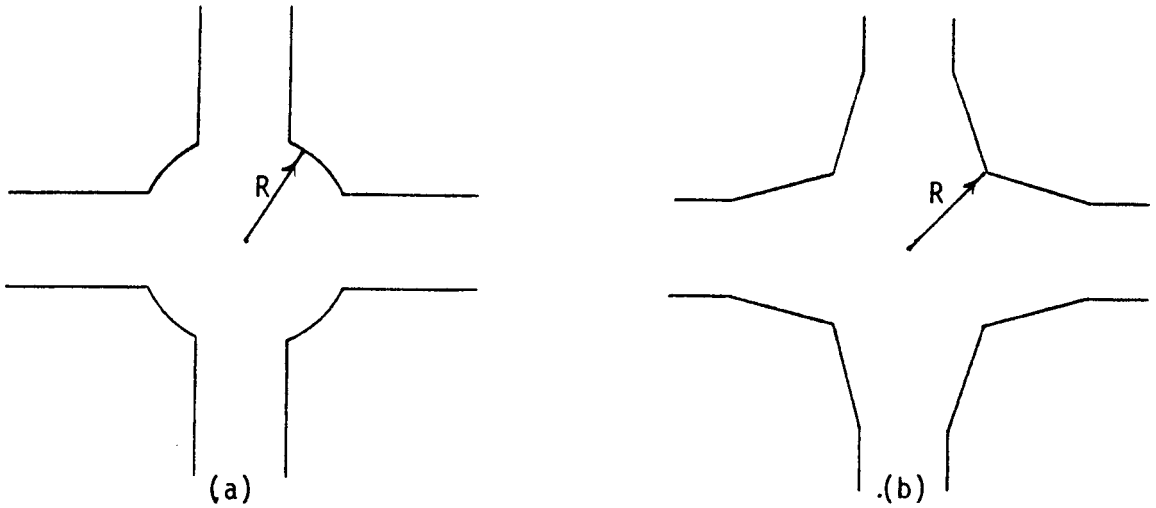

Figure 3.4-3. Four-port radial line combiner with cutout to expand the radial line region (a) and with tapered transitions (b).

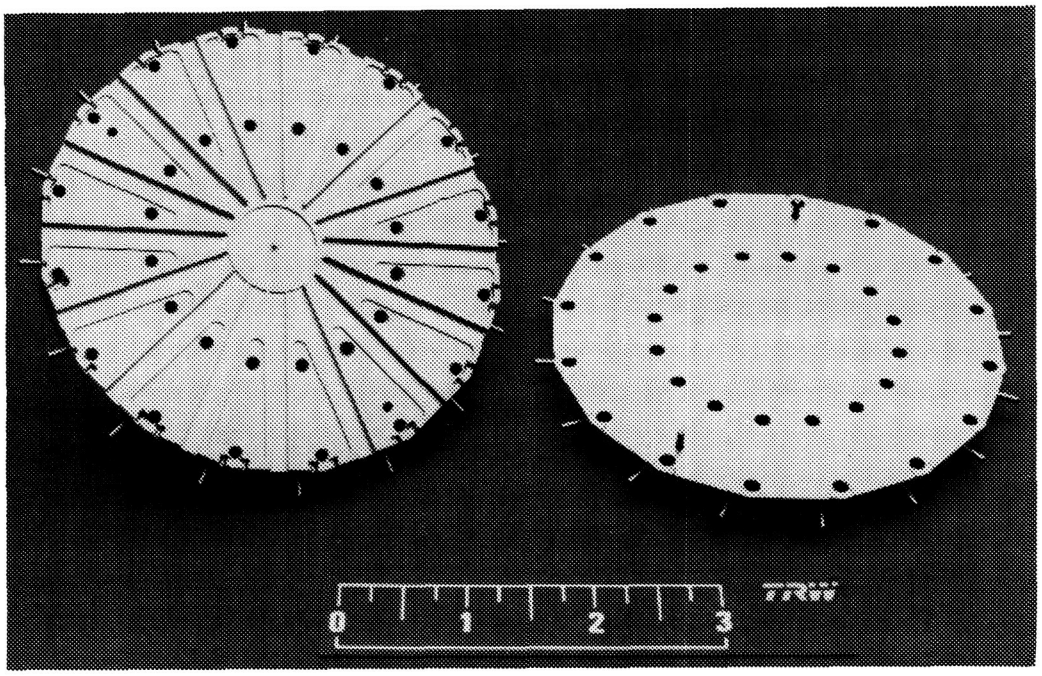

DISASSEMBLED UNIT

Figure 3.4-4. Disassembled 16-way V-band radial line divider/ combiner network.

line region, and, conceptually, a good transition to waveguide formed by the small angled wedges between each output port. From this, we will combine the power of only 4 out of the 16 output ports. This assembly will both demonstrate the technology and will stand as a foundation for future programs, where all 16 output ports will be used.

The relationship governing an ideal radial line combiner states that if signals with equal amplitude and phase from only 4 of the 16 ports are combined, and the remaining 12 ports are terminated with a matched load, the combined power at the output will equal that of the power incident at just one of the input ports (i.e., $P_o = P_i$). That is, three-fourths of the total power incident from 4 of the input ports is scattered or dissipated by the other 12 terminated ports, and only one-fourth of this power is summed at the output port. This is discussed in greater depth in Section 4.

To achieve this 1-W power level from each module, we must either drive the divider with an equally high power level (recall that the input power to each of the power modules is only 1/16 or -12 dB of the dividers input power) or use a high gain amplifier. Diodes fabricated at TRW are capable of producing 1 W as an oscillator at 60 GHz. To achieve 1-W output from stable

amplifier power modules would require either multiple stages per power module or a driver power to the divider of several watts; both methods are unacceptable. The alternative is to use a high gain injection-locked oscillator (ILO) in a single-stage power module.

3.5 FINAL AMPLIFIER DESIGN

A block diagram of the final amplifier configuration and its power budget is given in Figure 3.5-1. The amplifier is composed of a three-module driver stage and a four-module radial line combiner stage resulting in a peak output power of 0.4 W and a bandwidth of 1.5 GHz. This amplifier clearly does not meet the design specification; however, it does possess the capability to meet those required if all 16 ports were combined. It is due to this potential capability that this design was pursued.

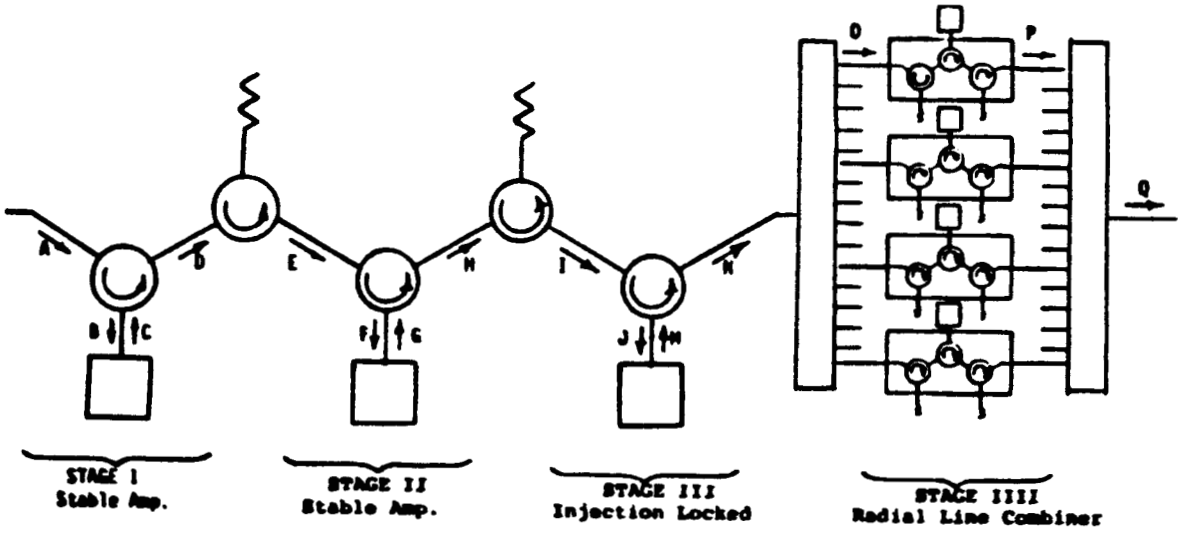

Location	A	B	C	D	E	F	G	H	I	J	M	N	O	P	Q
Power (dBm)	10	9.7	16.7	16.4	16.1	15.8	18.8	18.5	18.2	17.9	28.3	28.0	15.4	28.0	26.5

Figure 3.5-1. Amplifier block diagram.

The driver stage consists of two cascaded stable amplifiers and an ILO third stage. The power stage incorporates the 16-way radial line divider, but only four are employed for amplification using ILO modules. The resulting power from the four ILO power modules is recombined using a second 16-way radial line combiner. The results of this amplifier are presented in Section 5.

4. COMPONENT DEVELOPMENT

4.1 CONICAL WAVEGUIDE DIVIDER/COMBINER

A schematic of the four-diode conical line combiner for the proposed transmitter is shown in Figure 4.1-1. Wideband waveguide amplifier modules were coupled to the bottom of the conical transmitter line through step transformers for broadband matching. The conical line is tapered via a broadband coaxial-to-waveguide transition to a waveguide output. The overall structure involves nonresonant components capable of broad bandwidth.

To properly design a conical line power combiner, the transmission properties of a conical transmission line must be understood. We began by reviewing some of these properties in Section 3. Although this approach has demonstrated power combining at the microwave range, the complicated nonplanar structure of the conical line introduced many problems.

4.1.1 Transmission Characteristics

A conical transmission line is best described in terms of spherical coordinates r, θ, and ϕ as shown in Figure 4.1-2. The transmission direction is along the radius r, and the transmitted power is confined within the region bounded by cones of aperture θ_1 and θ_2.

The transmisssion characteristics of different modes in a conical line may be obtained by solving Maxwell's equations in spherical coordinates, together with the appropriate boundary conditions at the cone surface. The dominant E-mode is a transverse electromagnetic mode whose nonvanishing components are:

$$E_\theta = \frac{V(r)}{\ln\left[\frac{\tan(\theta_2/2)}{\tan(\theta_1/2)}\right]} \cdot \frac{1}{r \sin\theta} \qquad (4\text{-}1)$$

$$H_\phi = \frac{I(r)}{2\pi r} \quad \frac{1}{\sin\theta} \qquad (4\text{-}2)$$

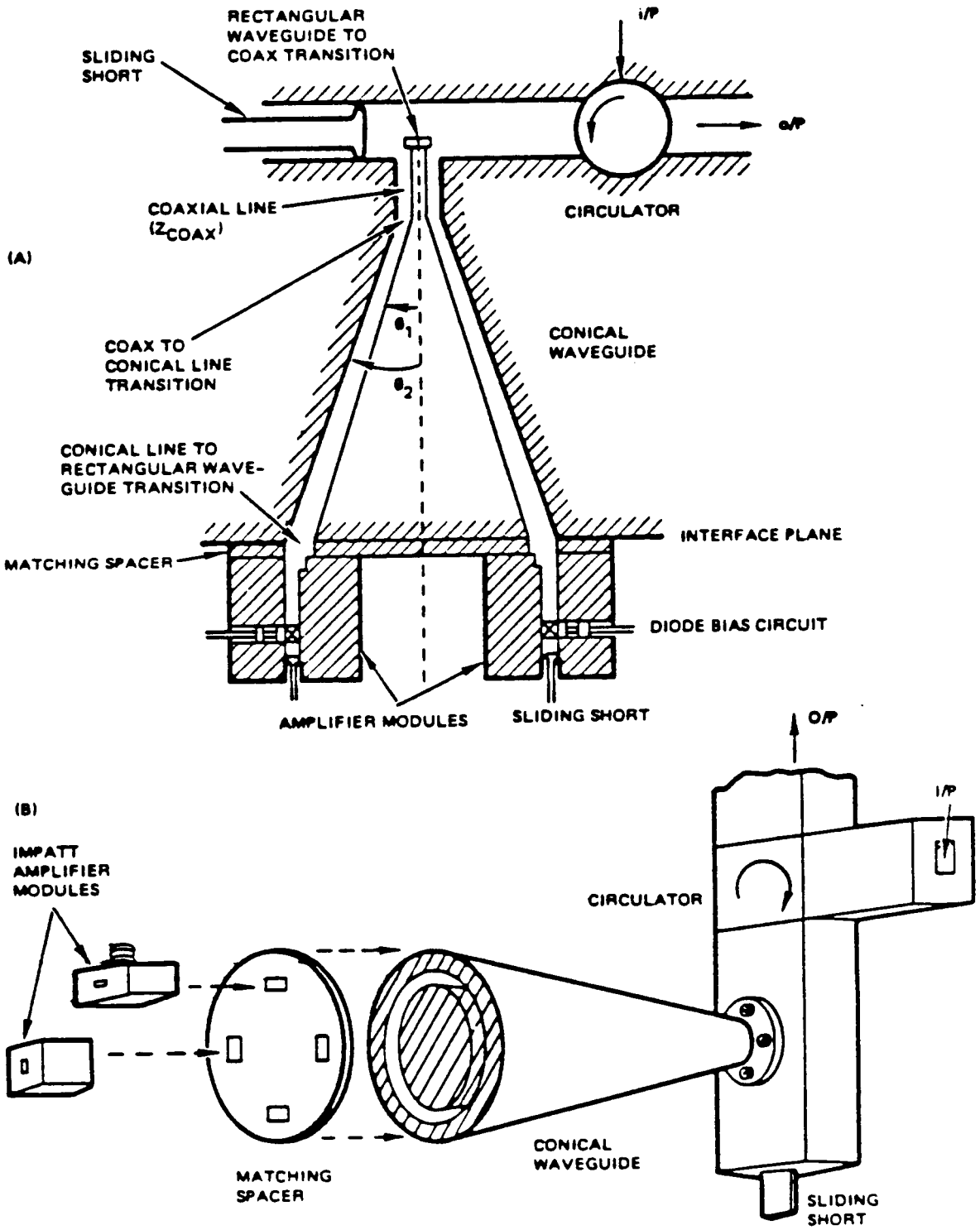

Figure 4.1-1. Four-diode conical power combiner.

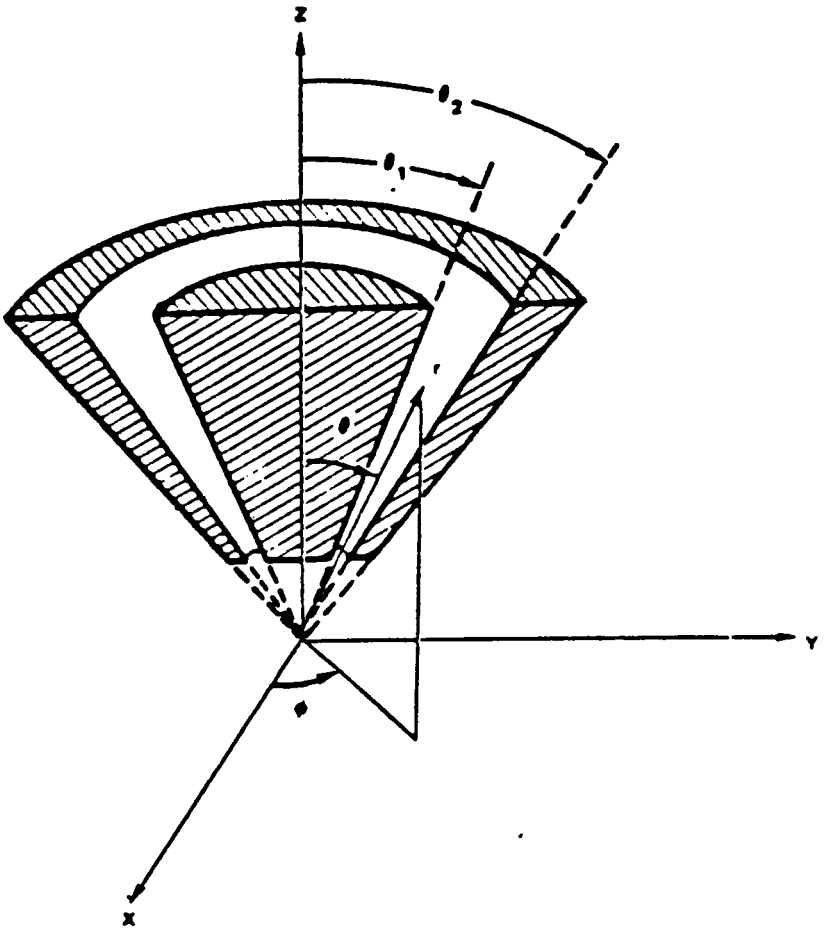

Figure 4.1-2. Conical transmission line coordinate system.

The dominant mode current I(r) and voltage V(r) are determined by the transmission line equations.

$$\frac{d^2I}{dr^2} + k^2 I = 0 \tag{4-3}$$

$$V = -\frac{j}{k} Z_c \frac{dI}{dr} \tag{4-4}$$

where $k = \omega/c$ is the free space propagation wave number assuming an exp $(-j\omega t)$ time dependence, and Z_c is the characteristic impedance of the dominant mode.

$$Z_c = \frac{1}{2\pi} \sqrt{\frac{\mu}{\varepsilon}} \ln \frac{\tan (\theta_2/2)}{\tan (\theta_1/2)}$$

Figure 4.1-3 plots Z_a as a function of the outer cone aperture θ_2 treating θ_1 as a parameter. This results in a family of curves for different θ_1's. Because of the azimuthal symmetry of the fundamental TEM mode, it is chosen as the principal mode for power transfer. However, higher-order modes having θ and ϕ dependence may also be generated if the excitation by the amplifier modules at the bottom of the cone possesses the amplitude and/or phase imbalance. Proper suppression of these higher-order modes is essential for efficient power combining. In Quines'*work, radially-machined slots filled with microwave absorbing material were implemented to overcome this isolation problem; however, it did not provide any design information to realize this mode filter. Therefore, an empirical technique is applied for producing the best performance.

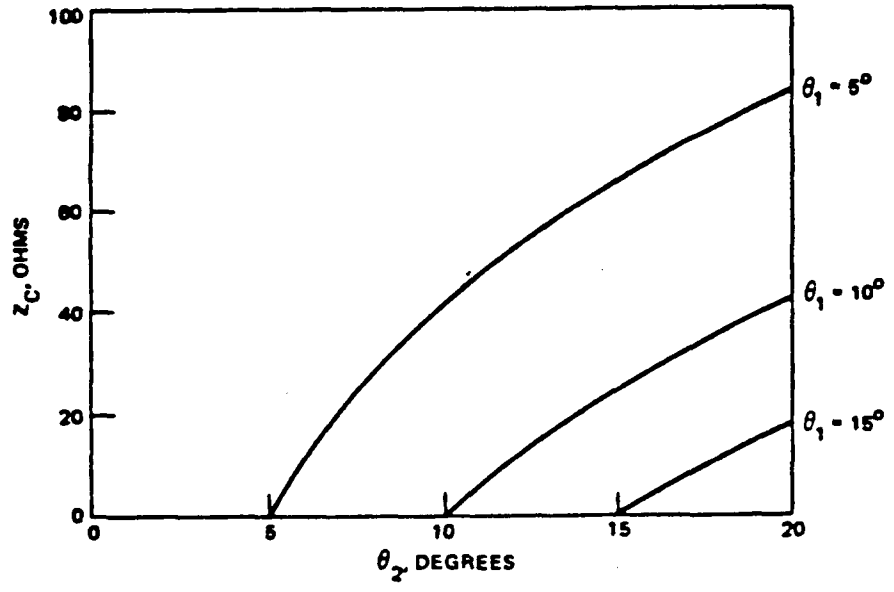

Figure 4.1-3. Characteristic impedance of a conical transmission line.

4.1.2 RF Characterization

To gain a complete understanding of the conical line combiner design and operation, a step-by-step approach has been adopted for development of this technology. The key steps are:

1) Develop broadband rectangular waveguide-to-coaxial line transition
2) Develop broadband coax-to-conical line transition
3) Develop broadband conical line-to-amplifier module transition.

*"Ku-band IMPATT Amplifier and Power Combiners," Catalog No. 786H1355-7 MTT, IEEE MTT-S, pp. 346-348

Steps 1 through 3 constitute the passive characterization of the combiner circuit and must be pursued in their respective order.

Broadband Waveguide-to-Coax-Transition

The waveguide-to-coax transition must be capable of the widest possible bandwidth with optimum impedance matching characteristics. The design at V-band was based on well-established commercial designs available at lower frequencies. To characterize the transition at 60 GHz, two identical transitions were placed in tandem as shown in Figure 4.1-4. Power was incident on one waveguide and coupled out of the other. Assuming the absence of unwanted resonances within the structure (which may easily be identified in the measured transmission characteristics), low insertion loss will indicate good impedance matching. The total insertion loss in dB divided by two gives the insertion loss of the waveguide-to-coax transition.

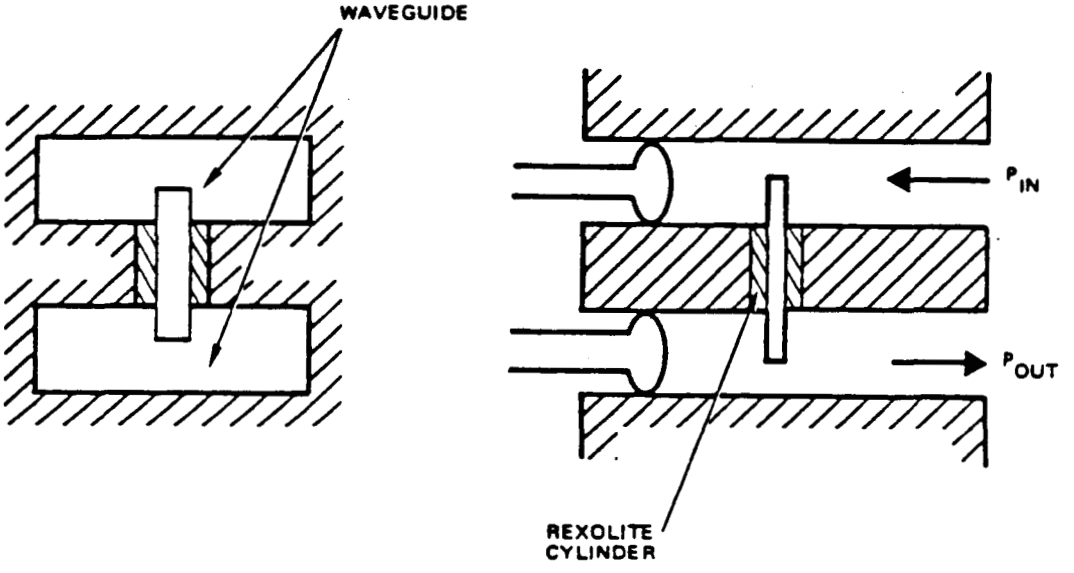

Figure 4.1-4. Tandem waveguide configuration for measuring waveguide to coax transition characteristics.

The measurements were obtained by tuning the tandem transition for maximum power by adjusting the tuning shorts and overall length of the center conductor. An impressive 9-GHz bandwidth was achieved with an average of 0.3-dB insertion loss per pass.

Coax-to-Conical-Line-Transition

Having fully understood the waveguide-to-coax transition, the next task was to design a broadband coax-to-conical line transition. Two conflicting requirements arose:

- The discontinuity at the coax-to-conical line interface increases with θ_1 and θ_2; therefore θ_1 and θ_2 must be kept reasonably small (say, no more than 15 degrees).
- On the other hand, if θ_1 and θ_2 are too small, the result would be a long conical line for combining a large number (8 to 12) of diodes. This would in turn result in higher ohmic loss.

After a preliminary mechanical tradeoff analysis, we chose θ_1 = 12° 7' and θ_2 = 14° 5' for the V-band design. Furthermore, instead of simply characterizing the coax-to-conical line transition, we characterized the waveguide-to-coaxial-to-conical line composite transition based on the previously matched waveguide-to-coaxial line transition. The V-band conical waveguide combiner hardware consists of the input and output waveguides, a coaxial line section, and a conical line section. To determine the impedance matching properties of this composite transition, gently tapered lossy material was inserted into the conical line to simulate a matched load. Deviations from this would represent a mismatch within the coax-to-conical line transition. Since the structure was physically symmetrical, phase information was not required, and the return loss at the waveguide input port was measured instead of the input impedance. Figures 4.1-5(a), (b), and (c) show the measured return loss for three tuning short positions. In all three cases, the coupling pin is 0.047 inch into the waveguide. With the tuning short 0.053 inch away from the coupling pin, better than 25 dB return loss (1.1:1 VSWR) was achieved between 57 and 60.5 GHz.

By moving the tuning short 0.047 inch away from the pin, an impressive 5.5 GHz bandwidth centered at 60 GHz was achieved with better than 20 dB return loss ($<$1.2:1 VSWR). When the tuning short was closest to the pin (0.037 inch), better than 25 dB return loss was again obtained at a higher frequency range between 60.5 and 63 GHz. Good impedance matching plus tremendous flexibility in frequency tuning can thus be achieved by merely adjusting the tuning short positions once an optimum pin length has been determined. Figure 4.1-6 is a photograph of some of the V-band conical combiner hardware.

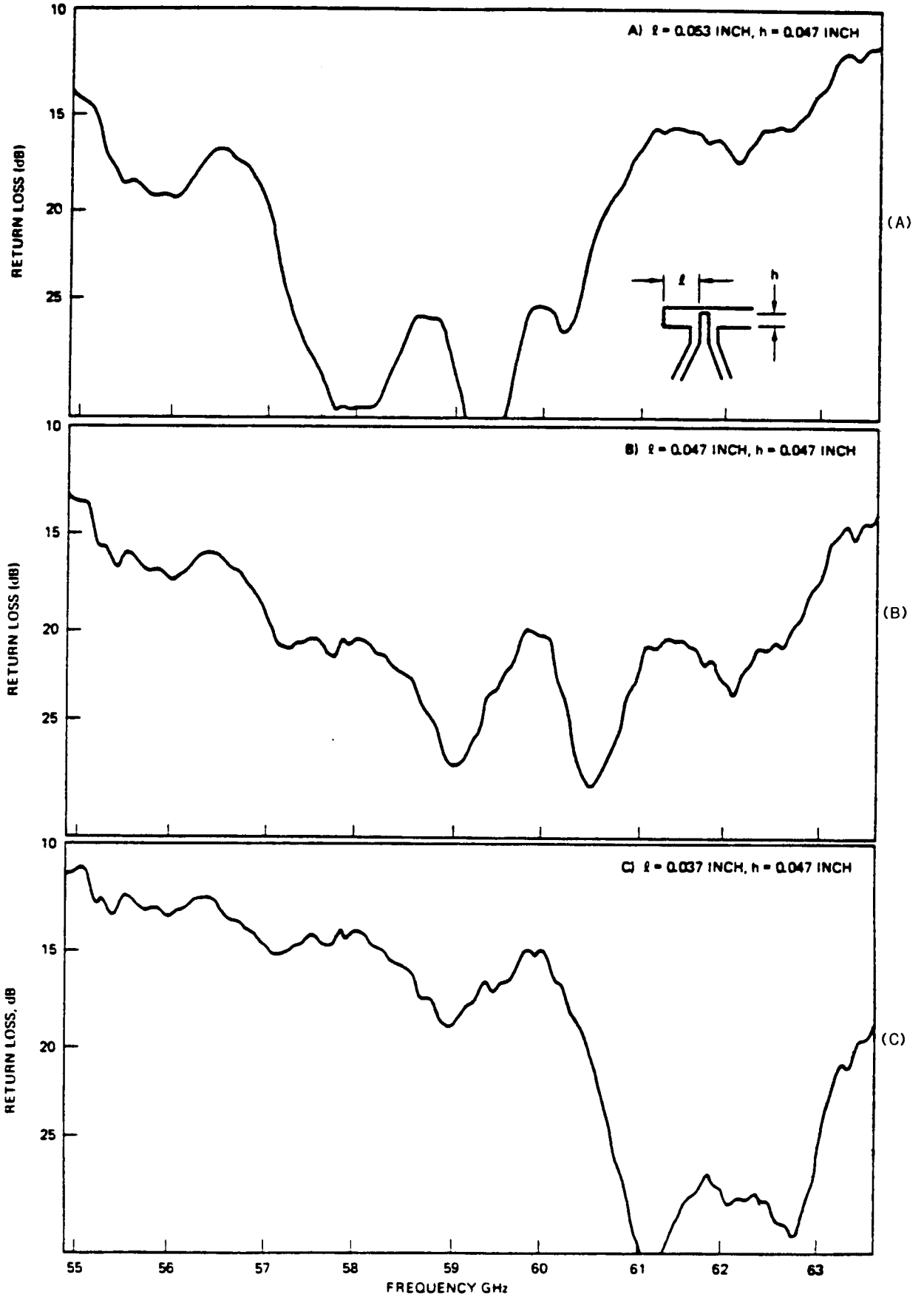

Figure 4.1-5. Waveguide-coaxial-conical line transition characteristics.

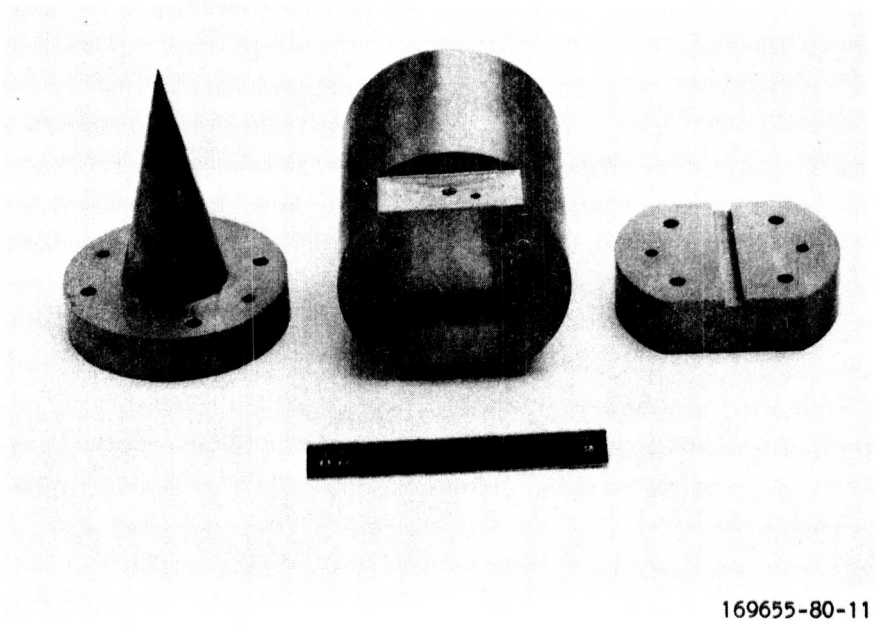

169655-80-11

Figure 4.1-6. V-band conical combiner hardware.

Conical Line-to-Amplifier Module Transition

The TEM wave propagating down the conical line must be equally divided and optimally coupled into four waveguide apertures in the matching plate. The fact that we have elected to combine four diodes created an artificial complication which will not appear in the more advanced (say eight-diode) version. In the four-diode configuration, the single-diode amplifier modules are the bolt-on type; the mechanical constraints require the waveguide openings to be configured as shown in Figure 4.1-7, where substantial metal areas separate adjacent waveguide openings (henceforth referred to as interstitial metal areas) on the module side (M-side) of the matching plate. If identical aperture geometry exists on the conical side (C-side) of the matching plate, two undesirable effects will result:

1) Metal areas have unit reflection coefficient so not all power in the TEM wave will get amplified. Combining efficiency is thus diminished.

2) Metal areas generate EM waves which are out of phase with those generated by the amplifier modules; this will give rise to higher order modes possessing azimuthal (ϕ) variations. These higher

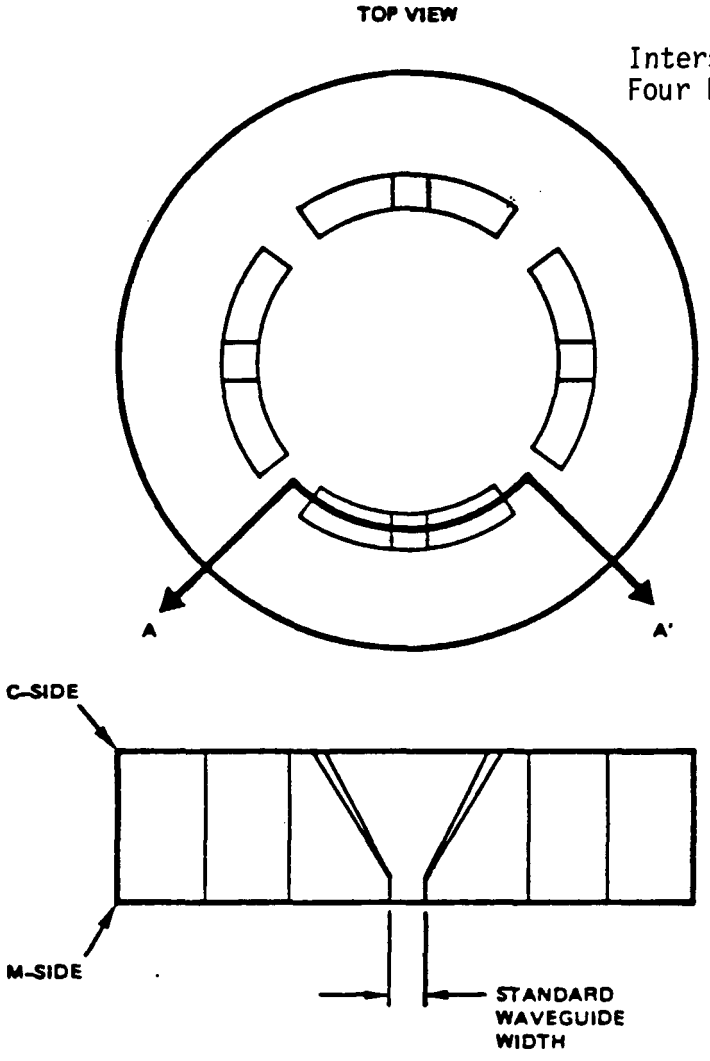

Figure 4.1-7. V-band matching plate with tapered transitions.

modes are of the TE or TEM variety and exhibit cutoff phenomena. As the conical line tapers toward the waveguide-to-coaxial transition, the diminishing coaxial cross-section eventually will reactively terminate all such higher order modes. If they are not properly attenuated, they will create high VSWR for the amplifier and poor port-to-port isolation.

To achieve the most optimum interface matching, the waveguide openings are increasingly tapered in width from the M-side to the C-side so that the interstitial metal areas on the C-side are reduced to a minimum, as seen in Figure 4.1-7. Any little metal areas remaining are masked off with Eccosorb (loss material) wedges which taper into the conical cavity.

Transmission measurements were performed at V-band by sending RF power (P_i) into the circulator waveguide port and observing the output power (P_o) from one of the amplifier module waveguide ports with the remaining three terminated in matched loads. If the conical combiner passive structure is an ideal four-way power divider, we must have $P_o/P_i = 1/4$, or 6 dB of loss from the circulator port to the amplifier module port. Any loss is excess of 6 dB will be due to impedance match and/or ohmic losses. Figures 4.1-8 and 4.1-9 are swept frequency measurements of P_o/P_i from 59 to 64 GHz with and without Eccosorb wedges between adjacent tapered waveguide transitions, respectively.

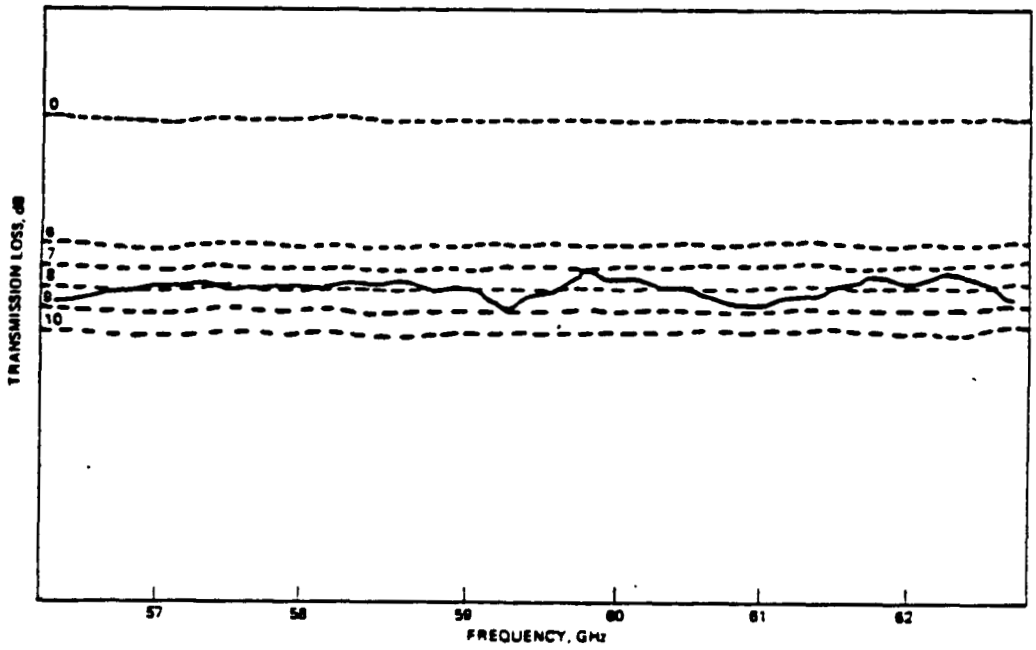

Figure 4.1-8. Transmission characteristics with Eccosorb wedges.

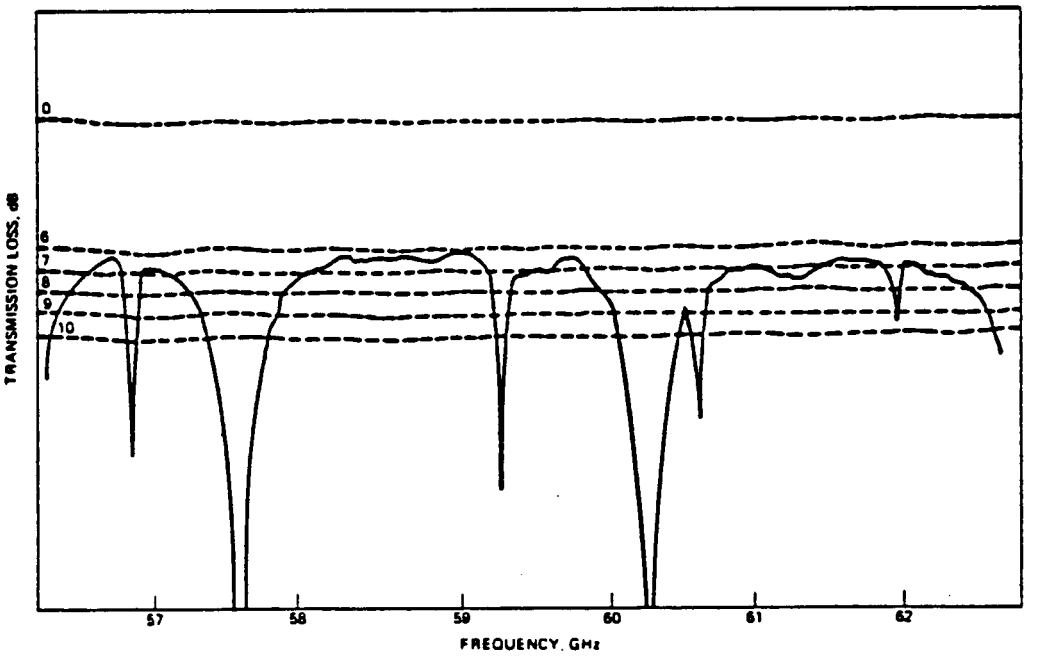

Figure 4.1-9. Transmission characteristics without Eccosorb wedges.

It is seen from Figure 4.1-9 that 0.5 dB of excess loss may be obtained for a maximum bandwidth of ≈ 1 GHz without using Eccosorb wedges. However, sharp resonances are present in the swept measurement because the minute interstitial metal areas behave as tiny point sources which excite higher-order modes. After Eccosorb wedges were inserted, the swept measurement showed an exceptionally flat response with approximately 1.5 dB excess loss, as shown in Figure 4.1-8.

The 1.5 dB excess loss may be further reduced by performing several iterations on the cone angles θ_1, θ_2, and the cone length to arrive at the most optimum compromise. An ultimate goal is a 0.5 dB excess loss over at least 2.5 GHz bandwidth, which translates into approximately 90-percent combining efficiency. An overall combining efficiency between 70 and 80 percent for four diodes is expected if losses due to amplitude and phase imbalance are included.

The matching plate design, the third step, has become critical for the overall conical line approach. Several versions of different designs, such as a simple gradual taper and the step-like transformers, have been tried. The simple gradual taper can be fabricated using an electronic discharge machining (EDM) technique. It can be seen from Figure 4.1-7 that a simple

gradual taper on the coaxial cylindrical structure actually involves two tapers rather than one because of the two different radii of a rectangular waveguide opening on the cylindrical structure. One disadvantage to this design is that once the hardware is fabricated, it would be difficult, if not impossible, to perform modifications. In addition, the EDM processing used to fabricate the hardware is extremely expensive. Some later versions of the matching plate included the step-like transformers, and although easier, they still did not succeed. This later design consisted of a stack of thin plates, each having four straight openings with widths different than the adjacent plates. In this manner, the stacks of plates simulated step transformers. Even with the added flexibility of this new design, we could not sufficiently optimize the conical line combiner.

4.2 RADIAL WAVEGUIDE POWER DIVIDER/COMBINER

This section describes a wideband power divider/combiner network using a section of radial waveguide as a basic transmission medium. The basic configuration of the N-way divider/combiner has one standard waveguide input port and N-symmetric waveguide output ports located in one plane and directed radially outward from the center. The network is a composite structure, since it will consist of input and output rectangular waveguides, a section of radial waveguide, and a section of coaxial line which is on the input line to excite the radial waveguide. All rectangular waveguides operate in the TE_{10} mode, and both coaxial and radial lines operate in their own TEM mode.

The input port must be well matched, and the network should have low insertion loss over the required bandwidth. The approach to developing this network is first to make a transition from the input waveguide to a coaxial line which has circular symmetry. Next, a transition is made from the coaxial line to a circular parallel plate radial line in the TEM mode, which also has circular symmetry. Finally, a transition is made from this radial line to the N rectangular waveguide ports.

The development of the N-way divider/combiner network, therefore, consists largely of three tasks, each of which concerns the impedance matching of junctions.

1) Matching the input waveguide to the coaxial line

2) Matching the coaxial line to a circular parallel plate radial line.

3) Matching the parallel plate radial line to the N-waveguide ports symmetrically placed about the radial line.

It is noted that all the different media are capable of wideband and high power transmission except for the transition region. Therefore, to have wideband characteristics throughout the whole power divider/combiner network, a transition using nonresonant schemes is desired. The following subsections discuss the propagation characteristics of the radial waveguide; the development of three tasks will be illustrated and measured results presented.

4.2.1 Propagation Characteristics of the Radial Waveguide

A parallel plate radial waveguide illustrated in Figure 4.2-1 can support two types of waveguide modes: E_{mn}-type modes for which $H_Z = 0$ and H_{mn}-type modes for which $E_Z = 0$.

E-Type Modes

The field components of an E-type mode in the radial guide of Figure 4.2-1 can be represented as:

$$E_z = - V_i' \frac{\varepsilon_n}{b} \cos \frac{n\pi}{b} z \begin{matrix}\cos \\ \sin\end{matrix} m\phi ,$$

$$E_\phi = \mp V_i' \frac{\varepsilon_n}{b} \frac{m}{\kappa_n r} \frac{n\pi}{\kappa_n b} \sin \frac{n\pi}{b} z \begin{matrix}\sin \\ \cos\end{matrix} m\phi , \qquad (4\text{-}5a)$$

$$E_r = - j\zeta I_i' \frac{\varepsilon_m}{2\pi r} \frac{\pi}{kb} \sin \frac{n\pi}{b} z \begin{matrix}\cos \\ \sin\end{matrix} m\phi ,$$

$$H_z = 0,$$

$$H_\phi = I_i' \frac{\varepsilon_m}{2\pi r} j \cos \frac{n\pi}{b} z \begin{matrix}\cos \\ \sin\end{matrix} m\phi , \qquad (4\text{-}5b)$$

$$H_r = \pm 2j\eta V_i' \frac{\varepsilon_n}{b} \frac{K}{\kappa_n} \frac{m}{\kappa_n r} \cos \frac{n\pi}{b} z \begin{matrix}\sin \\ \cos\end{matrix} m\phi ,$$

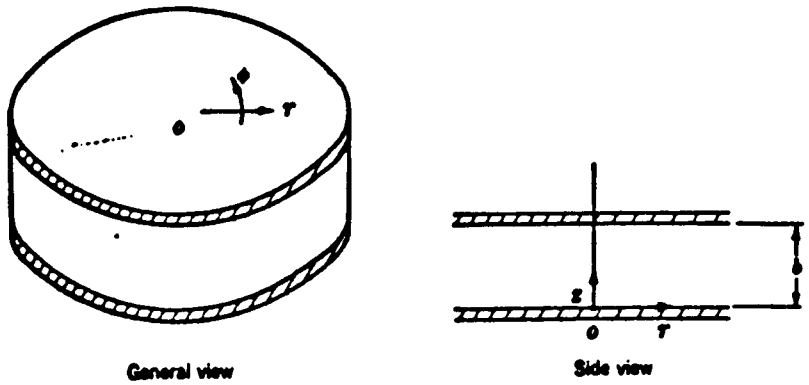

Figure 4.2-1. Radial waveguide of cylindrical cross section.

where

$$\kappa_n = \sqrt{k^2 - \left(\frac{n\pi}{b}\right)^2}$$

$$\varepsilon_n = 1 \quad \text{if } n = 0,$$

$$\varepsilon_n = 2 \quad \text{if } n \neq 0,$$

$$m = 0,1,2,3,\ldots,\ n = 0,1,2,3,\ldots$$

The z dependence of the E-type mode is determined by the transmission line behavior of the mode voltage V'_i and current I'_i. The latter quantities satisfy the transmission-line equations.

$$\frac{dV}{dt} = -jkZI \tag{4-6a}$$

$$\frac{dI}{dt} = -jkYV \tag{4-6b}$$

$$Z'_i = \zeta \frac{b\varepsilon_m}{2\pi r_n} \frac{\kappa_n^2}{\kappa'_i k'}$$

$$\kappa'_i = k^3 = \left(\frac{n\pi}{b}\right)^2 - \left(\frac{m}{r}\right)^2$$

$$\kappa_n = k^2 - \left(\frac{n\pi}{b}\right)^2 \tag{4-7}$$

For either m = 0 or n = 0 the transverse electric and magnetic fields of each mode have only a single component. As is evident from the form of equations (4-5), two independent E-type modes with different polarizations exist; the amplitudes of these degenerative modes are different from each other, although this has not been explicitly indicated.

H-type Modes

The field components of an H-type mode in the radial guide of Figure 4.2-1 are given by:

$$E_z = 0$$

$$E_\phi = V_i'' \frac{\varepsilon_m}{2\pi r} \sin \frac{n\pi}{b} z \begin{matrix}\sin \\ \cos\end{matrix} m\phi$$

$$E_r = j\zeta I_i'' \frac{\varepsilon_n}{b} \frac{k}{\kappa_n} \frac{\varepsilon_m}{\kappa_n r} \sin \frac{n\pi}{b} z \begin{matrix}\cos \\ \sin\end{matrix} m\phi \qquad (4\text{-}8a)$$

$$H_z = I_i'' \frac{\varepsilon_n}{b} \sin \frac{\pi}{b} z \begin{matrix}\sin \\ \cos\end{matrix} m\phi$$

$$H_\phi = \pm I_i'' \frac{\varepsilon_n}{b} \frac{m}{\kappa_n r} \frac{n\pi}{\kappa_n b} \cos \frac{n\pi}{b} z \begin{matrix}\cos \\ \sin\end{matrix} m\phi \qquad (4\text{-}8b)$$

$$H_r = -j\eta V_i'' \frac{\varepsilon_m}{2\pi r} \frac{\pi}{kb} \cos \frac{\pi}{b} z \begin{matrix}\sin \\ \cos\end{matrix} m\phi$$

where

$$\kappa_n = k^2 - \left(\frac{n}{b}\right)^2$$

$$m = 0,1,2\cdots, \quad n = 1,2,3\cdots.$$

The z dependent mode voltage V''_i and current I''_i obey the radial transmission line equation (4-6) with

$$Z_i'' = \frac{2\pi r \varepsilon_n}{b \varepsilon_n}$$

$$\varepsilon_i'' = k^2 - \left(\frac{n\pi}{b}\right)^2 - \left(\frac{m}{r}\right)^2 \qquad (4\text{-}9)$$

The existence of two distinct H-type modes with different polarizations is to be noted. E_{mn}-type modes have the identical cutoff frequency $f_{c_{mn}}$ expressed as:

$$f_{cjmn} = C\sqrt{\left(\frac{n}{2b}\right)^2 + \left(\frac{m}{2\pi r}\right)^2} \qquad (4\text{-}10)$$

The dominant mode in the radial waveguide is an E-type mode with $m = n = 0$, and is seen to be a transverse electromagnetic mode. The non-vanishing field components of this TEM mode follow from equation (4.4) as:

$$E_z = \frac{-V(r)}{b} \qquad (4\text{-}11a)$$

$$H_p = \frac{I(r)}{2\pi r} \qquad (4\text{-}11b)$$

and the corresponding characteristic impedance and mode constant as:

$$Z = \zeta \frac{b}{2\pi r} \quad \text{and} \quad k \qquad (4\text{-}12)$$

For an N-way radial waveguide power divider/combiner, the radial waveguide is actually operating in the multimode region. Because of the physical symmetry and geometrical structure, this radial waveguide will support finite E_{mn}-type modes for $n = 0$ and $m = 1, 2 \ldots M$. For these modes, there are only three field components; i.e, E_Z, H_ϕ, and H_r.

4.2.2 Rectangular Waveguide-to-Coaxial Line Transition

A V-band symmetric back-to-back waveguide-to-coaxial-to-waveguide transition test fixture was fabricated to develop a suitable low loss, wideband, matched configuration for this transition. Varieties of matching-element bead pairs were made to be placed at each of the two ends of the coaxial conductor protruding into the two waveguides. The configuration of this test fixture is shown in Figure 4.2-2. The coaxial line is a 60-ohm system to minimize losses, and its OD and ID are 0.060 and 0.023 inch, respectively, in the air-dielectric region and allow single-mode propagation. Standard V-band waveguides are adopted for their compatibility with the available measuring systems.

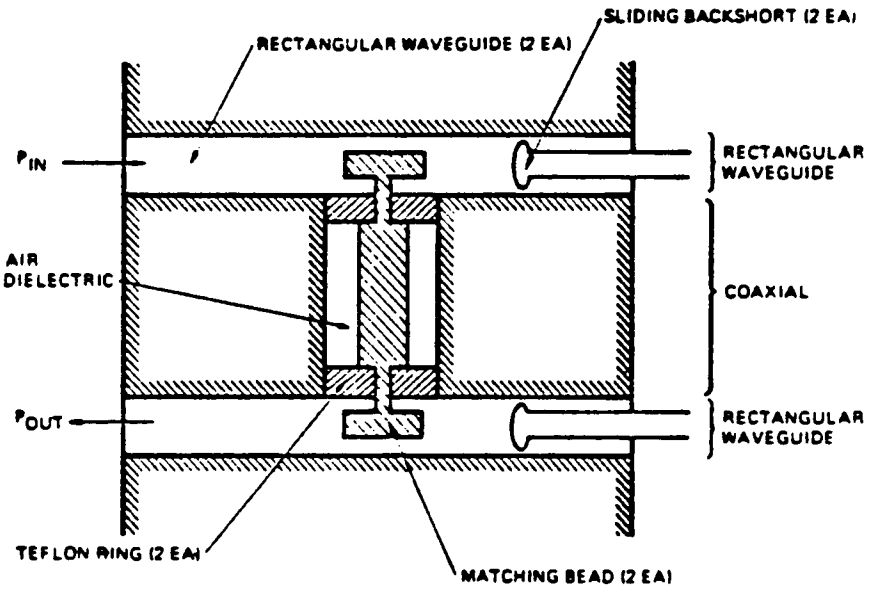

Figure 4.2-2. Back-to-back waveguide-to-coax test fixture for developing a low insertion loss, low VSWR V-band waveguide-to-coax transition.

Development of matching for the waveguide-to-coaxial transition consisted of experimentally determining the dimensions of the matching bead, its height above the floor of the waveguide, and the position of the sliding backshort which produces a sufficiently low VSWR, low insertion loss, and broad bandwidth. The insertion loss and VSWR were measured using a laboratory V-band transmission/reflection test set. Excellent results were obtained using a bead with a diameter of 0.045 inch, a height of 0.040 inch, and which protrudes into the waveguide with a total height of 0.055 inch.

Figure 4.2-3 shows the results of the insertion loss measurement of the final matching element configuration. A single-pass insertion loss of better than 0.4 dB over the 55 to 65 GHz band is indicated.

4.2.3 Coaxial Line-to-Radial Waveguide Transition

A second special test fixture was constructed to develop the matched coax-to-radial waveguide transition (Figure 4.2-4). The matched rectangular waveguide-to-coax transition developed in the previous steps is included on the fixture to allow using standard waveguide test equipment to perform measurements.

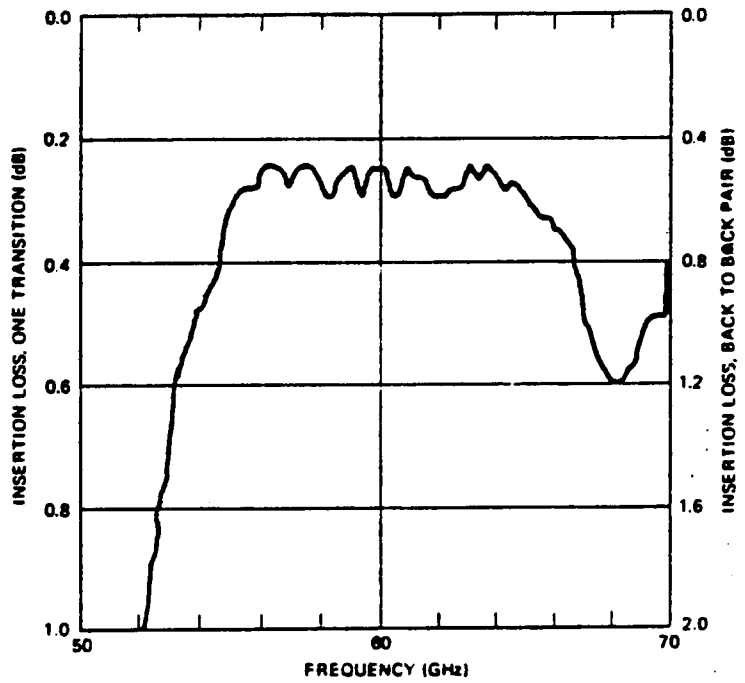

Figure 4.2-3. Insertion loss of the V-band symmetric back-to-back waveguide-to-coax test fixture after a suitable matching bead was developed.

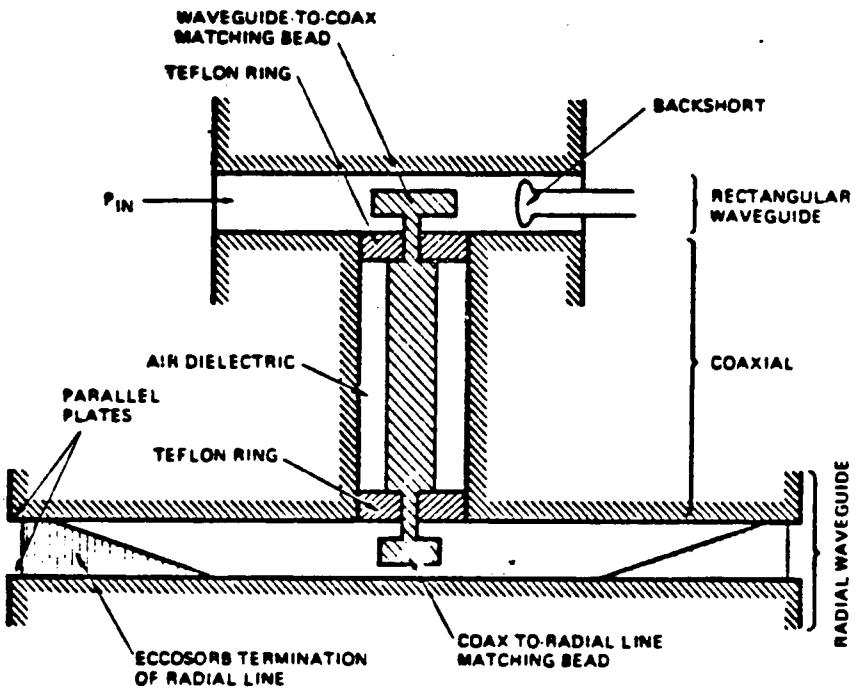

Figure 4.2-4. Test fixture for developing a matched V-band coax-to-radial line transition. Upper section is the matched waveguide-to-coax transition previously developed.

The parallel plate radial line section is terminated at its periphery with sections of tapered microwave absorbing material. A suitable configuration for a matching bead at the coax-to-radial transition was determined to have a diameter of 0.045 inch and height of 0.040 inch; the bead protrudes into the waveguide with a height of 0.066 inch.

The measurement of the return loss versus frequency for this configuration is shown in Figure 4.2-5. A return loss of better than 20 dB over the 55 to 65 GHz band is indicated. A short-circuiting metallic ring placed within the parallel plate radial line section, making contact with both the top and bottom parallel plates on the radial line, will allow a measurement of the double-pass insertion loss. This is performed by measuring the return loss at the waveguide port when the shorting ring is in place within the parallel plate radial line. The single-pass insertion loss of this fixture cannot be measured directly because there are no practical means of directly measuring the power in the radial line.

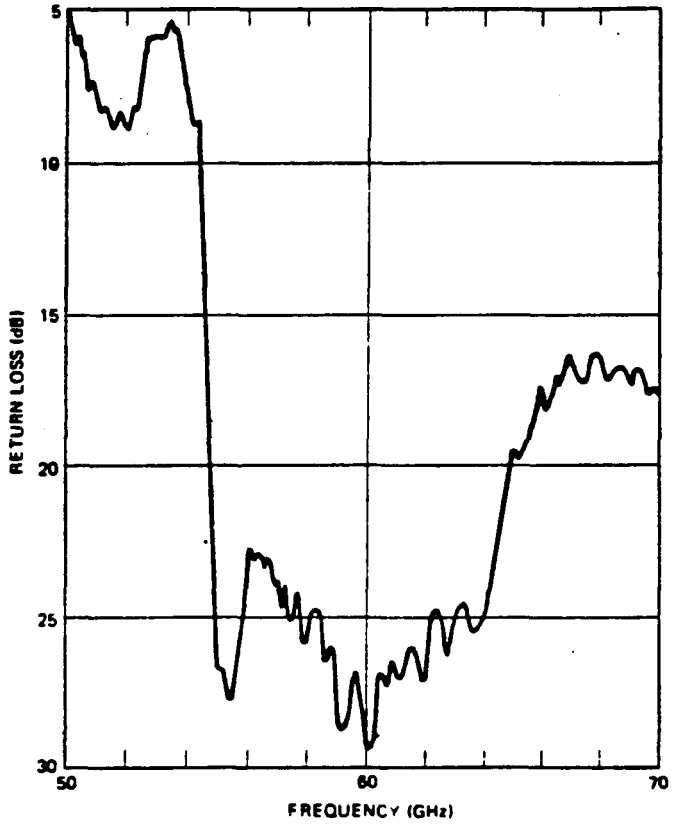

Figure 4.2-5. Return loss for an optimized V-band coaxial-to-radial waveguide transition test fixture in which tapered Eccosorb loads are placed around the circumference of the radial line to terminate the radial line mode.

The measured return loss for this configuration was about 1.3 dB over the 59 to 64 GHz frequency range. Therefore, the single-pass insertion loss of the circuit is about 0.65 dB over the 59 to 64 GHz band. One phenomenon observed is that the response showed much more ripple over the frequency; we believe this is due to asymmetry of machined parts and position of short-circuiting ring.

4.2.4 Radial Waveguide-to-N-Way Rectangular Waveguide Ports

The initial goal to meet the program requirements is to demonstrate the power combining techniques to combine four IMPATT diodes to reach a power output of 1 W minimum. On the other hand, it is believed that one of the advantages of an N-way radial waveguide power divider/combiner is to use a large radius of the radial waveguide; i.e., a large N. Therefore, a 16-way radial waveguide power divider/combiner is designed and fabricated instead of a four-way; four amplifiers will mount to this power divider/ combiner with the remaining ports terminated to demonstrate the combining techniques. This will be illustrated in the section on amplifier integration.

A photograph of the final hardware is shown in Figure 4.2-6. The radius and height of this radial waveguide are 0.402 and 0.074 inch, respectively. The block is made of brass for ease of machining, and is gold-plated. Sixteen rectangular waveguides are machined and symmetrically directed radially outward from the center. The unit is fabricated using numerically-controlled machining techniques, where tight machining tolerances and good physical symmetry can be controlled.

The complete 16-way V-band radial waveguide power divider/combiner network is constructed by using the two previously matched transition elements. The impedance matching of the radial waveguide to the 16 symmetrically placed rectangular waveguides on the final hardware was done by symmetrically placing a set of uniform dielectric chips near the interface of the radial waveguide and the array of rectangular waveguide. A close-up view of these dielectric chip matching elements is shown in Figure 4.2-7.

Excellent results have been achieved from the final unit. An insertion loss of 1 ± 0.3 for the 26 power division coefficients and a return loss at the input port better than 12 dB over the 55 to 67 GHz frequency range were measured. The average power division coefficient of the 16 output ports is

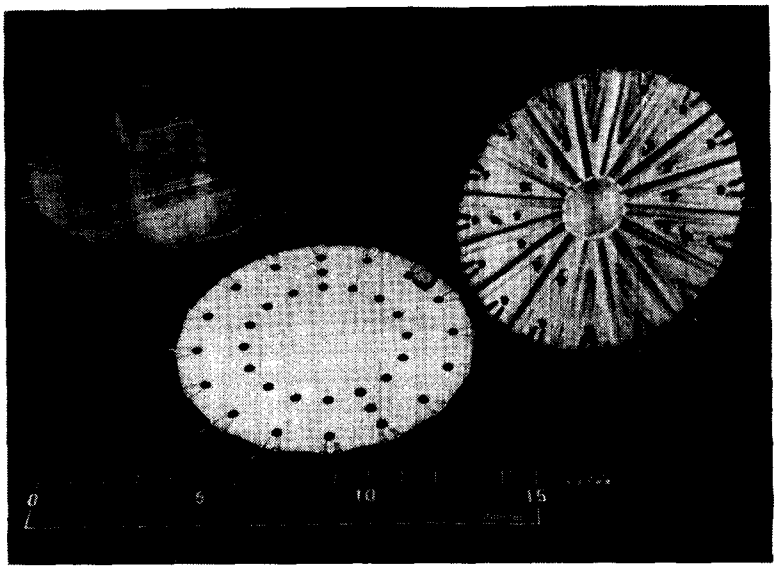

Figure 4.2-6. 16-way V-band radial line divider/combiner network.

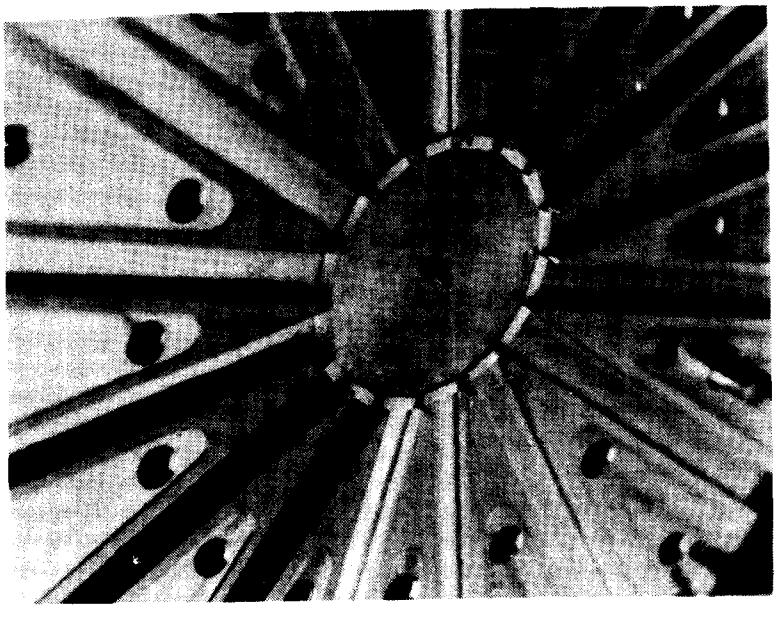

Figure 4.2-7. Close-up view of dielectric chip matching elements.

plotted versus frequency in Figure 4.2-8. The power imbalance over the output ports is ±0.6 dB, and is probably a result of imperfections in the machining of the unit and/or of the matching elements. Figure 4.2-9 shows the return loss of the input port and a typical output port of this network. Isolation coefficients between output ports have also been measured; the

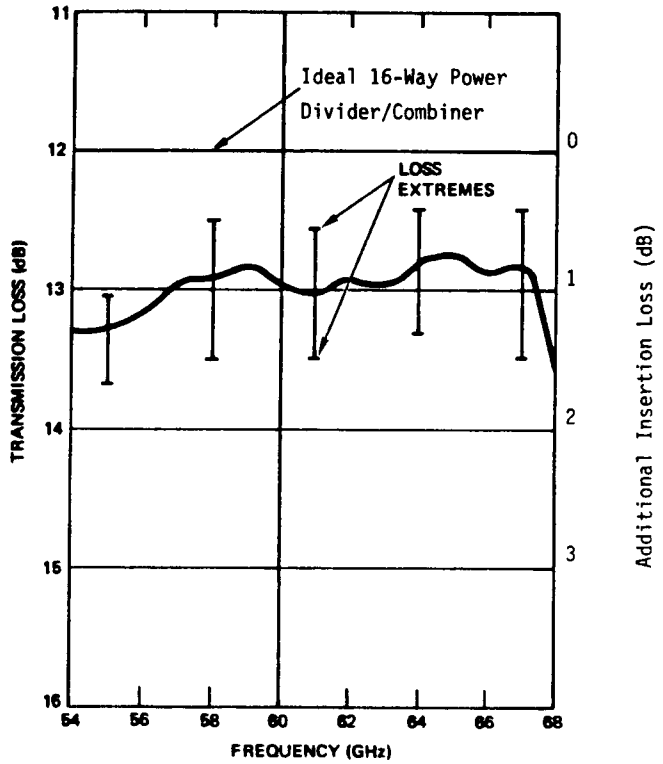

Figure 4.2-8. Measured transmission loss from the input (common) port to one of the output (radial) ports of the 16-way radial waveguide power divider/combiner. The ideal transmission loss is 12 dB.

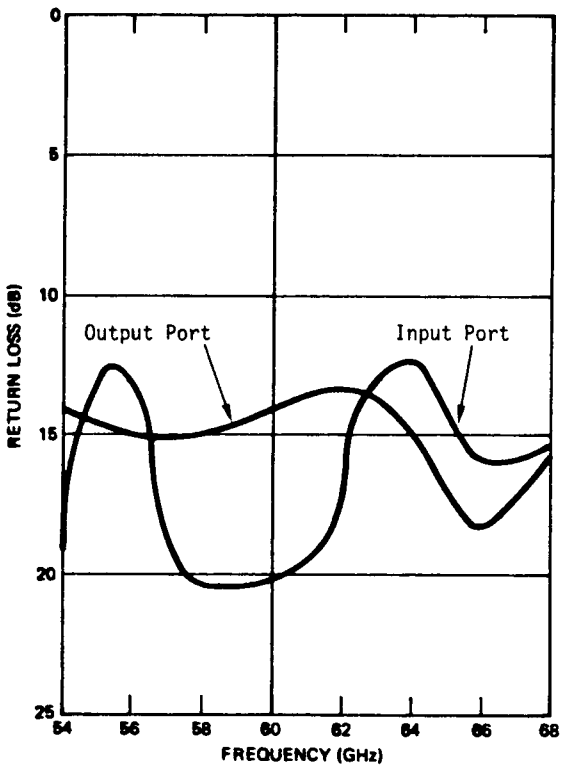

Figure 4.2-9. Return loss of both input (common) port and a typical output (radial) port on the 16-way radial waveguide power divider/combiner.

lowest isolation is observed between directly opposing output ports. Results of the measurements of the isolation coefficients of this power divider/combiner are presented in Figure 4.2-10.

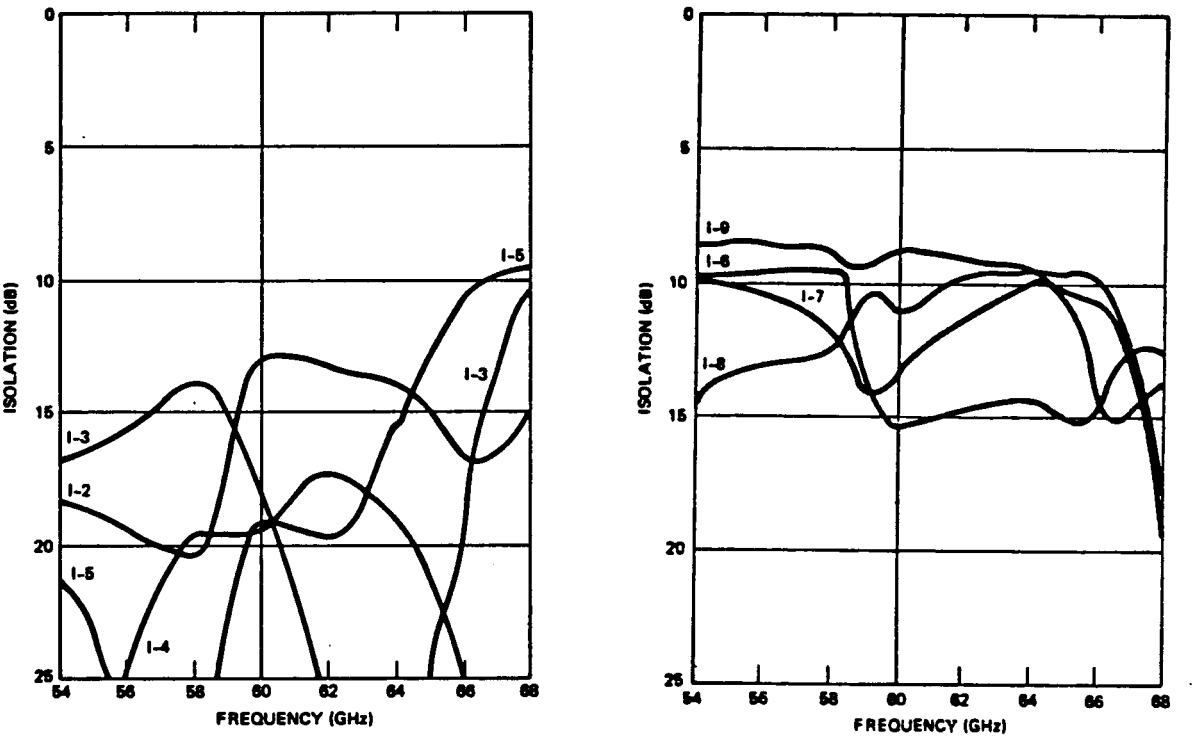

Figure 4.2-10. Isolation between output ports on the 16-way radial waveguide power divider/combiner (a) ports 1-2, 1-3, 1-4, and 1-5; (b) ports 1-6, 1-7, 1-8, and 1-9.

The radial line combiner as designed is a lossless structure; i.e., there are no terminations in the network to suppress higher-order modes within radial waveguide which has circumferential (ϕ) variation. Consequently, this network does not provide high port-to-port isolation, which is required for power combining IMPATT power amplifiers. Poor isolation can be improved by using external circulators. A configuration for an IMPATT amplifier power combiner scheme, using a pair of radial lines and combining the power of 16 matched two-port circulator-coupled amplifier modules, is shown schematically in Figure 4.2-11. A representative configuration sketch of the actual hardware for such a unit is shown in Figure 4.2-12.

In this configuration, each of the 16 two-port circulator-coupled amplifier modules has an isolator (i.e., a terminated circulator) on the input and

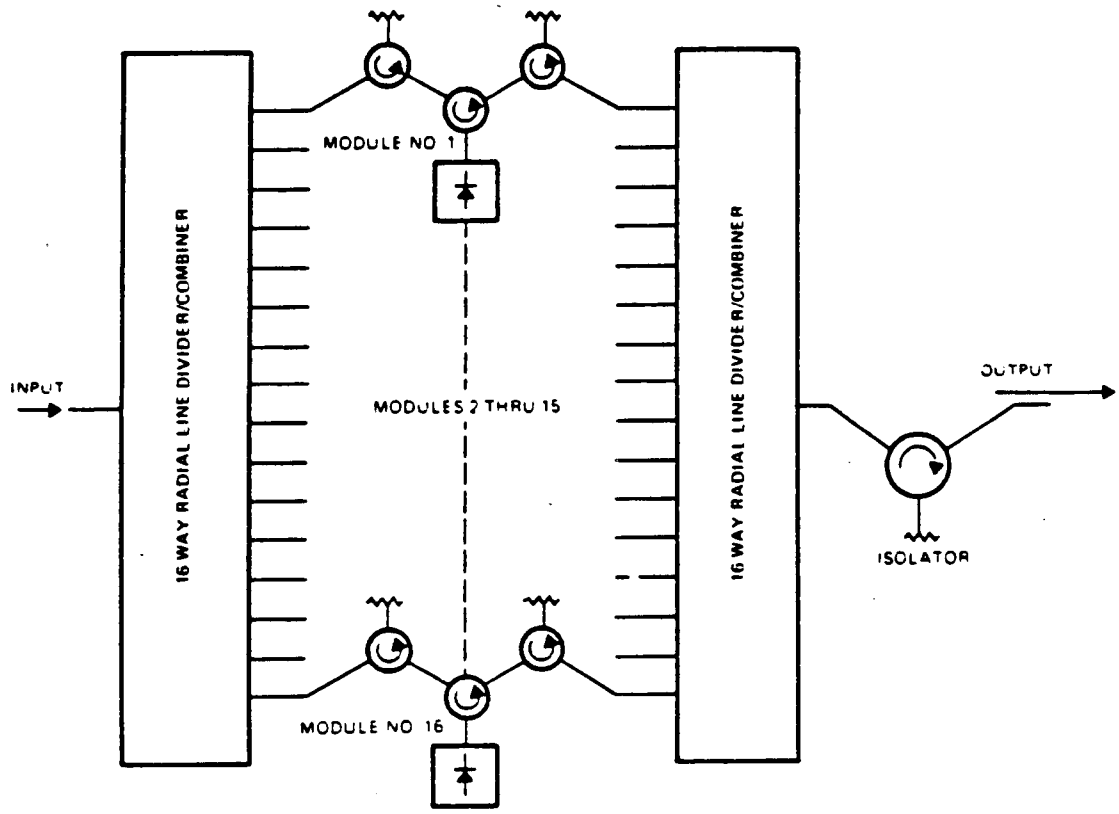

Figure 4.2-11. Module-level power combining of N two-port reflection amplifiers by means of a pair of N-way divider/combiner networks. Generally, N single-stage amplifiers can be replaced by N amplifier chains of stages.

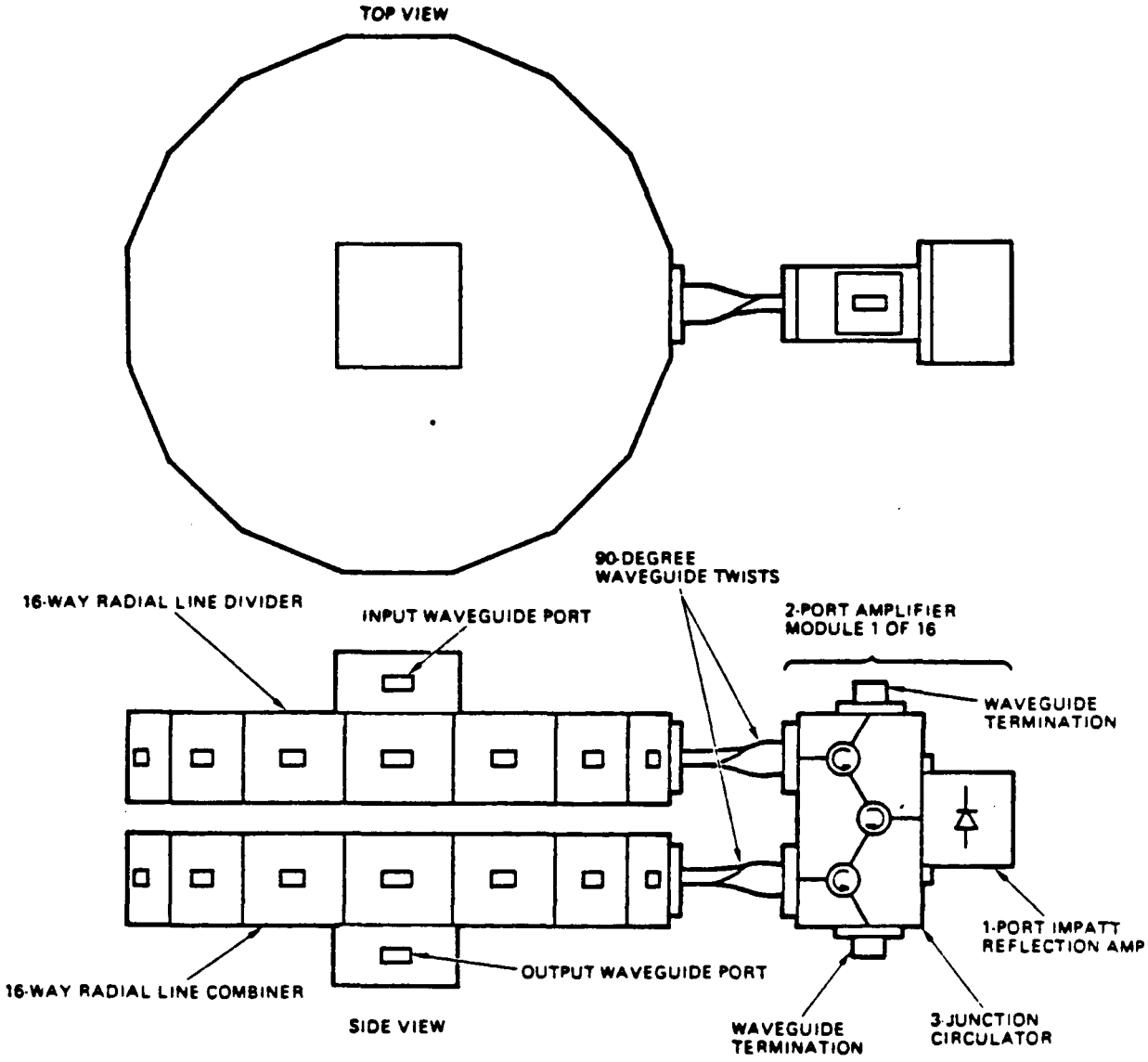

Figure 4.2-12. Conceptual design of 16-way radial line module-level power combiner configuration.

the output sides of each module. This is required to provide low VSWR and a high degree of module-to-module isolation, which an N-way divider/ combiner network alone generally could not provide.

TRW's V-band circulators have an isolation of about 25 dB over a wide (6 GHz) bandwidth. Since there are two circulator passes on the input and output sides of each amplifier module, this configuration provides at least 50 dB of module-to-module isolation. This high degree of isolation, provided by external ferrite components, is an outstanding advantage of the radial line power combiner.

Radial waveguide power divider/combiners using higher-order modes have also been considered; such schemes offer some very attractive features:

1) Higher-order modes, particularly circular electric TE_{10} mode of a radial waveguide, provide low loss and high power propagation characteristics.

2) The E-field polarization of the circular electric mode is in the direction, making it easier to implement mode suppressions within the network.

3) Again, due to field polarization, the additional waveguide twists for the previous power combining technique can be eliminated. A conceptual configuration of the power mode is shown in Figure 4.2-13.

In summary, TRW has developed a novel wideband power divider/combiner network during the present program period. This network uses the radial waveguide as a basic transmission medium. For a 16-way radial waveguide power divider/combiner, an insertion loss of less than 1.0 dB and return loss better than 12 dB have been obtained over a frequency range of 55 to 67 GHz. This power divider/combiner network is suitable for applications such as power combining solid state amplifier modules as well as phased array antennas. To power combine IMPATT amplifier modules, it will be necessary to use external ferrite components to obtain sufficiently high module-to-module isolation.

4.3 WIDEBAND, LOW LOSS CIRCULATORS

The three-port circulator is one essential component found in most injection-locking oscillators or reflection amplifiers employing IMPATT diodes. The circulator decouples the input circuit from the output circuit and, in effect, transforms a one-port network into one with two ports. Since both the input and output signals are transmitted through the circulator, the electrical characteristics of the circulator have a profound influence on overall circuit performance. The requirements imposed on the circulators used in the proposed program are stringent. They must be capable of handling the signal power and have a wide bandwidth (with low SWR) for proper circuit operations, and an adequate isolation for input/output decoupling. Moreover, the circulators must have an extremely low insertion loss (in the vicinity of 0.3 dB) so as not to further degrade the relatively poor efficiency of IMPATT devices. TRW has developed and patented such high performance circulators.

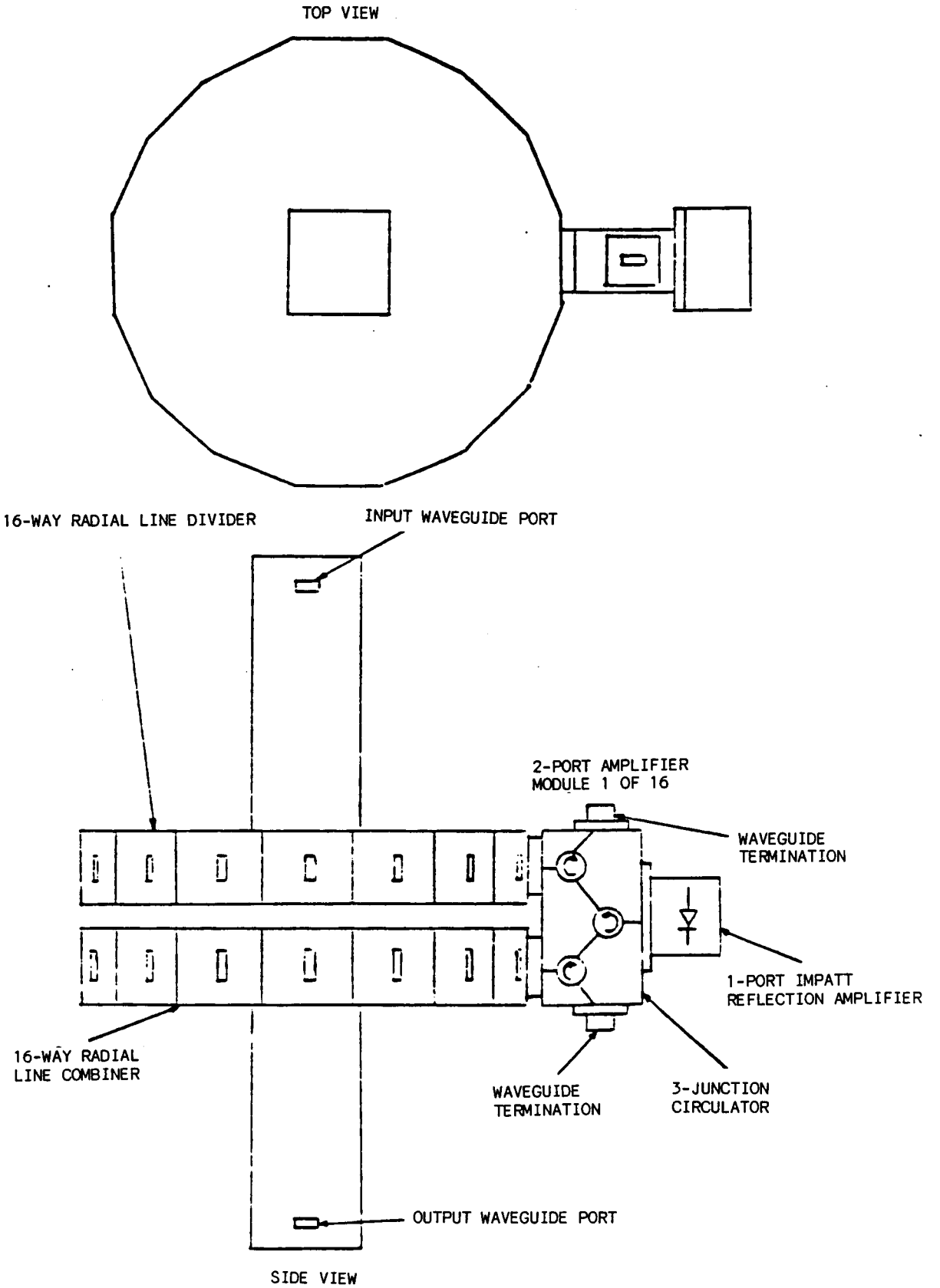

Figure 4.2-13. Conceptual design of radial line power combiner using circular electric TE_{01} wave.

Figure 4.3-1 depicts the simplified construction of a three-port junction circulator consisting of three TE_{10} rectangular waveguides which are 120 degrees apart and intercept to form a symmetric junction. A ferrite post is placed at the center of the junction. An external static magnetic field, H_a, is required to bias the ferrite post. Commercially available circulators employ ferrite posts with a triangular cross-section as shown in Figure 4.3-2. The triangular geometry was considered to have potential of offering a wide circulator bandwidth; however, due to fabrication and mechanical alignment difficulties, the wideband potential was never practically realized. In fact, each triangular geometry circulator has to be individually tuned to meet the electrical requirements. TRW, on the other hand, adopted the cylindrical ferrite post as shown in Figure 4.3-2(b). It was found that the cylindrical geometry offers not only superior mechanical properties, but also electrical performance that equals or surpasses that of the triangular geometry. Individual tuning of the TRW circulators is not required once the proper junction design is completed.

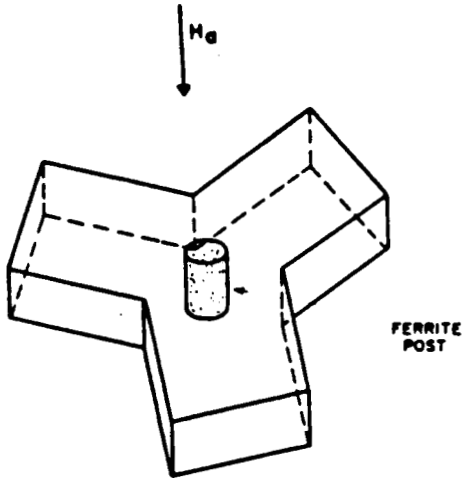

Figure 4.3-1. Simplified construction of a 3-port circulator.

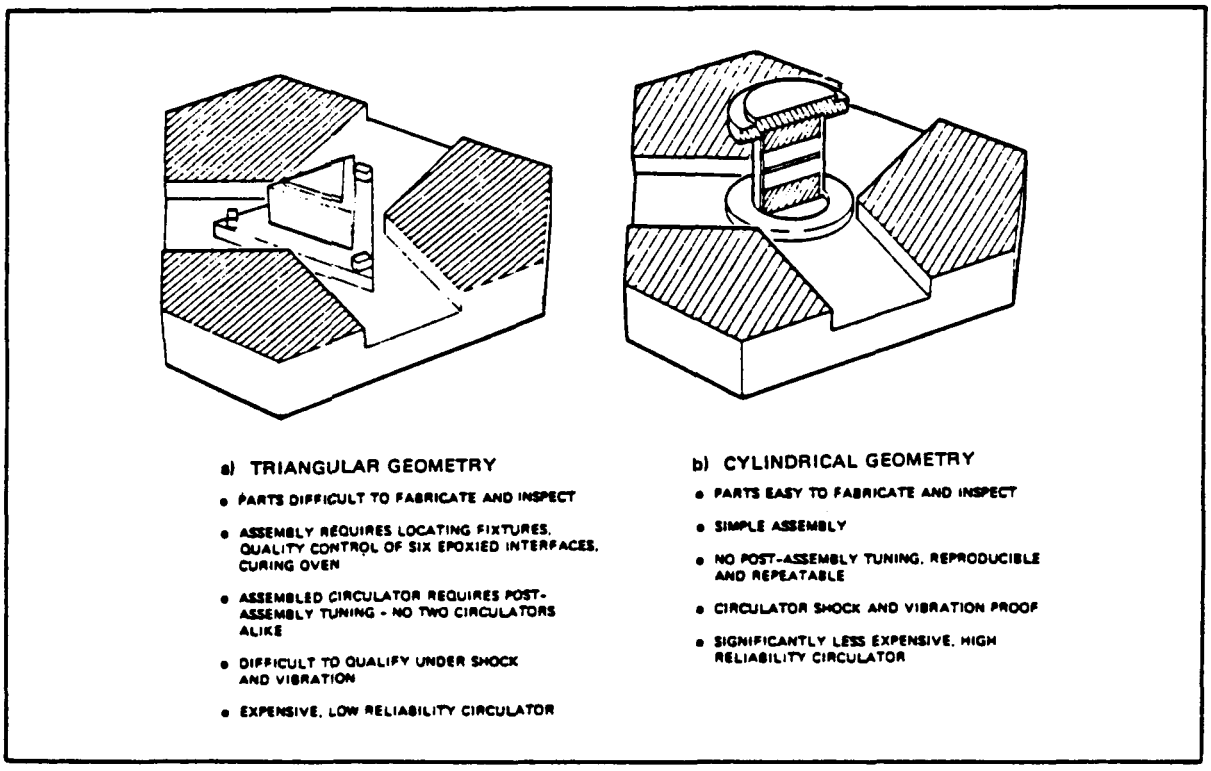

Figure 4.3-2. Comparison of conventional triangular and TRW's cylindrical circulator junctions.

A detailed graphic representation of the TRW circulator junction is depicted in Figure 4.3-3. The junction consists of one ferrite disc, two dielectric spacers, and a dielectric tube enclosing the above parts. This junction assembly is nested in metallic transformer discs indexed precisely in the circulator housing formed by three intersecting waveguides. The operation of a junction circulator is best explained with the aid of Figures 4.3-4(a) and (b). Notice that the symmetric junction formed by the waveguides behaves as a TM_{110} mode cylindrical cavity. When the external magnetic bias H_a is removed and the cavity is excited by the TE_{10} wave from one waveguide, the resulting TM_{110} field pattern is oriented in the direction shown in Figure 4.3-4(a). The pattern orientation is identical to that when no ferrite post is present. The reason that the ferrite post does not change the pattern orientation is as follows. In the absence of an external magnetic bias, the electromagnetic left and right polarized waves existing inside the ferrite have the same propagation constant. The two waves emerge from the ferrite in-phase, and no rotation of the cavity field pattern takes place. As shown in Figure 4.3-4(a), the presence of electric and tangential

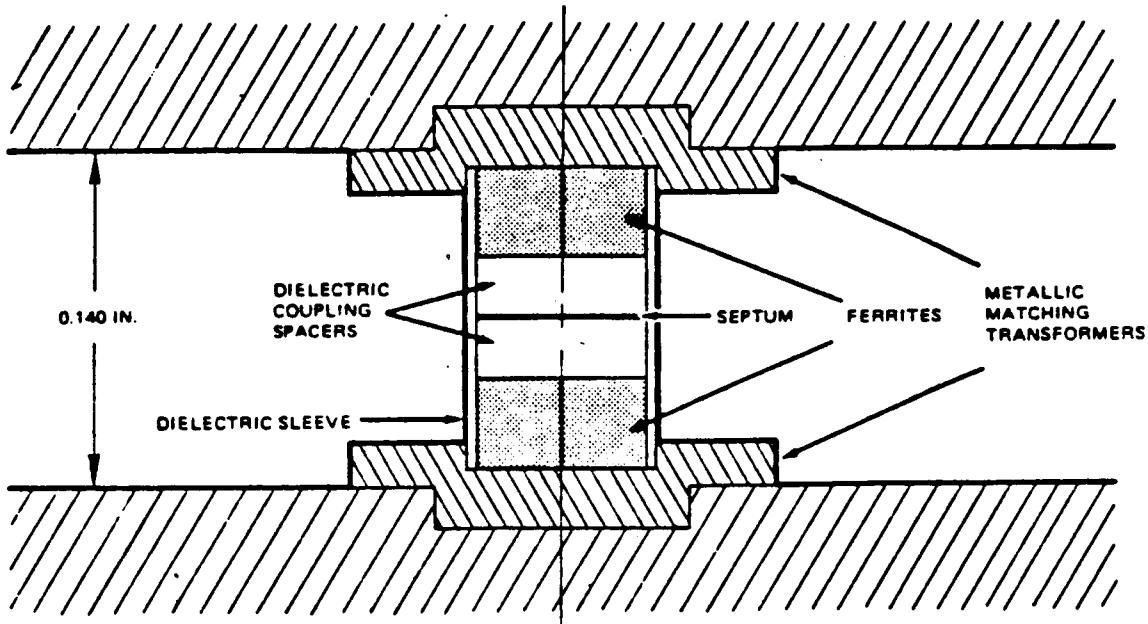

Figure 4.3-3. Graphic presentation of TRW's circulator junction.

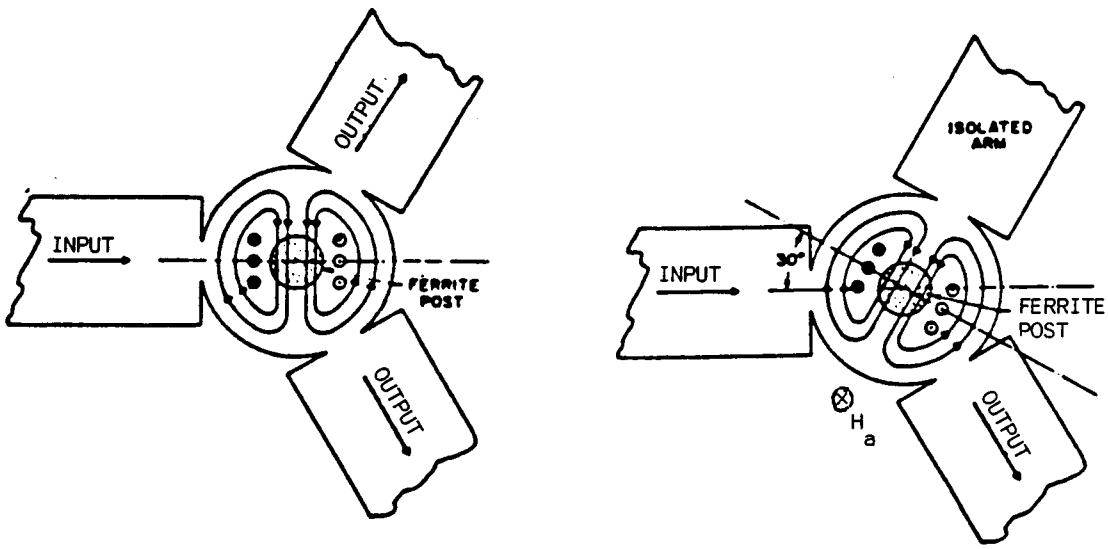

(A) WITH NO MAGNETIC BIAS

(B) WITH MAGNETIC BIAS H_a

Figure 4.3-4. Field pattern for H-plane waveguide circulator using TM_{110} mode. magnetic fields at the waveguide-cavity interface allows excitation of the TE_{10} wave in the two output waveguides.

When the external magnetic bias, H_a, is applied, the situation is changed. The two polarized waves in the ferrite no longer have the same propagation constant, resulting in rotation of the mode pattern of the cavity by 30 degrees, as shown in Figure 4.3-4(b). The final outcome is that one output waveguide stays unchanged, while the remaining waveguide is isolated

(i.e., no output). The cavity field pattern has altered so much that there are no electric and tangential magnetic fields at the waveguide-cavity interface to excite the TE_{10} wave in the isolated waveguide.

Figure 4.3-5 indicates the electrical performance of a typical TRW V-band circulator. The upper curve represents the SWR data and the lower curve, insertion loss data. It can be seen that for a SWR of 1.2, the circulator has a passband from 59 to 62 GHz, a bandwidth of 3 GHz. The insertion loss in the passband is less than 0.5 dB. The applicability of the circulator is further enhanced by various housing designs. Figure 4.3-6 shows the circulator construction using a multiple junction housing. Successful assembly of the multiple junction housing is primarily due to the repeatability of the cylindrical junction circulator developed at TRW. The assembly shown in Figure 4.3-6 houses three circulator junctions. Six assemblies of this type were used in the construction of the V-band amplifier. Each of the four power stage amplifier modules required one each of these assemblies. The two end circulators are used as isolators to achieve the necessary port-to-port isolation required by the radial line combiner.

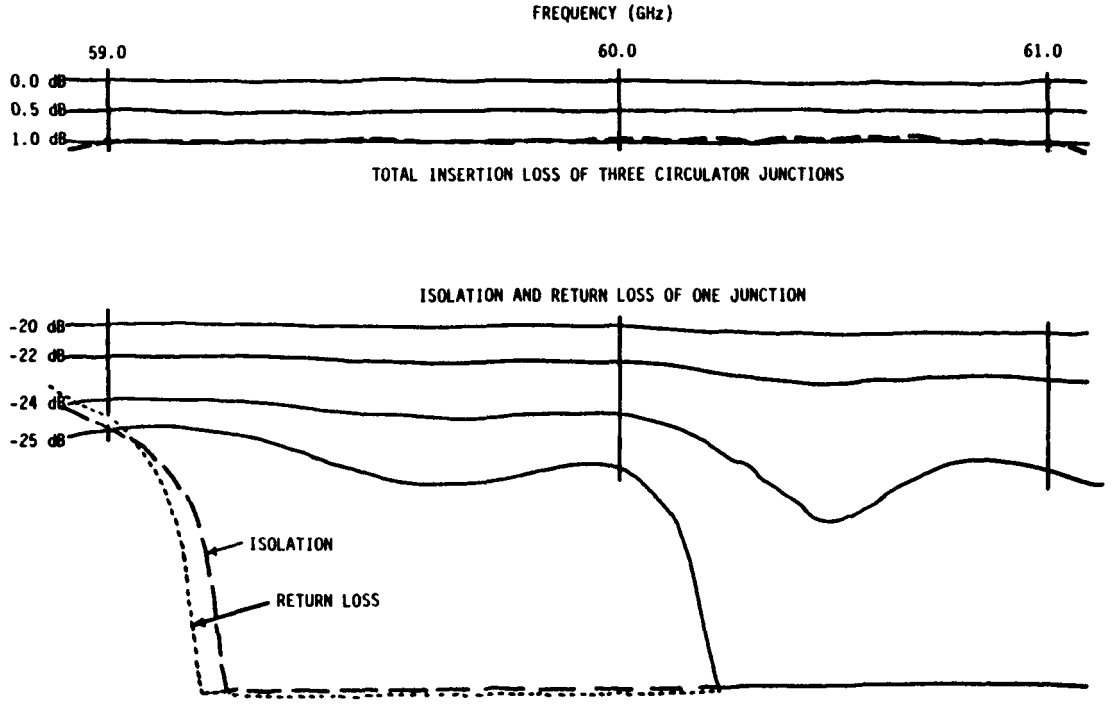

Figure 4.3-5. Swept frequency response of a three-junction circulator.

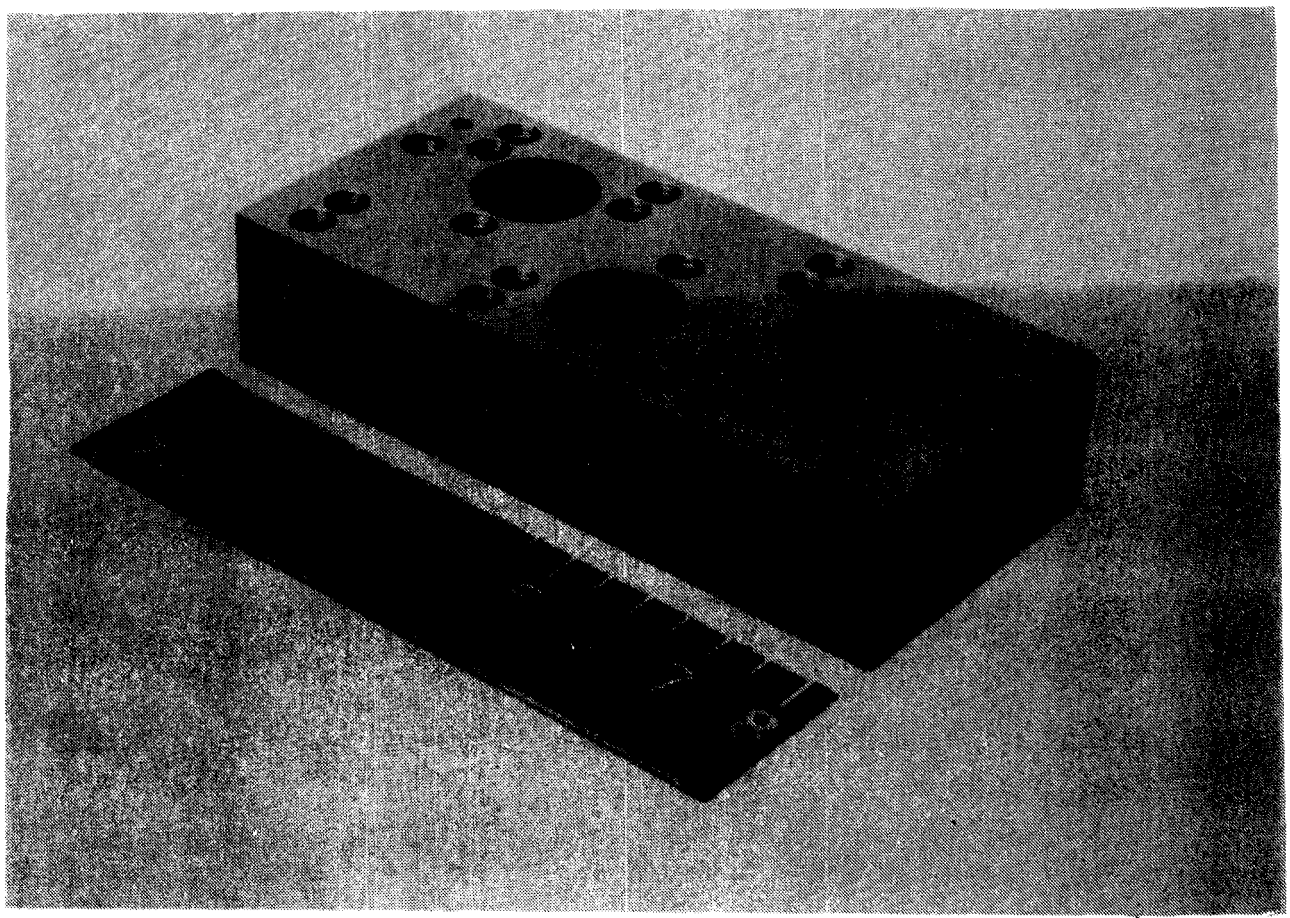

156766-79

Figure 4.3-6. Three-junction circulator assembly.

The implementation of this multiple junction circulator has greatly simplified the integration of the radial line combiner. First, because these waveguide circulator junctions have been assembled into one compact assembly, the overall dimensions of the amplifier have been reduced. Second, the electrical path length through the isolator-circulator-isolator network over the operating frequency is identical from housing-to-housing because no interconnecting waveguide sections are required to bolt the various components together, and because each circulator junction is identical. No additional dielectric tuning chips are necessary in their assembly. It is essential to the operation of the radial line combiner that the power entering each of the combiner arms is in phase across the frequency of interest. Any phase error between power module arms will degrade the overall performance of the amplifier.

4.4 SILICON IMPATT DIODE DEVELOPMENT

Development of V-band silicon IMPATT diodes was funded in part by an internal research program at TRW, and was not a contractual task in developing this radial line combiner. It is, however, an important subject, and we will report its achievements.

The IMPATT diode is shown schematically in Figure 4.4-1. It consists of a hermetically sealed ceramic ring package on a copper disk, with the diode chip thermal compression-bonded on a Type II-A diamond heatsink for efficient heat dissipation. The diamond heatsink is gold plated and pressed into a 0.060-diameter copper disc. Electrical contact to the diode mesa is provided by a gold ribbon which provides the proper series inductance ($\approx$ 0.12 nH) to the diode mesa, as shown in the equivalent circuit of Figure 4.4-2. The copper disc is then soldered onto a copper heatsink. The diodes are tested as oscillators using the test setup shown schematically in Figure 4.4-3. A histogram showing the results of four diode lots fabricated in 1984 is given in Figure 4.4-4. In reviewing these histograms, we find that at a junction temperature of 250°C, 86 percent of the diodes tested produced at least 28 dBm (or$\geqslant$794 mW). The power budget was determined for this amplifier from these results(refer to Section 3.5).

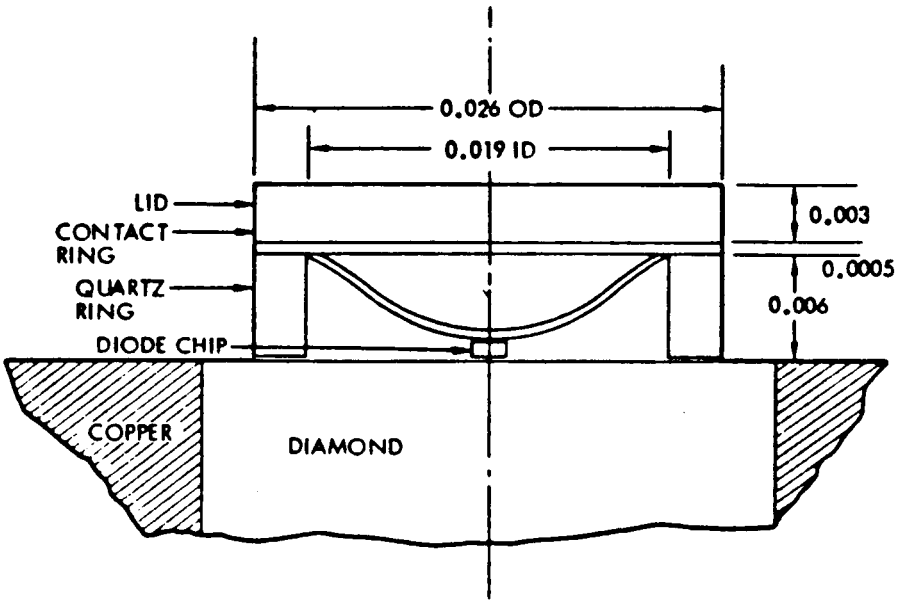

Figure 4.4-1. IMPATT diode package.

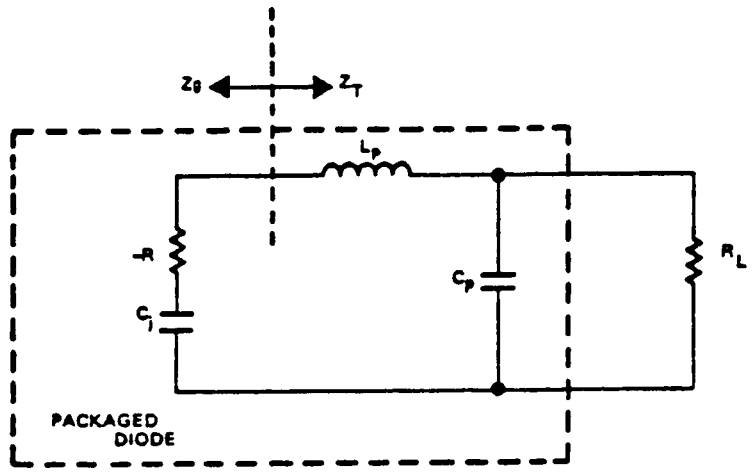

WHERE $-R$ IS THE NEGATIVE RESISTANCE
C_j IS THE JUNCTION CAPACITANCE
L_p IS THE PACKAGE INDUCTANCE
C_p IS THE PACKAGE CAPACITANCE
R_L IS THE TRANSFORMED LOAD IMPEDANCE

Figure 4.4-2. Schematic diagram of an IMPATT diode and its package parasitics.

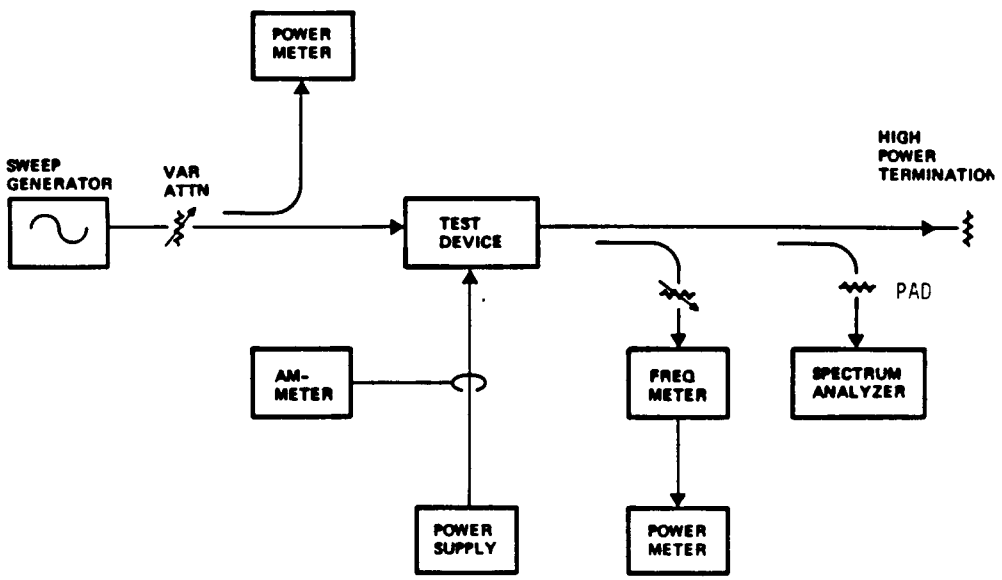

Figure 4.4-3. Block diagram of diode test station.

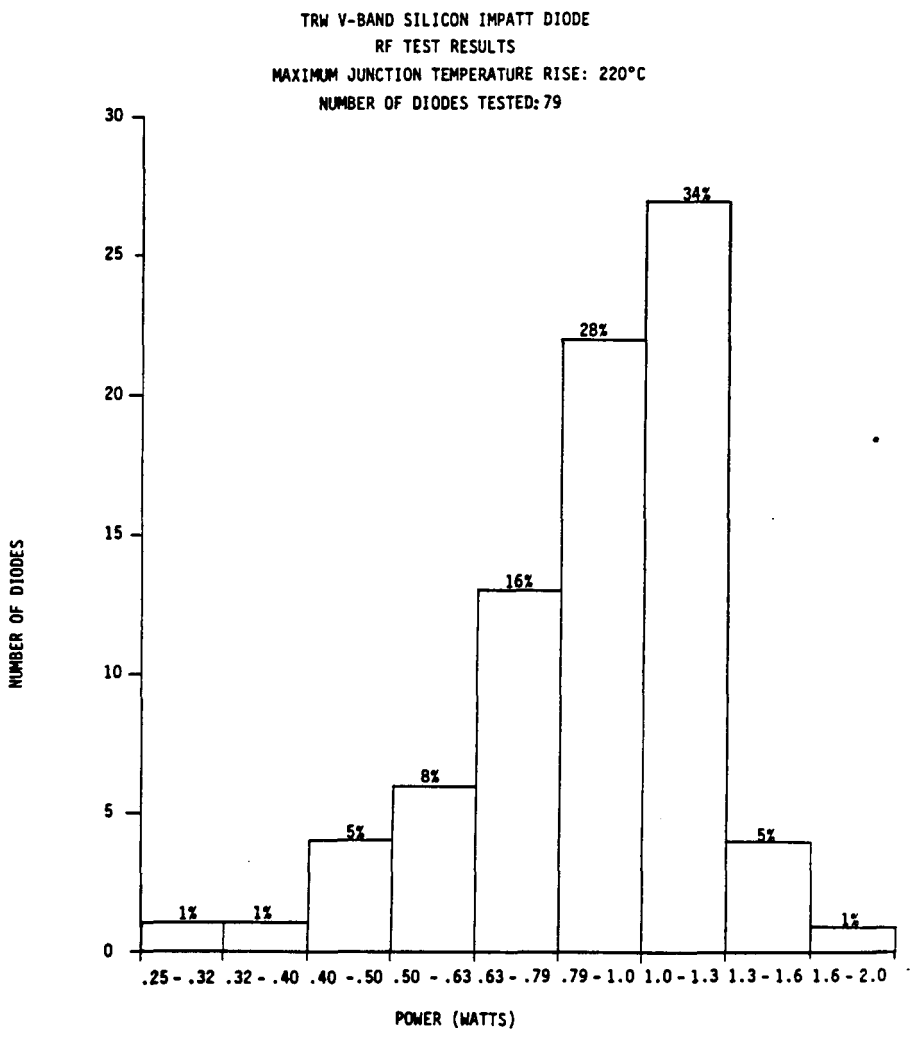

Figure 4.4-4. Typical TRW silicon IMPATT diode test results.

Extensive development of TRW's 60-GHz silicon double-drift IMPATT diodes began in 1981. The primary goal of this early effort was to produce a high power V-band diode. Evaluating the diode as oscillators revealed several diode lots which could produce 1 W of RF power. It was essential for this program that the diodes used produce their maximum power at 60.0 GHz with an efficiency greater than 6 percent and a junction temperature less than 250°C. The added constraints on the diode operational requirements demanded further diode development. We had the capability to produce a higher power IMPATT diode, but now the diode had to be optimized for maximum performance at a selected frequency, 59 to 61.5 GHz.

Optimization of the IMPATT diode was accomplished in two steps. The first was to optimize the diffusion profile of the diode chip and the second,

to optimize the package parasitics to the particular profiles. The objective was to produce a high power, high efficiency, 60-GHz diode. Previous V-band diode results revealed a consistently high operational frequency, approximately 66 GHz. Because of this high oscillation frequency, the drift region of the diodes was lengthened. In addition, the dopant concentrations were adjusted in an effort to improve device efficiency. During 1983 and 1984, 26 V-band IMPATT diode wafers were fabricated and RF evaluated. From these 26 lots, there were 75 separate diode deliveries totaling 594 individual diodes. Each diode was tested for its DC characteristics, thermal resistance, and RF performance. For every diode, the RF evaluation consisted of an average of six adjustments in the coaxial shims, or bias pins, in addition to numerous adjustments in DC operation levels, choke, and backshort positions. Clearly, RF evaluation is the most tedious and time consuming process. From this effort we have achieved the test results shown in Table 4.4-1.

Table 4.4-1. V-band silicon IMPATT diodes best test results.

	DIODE NO.	EFFICIENCY	POWER (W)	FREQUENCY	Tj (°C)
HIGHEST POWER DIODE	112E-1	9.8	2.00	53.12	335
HIGHEST EFFICIENCY DIODE	112E-1	10.0	1.66	53.35	272
HIGHEST POWER AND HIGHEST EFFICIENCY DIODE	109B-14	9.5	1.15	61.1	181
AT $\Delta T_j \leq 215°C$ $T\Delta = 25°C$ FREQUENCY = 60 GHz					

The IMPATT diodes used in this program were selected from three diode lots for their RF power capability at a given junction temperature. Table 4.4-2 presents test results for each of the seven delivered diodes at the operating current level used in the delivered amplifier.

Table 4.4-2. IMPATT diode oscillator test results for the seven delivered diodes.

DIODE NO.	V_{op}	I_{op}*	f	P_o	T_j	POSITION
109A6	26.9	500	66.90	28.6		DRIVER STABLE
109B13	23.5	250	56.00	22.0		DRIVER STABLE
109B9	26.7	600	59.98	29.7		DRIVER ILO
112B1	28.7	500	59.18	30.1		POWER MODULE ILO
112B2	29.3	375	61.04	29.9		POWER MODULE ILO
112G6	29.2	450	59.62	30.3		POWER MODULE ILO
113A1	27.7	500	60.32	29.2		POWER MODULE ILO

*RESULTS ARE GIVEN AT THE SAME CURRENT LEVELS USED IN THE DELIVERED AMPLIFIER.

5. AMPLIFIER INTEGRATION

5.1 SYSTEM SCHEMATIC

The system schematic of the entire amplifier, shown in Figure 5.1-1, consists of a driver stage and a 16-way radial line combiner power stage.

The driver stage is composed of two three-junction circulators, three single-diode amplifier modules, and their respective current regulators. The power stage combines four power modules using a 16-way radial line combiner. Each power module consists of a three-junction circulator, single-diode injection-locked oscillator module, and necessary regulator circuitry. All these components were described in detail in Section 4. The amplifier requires only one regulated dc input drive of approximately +30 V at 3 A.

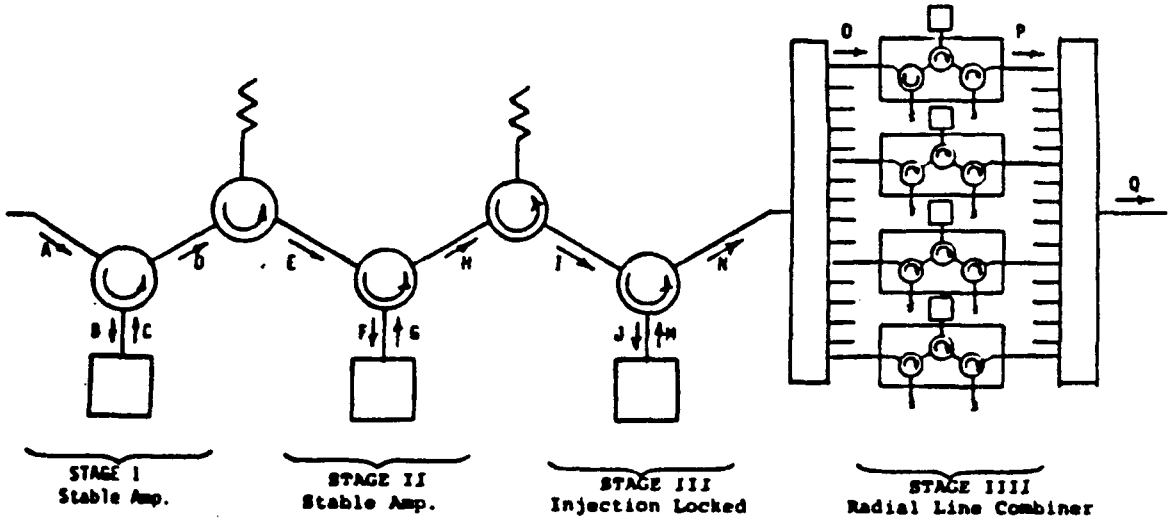

Location	A	B	C	D	E	F	G	H	I	J	M	N	O	P	Q
Power (dBm)	10	9.7	16.7	16.4	16.1	15.8	18.8	18.5	18.2	17.9	28.3	28.0	15.4	28.0	26.5

Figure 5.1-1. Amplifier block diagram.

Amplifier cooling is achieved by passive radiation for short term operation. The driver stage is mounted to the baseplate and dissipates approximately 31 W. Each power module has been mounted to a heatsink and dissipates approximately 13 W each. For extended operation, forced air circulation is required on each of the power modules.

5.2 INTERFACE REQUIREMENTS

Both RF input and output connectors are via standard WR-15 waveguide with a MIL-F-3922/67B-008 flange. Both the source and load SWR should not exceed 1.3:1. The input RF signal should be of a single frequency within the range of 59.2 to 60.7 GHz and not exceed 0.03 W CW. DC input to the unit is connected through a standard banana jack at +32 V (red) and ground (black).

5.3 AMPLIFIER EVALUATION

The amplifier for this program was developed in stages and later assembled into its final configuration. Test results of the basic stages which construct the amplifier will be discussed in detail below. These basic stages are categorized as follows:

- Stable amplifier driver pair
- Single-diode injection locked oscillator (ILO) driver output stage.
- Radial line divider/combiner
- Power module (four each)
- Bias circuitry (seven each).

The goal of this program was to develop a solid state amplifier with the following RF performance:

- Power out 1 W (minimum)
- Dynamic RF band 59 to 61.5 GHz
- RF gain 17 dB

The only test required to determine these specifications is a power measurement. No noise measurements were conducted, but the amplifier was tuned to eliminate any visual spectral noise. The test setup used for amplifier measurements is schematically represented in Figure 5.3-1.

5.4 STABLE AMPLIFIER DRIVER PAIR

The first two amplifier modules within the driver section are stable amplifiers due to the low input drive level available. Injection-locked modules at this location would probably produce too narrow a bandwidth. The configuration of this stable amplifier stage, shown in Figure 5.4-1, consists of two circulator junctions, one isolator, and two amplifiers. Figure 5.4-2 presents a point-by-point response of the two cascaded stable amplifiers.

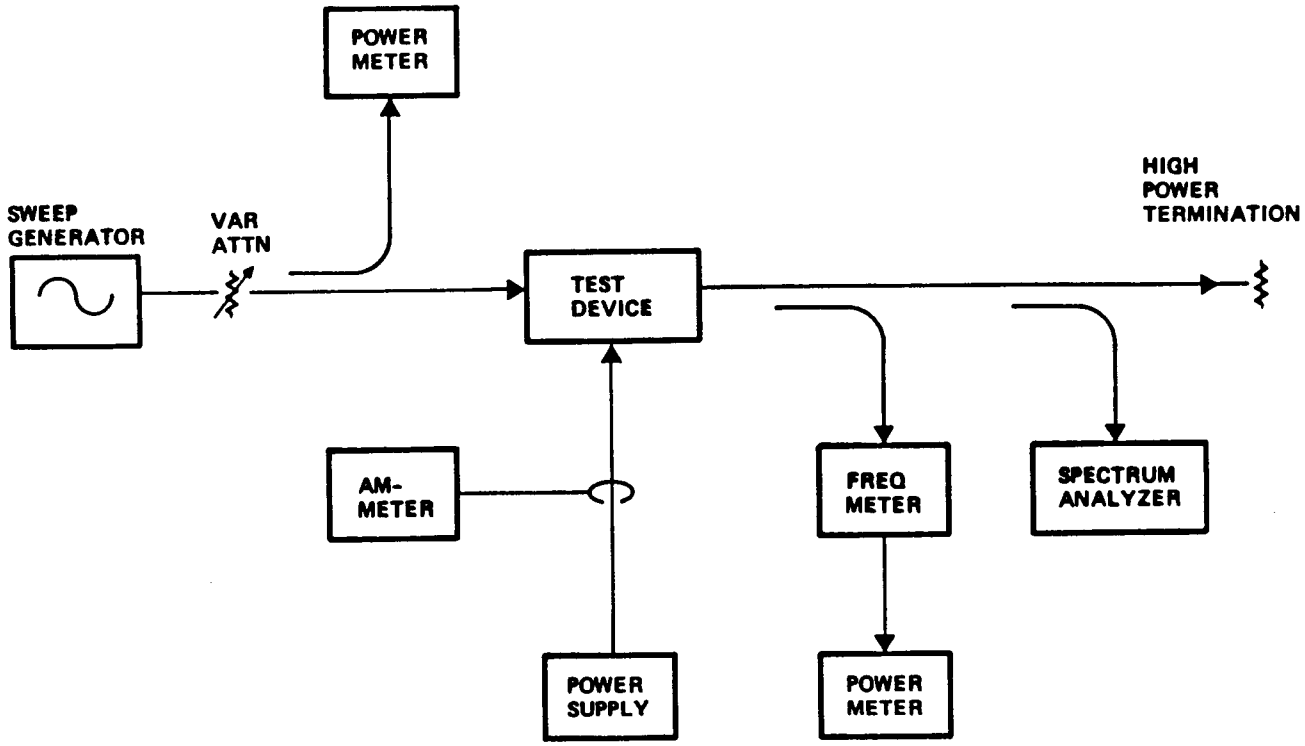

Figure 5.3-1. Test circuit schematic.

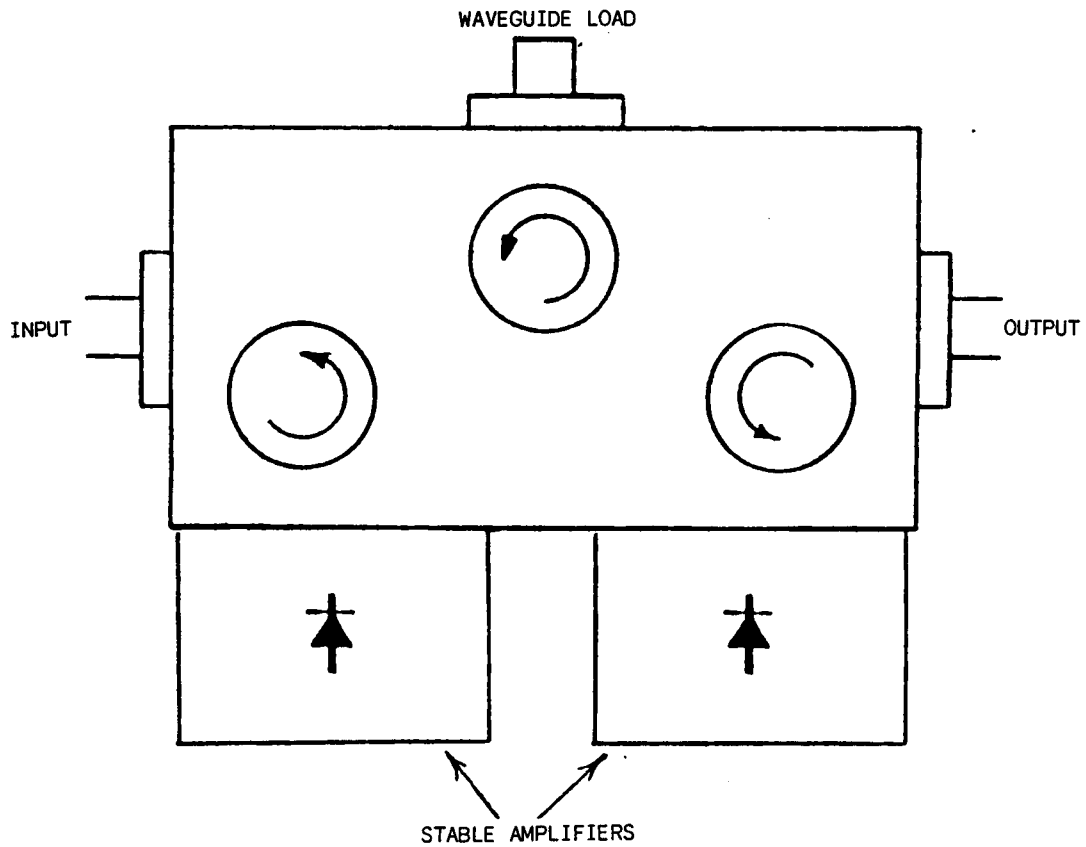

Figure 5.4-1. Stable amplifier driver stages.

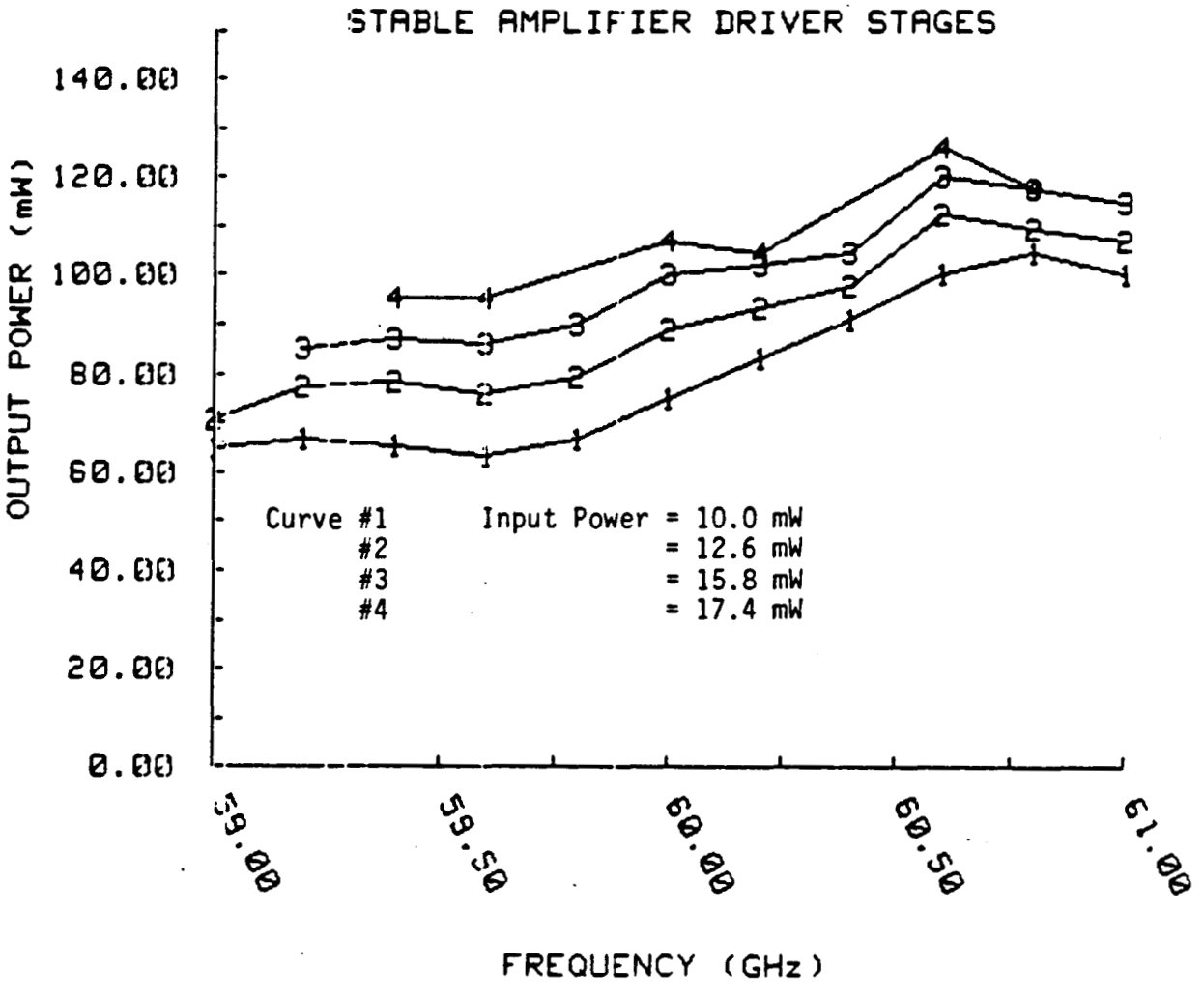

Figure 5.4-2. Swept frequency response of the two-stage stable amplifier driver.

This method of recording was chosen over a swept response due to the ripple of our sweeper source. The typical gain for this amplifier pair is about 9 dB with a ±1 dB ripple. There is evidence of gain compression at about 60.25 GHz for drive levels above 12 dBm. This compression does not significantly affect the overall performance of the amplifier. Figure 5.4-2 does not imply that the bandwidth of this stage is reduced at the higher drive levels. Simply, the sweeper used for this measurement was limited in its output power capability. The sweeper bandwidth is narrower at the higher output levels. We will assume a constant drive level of 10 dBm at the input port of the amplifier. Minor variations from this drive level will normally alter only the bandwidth of the overall amplifier. Using this stable amplifier, we were then able to test the ILO driver output stage.

5.5 ILO DRIVER OUTPUT STAGE

The last amplifier of the driver chain is an injection-locked oscillator. We chose the ILO amplification method because of its high gain, high power capabilities. Figure 5.5-1 presents a schematic of this stage, which consists of two isolators on either side of a circulator attached to the ILO housing. The frequency versus power relationship of this ILO is plotted in Figure 5.5-2 for an input drive level of 50 mW. This includes the losses due to both isolators and the circulator. From this graph we find a locking bandwidth of 1.6 GHz with a gain of approximately 11.4 ± 0.33 dB. Figure 5.5-3 relates the normalized bandwidth of the ILO to its gain. For an ILO amplifier, the expression relating the normalized bandwidth to its gain can be approximated with the following expression (assuming that $P_o \gg P_i$).

$$\frac{dF}{F_o} = \frac{1}{Q_{ext}} \sqrt{\frac{P_d}{P_o}}$$

where Q_{ext} is the external quality of the circuit. A straight line drawn through the measured points on Figure 5.5-3 obeys the above expression and indicates an external Q for the circuit to be $Q_{ext} = 15$, which is considered a relatively low value. Note that an external Q = 15, and a gain of 11.4 dB defines a locked bandwidth of over 2 GHz. This 2-GHz bandwidth is not reflected in Figure 5.5-2 due to a drop in the output power level at the band edges. We set the output ripple at the 1/3-dB level in Figure 5.5-2, which yields the 1.6-GHz bandwidth.

5.6 RADIAL LINE COMBINER/DIVIDER

The key element to this amplifier program is the radial line combiner and divider. Section 4.2 presented a detailed analysis of the radial line and its port-to-port isolation, input-to-output insertion loss, and SWR measurements. For optimum integration of a perfectly symmetric radial line power combiner, the power entering the radial line from each of the 16 radially directed ports must be equal in amplitude and phase at each frequency. To obtain this optimum operating condition using an actual, imperfect radial line network, the amplitude and phase difference from the central input port to each of the 16 radial waveguide ports must be determined and corrected. This measurement must be performed for both the divider network and combiner network.

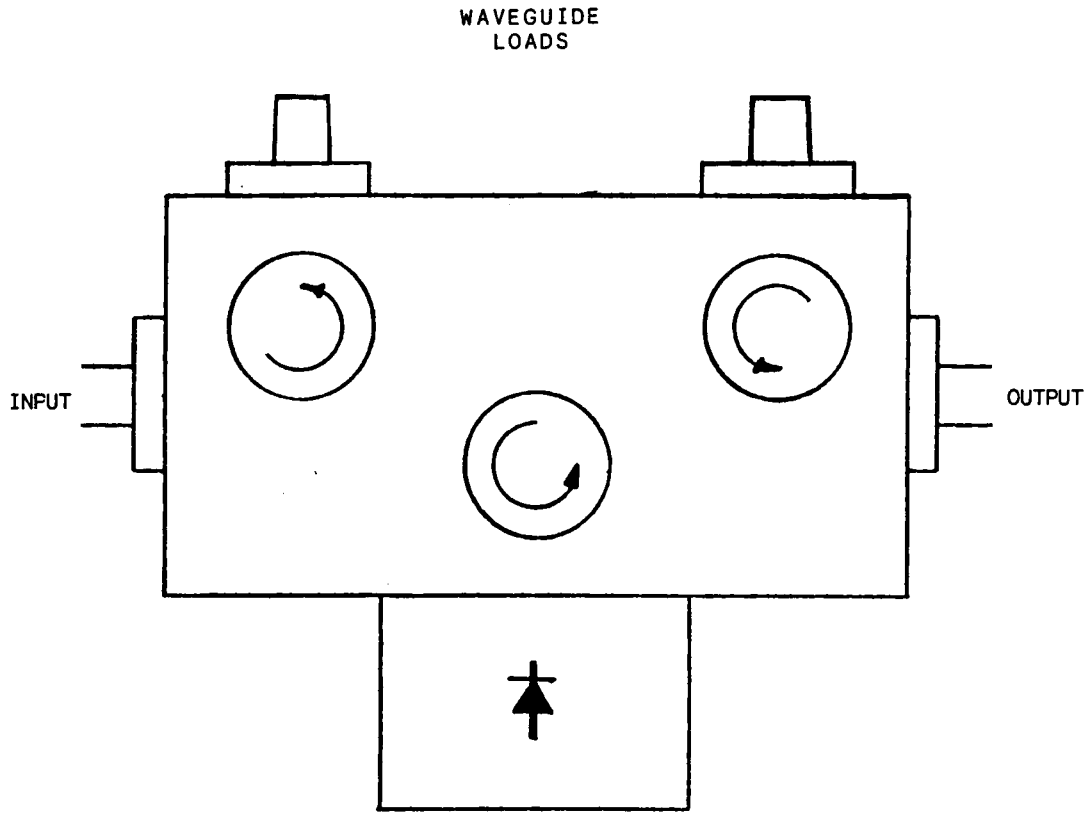

Figure 5.5-1. Driver injection-locked oscillator stage with input and output isolators.

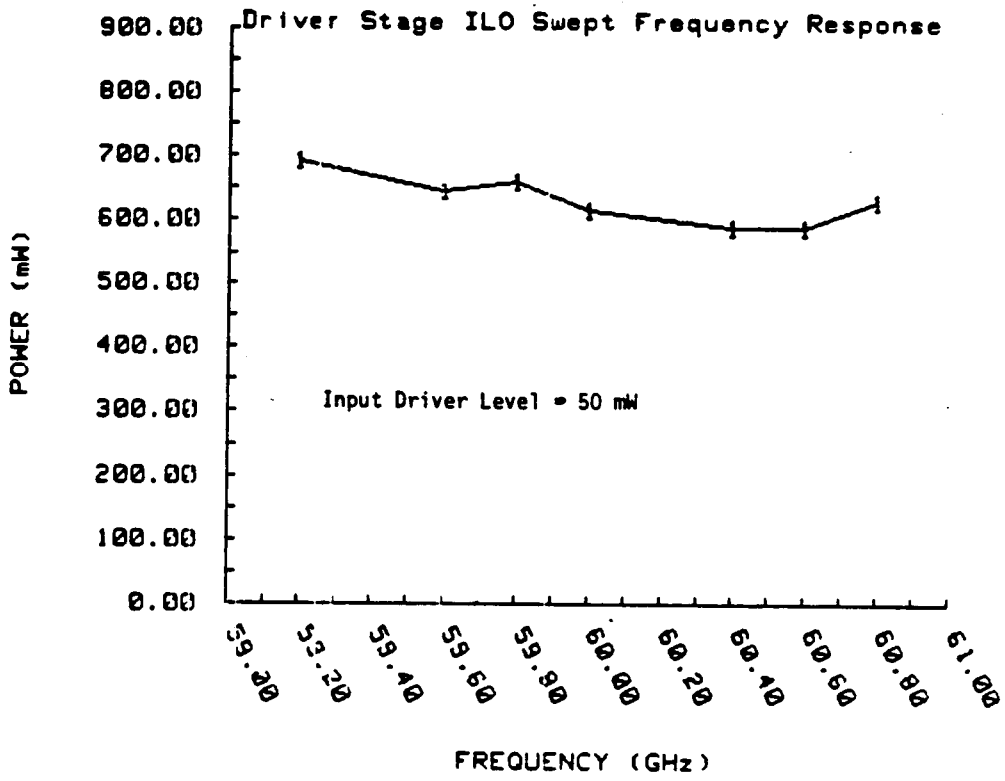

Figure 5.5-2. Swept frequency response of the driver ILO.

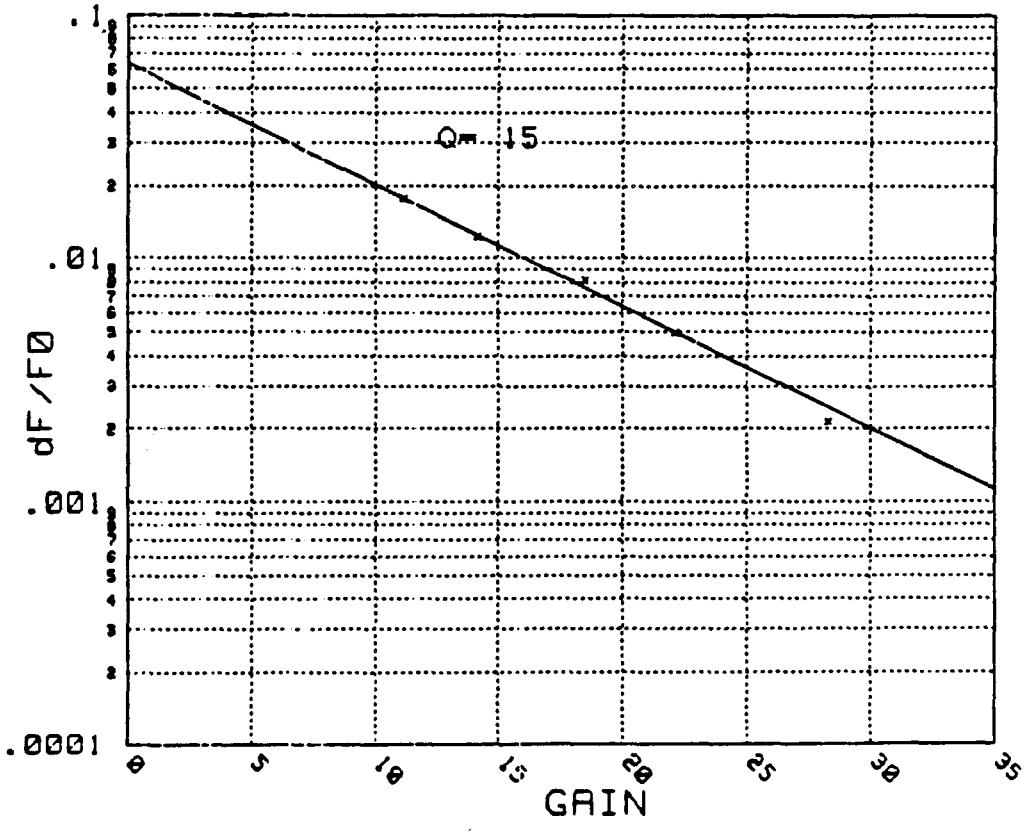

Figure 5.5-3. Normalized bandwidth vs gain for the driver stage ILO.

The ideal method for this type of phase and amplitude balance measurement would use an automatic vector network analyzer. Although such analyzers are available, the configuration of the 16-port divider/combiner makes it incompatible with our present network analyzer system. This is because each of the 16 output ports is oriented in 16 different directions in relation to the input port, the central port on the top of the divider. Using the present network analyzer, it is not possible to bend a waveguide each time to examine each of the 16 output ports.

A network analyzer with a downconverter on the end of a flexible coaxial line on the input arm has been developed but is not presently available at V-band. Therefore, an alternate method of determining the relative phase of each output port in reference to one another was devised. This method measures the return loss of the top port (divider input port) over frequency with each of the 16 radial waveguides terminated using a matched load. The swept return loss of the signal for this case shows a matched circuit; i.e., low VSWR. Replacing one of the 16 matched terminations with an adjustable

short will change the swept return loss measurement so the plot of return loss versus frequency has a characteristic shape; and, in fact, has a clearly defined resonance within band. As the position of the short is adjusted in and out, the resonant spike translates higher and lower in frequency, respectively. The position of the back short can be adjusted for each of the 16 ports, so they all result in almost the same characteristic return loss curve versus frequency (Figure 5.6-1).

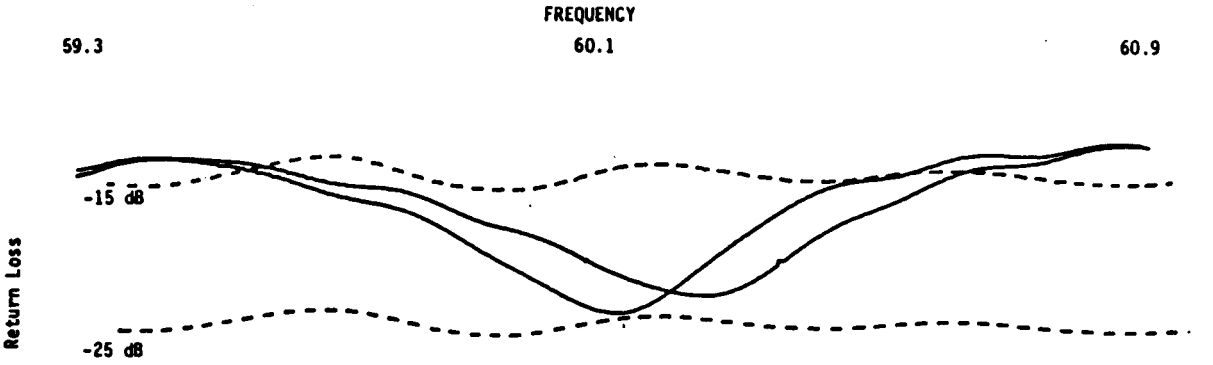

Figure 5.6-1. Swept response of return loss at the central port of the 16-way divider. The 16 output ports have all been terminated with matched loads except one which is terminated with a variable short. The two curves represent a resonance within the circuit with the short positioned at two different distances. The difference in the short position is 0.012 inch.

Performing this, we noted that for the 16 radial ports there is a maximum change in the position of the short of only 0.005 inch at 60 GHz. This is equivalent to 6.4 degrees maximum phase change for WR-15 waveguide.

5.7 POWER MODULES

For optimum performance, each of the four power modules surrounding the diode/combiner networks should have equal gain and phase response at each frequency. For this reason identical isolators, circulators, diodes, and amplifier circuits are desirable.

Gain/Amplitude Measurements

The output power versus frequency of the four power modules is presented in Figure 5.7-1. The input drive level for each module is 40 mW which is the power available at the output ports of the radial line divider. From this we observe an average power of 700 mW with a typical ripple of 0.35 dB. Module

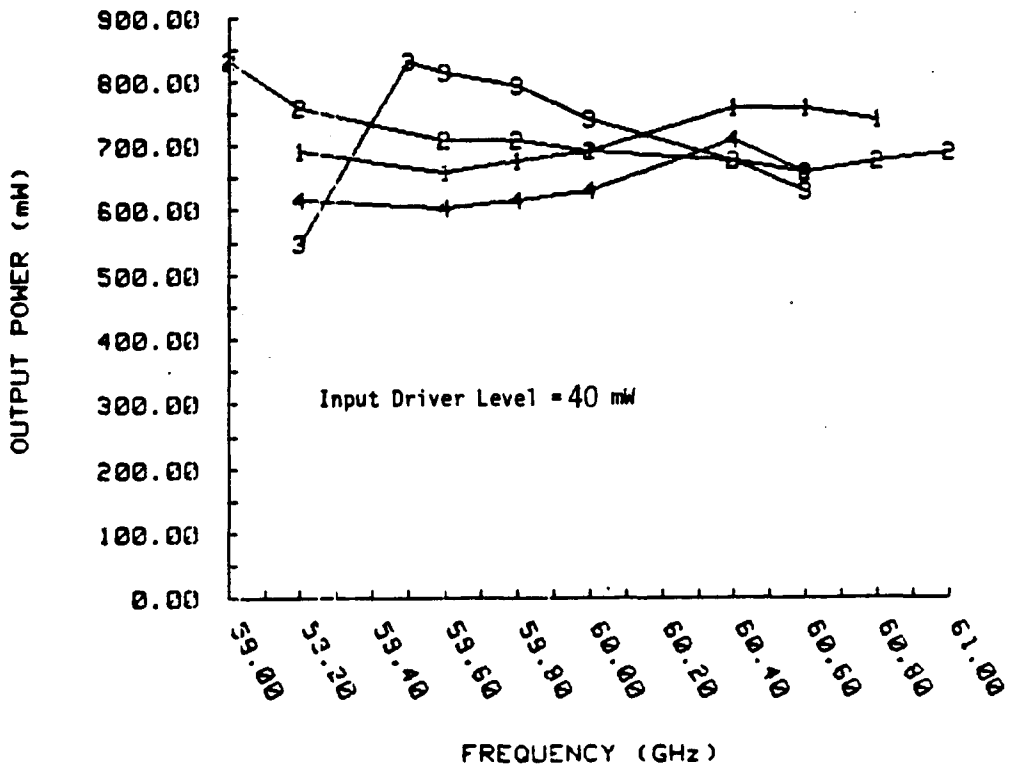

Figure 5.7-1. Swept frequency response of each of the four power stage ILOs.

number three is the worst case with a ripple of 0.9 dB over the same frequency range. A plot of normalized locking bandwidth versus gain for the four power modules is presented in Figure 5.7-2. The straight line drawn corresponds to an average of the data points assuming the Adler relationship (Equation 5.5-1). The corresponding quality for this averaging line is Q = 15.

Phase Measurement

It is essential that the electrical line length be equal for each of the four power stage modules across the frequencies of interest. Phase matching for each of the four power module arms is accomplished using the magic-tee circuit shown in Figure 5.7-3. If the phase of each module under test is identical, there will be no power present at the difference port (Δ) of the second magic-tee. Shims are added to the module arms until minimum power is observed at the difference port of the second magic-tee across frequencies from 59.5 to 61.0 GHz. All four module arms are phase matches using this technique.

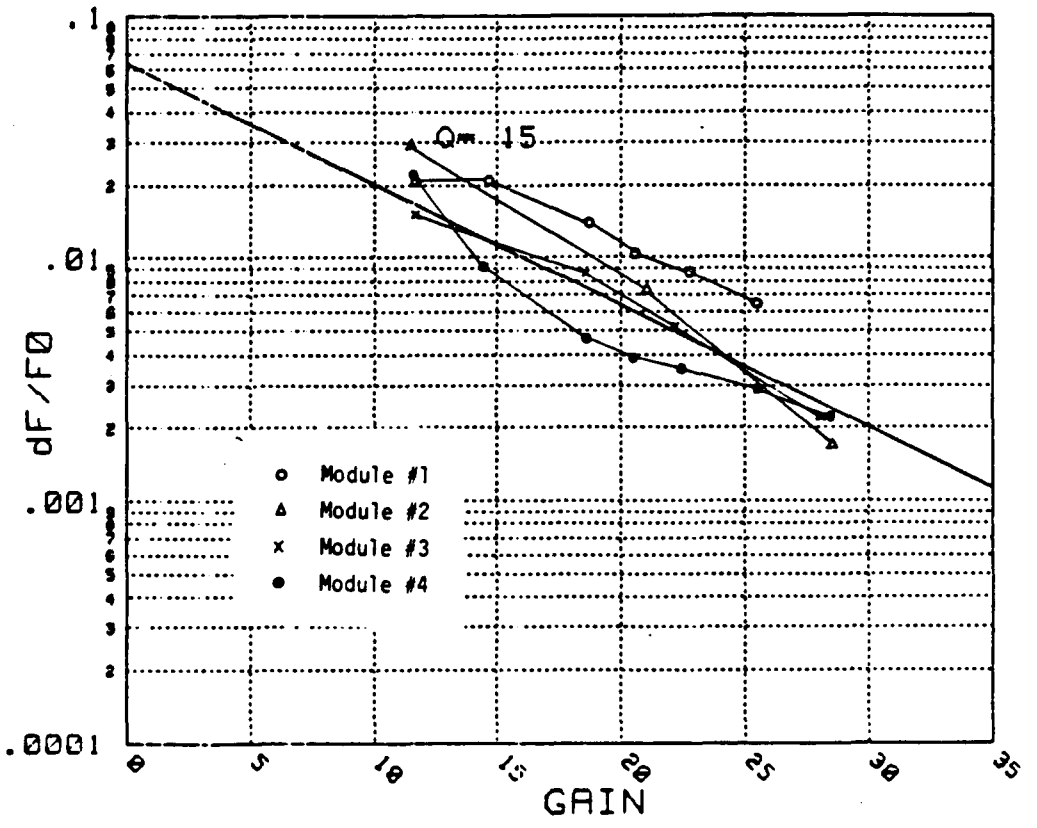

Figure 5.7-2. Normalized bandwidth vs gain for each of the four power modules.

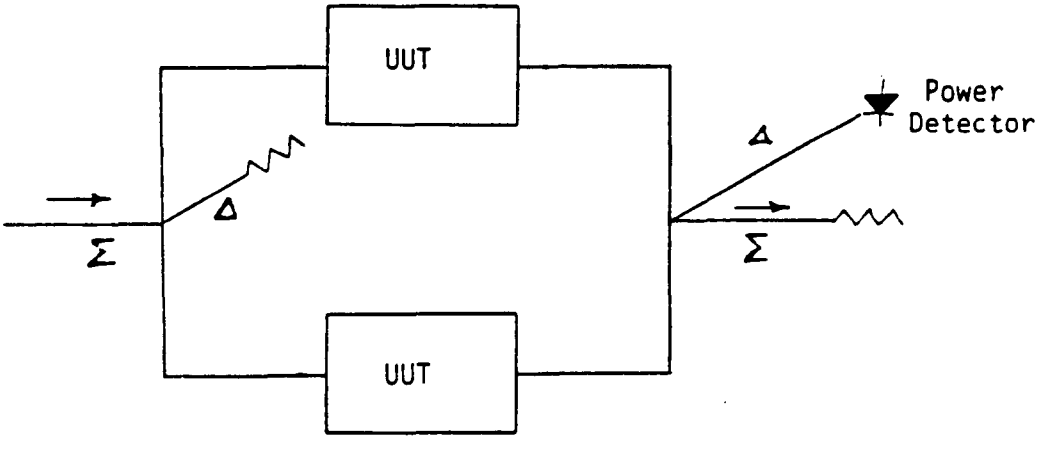

Figure 5.7-3. Magic-tee network for phase matching the power modules (UUT).

5.8 RADIAL LINE COMBINER WITH ILO DRIVER

The power versus frequency response for the radial line combiner integrated with four power modules and the ILO driver is presented in Figure 5.8-1. The two curves represent two different drive levels presented to the driver ILO input. Note that the band edges are most affected by varying the input drive levels. The bandwidth of the combiner versus gain is presented in Figure 5.8-2.

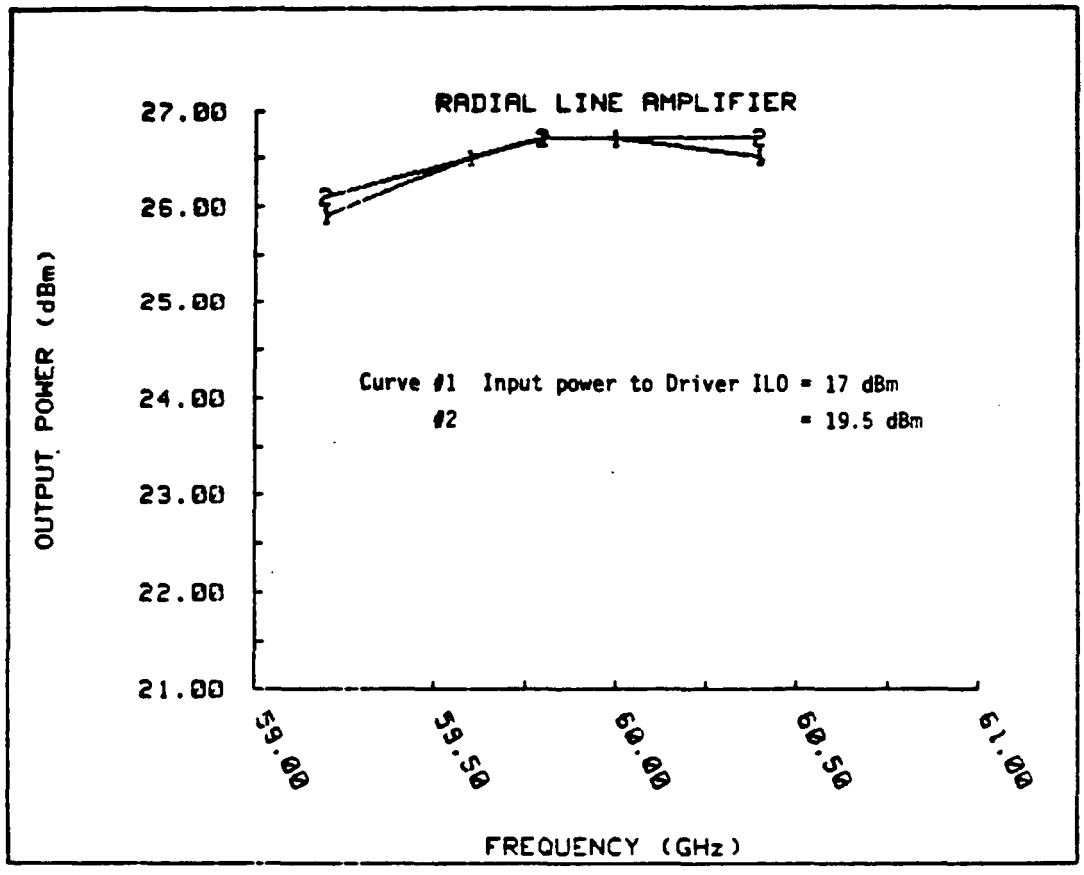

Figure 5.8-1. Swept frequency response of the radial line combiner.

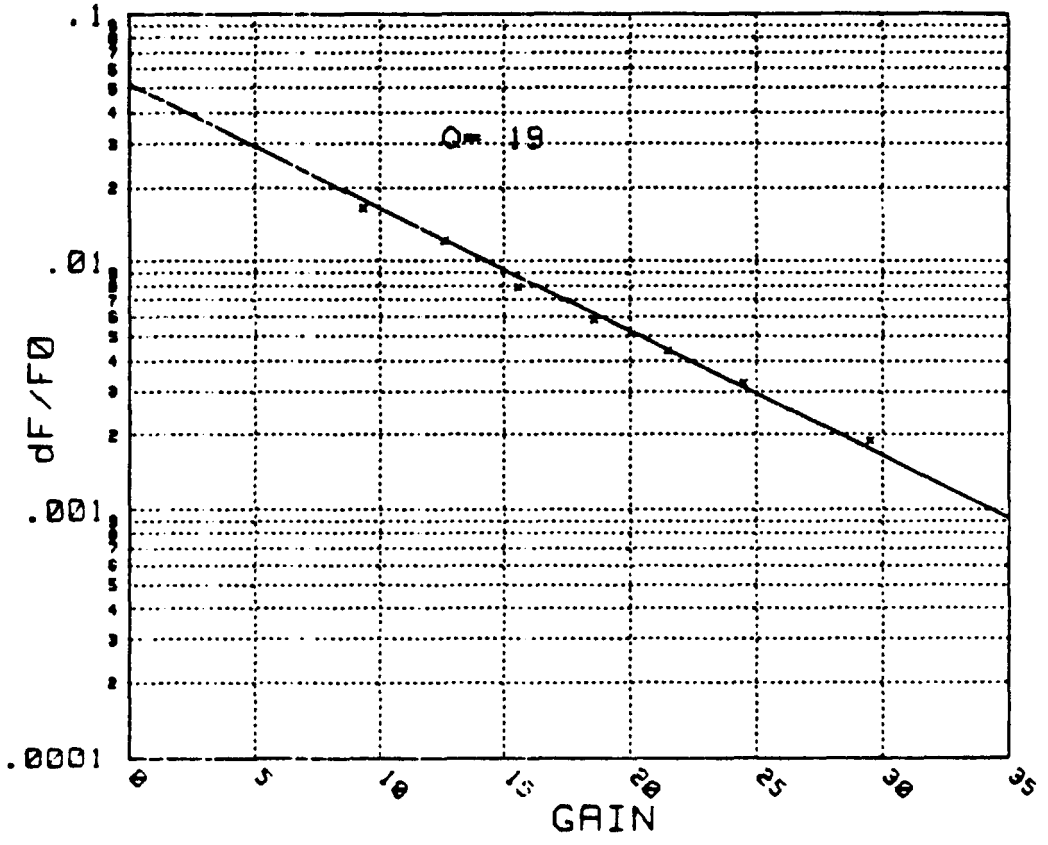

Figure 5.8-2. Normalized bandwidth vs gain for the radial line combiner.

5.9 ASSEMBLED AMPLIFIER

The assembled amplifier includes the stable amplifier driver stages and circuit assembly described in Section 5.8. The output power of the final amplifier was checked against the results of Figure 5.8-1 and shown to be identical. The performance of the amplifier is plotted in Figure 5.9-1. A photograph of the V-band IMPATT amplifier is shown in Figure 5.9-2.

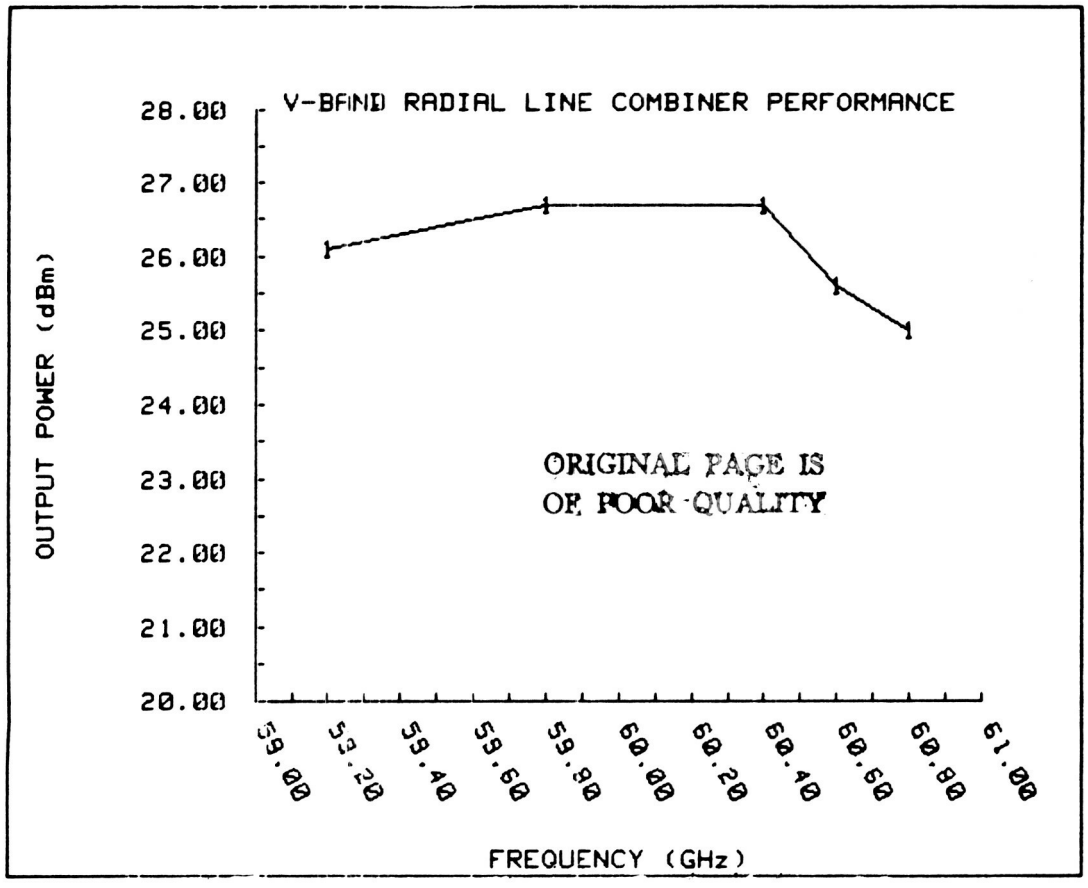

Figure 5.9-1. Swept frequency response of V-band amplifier.

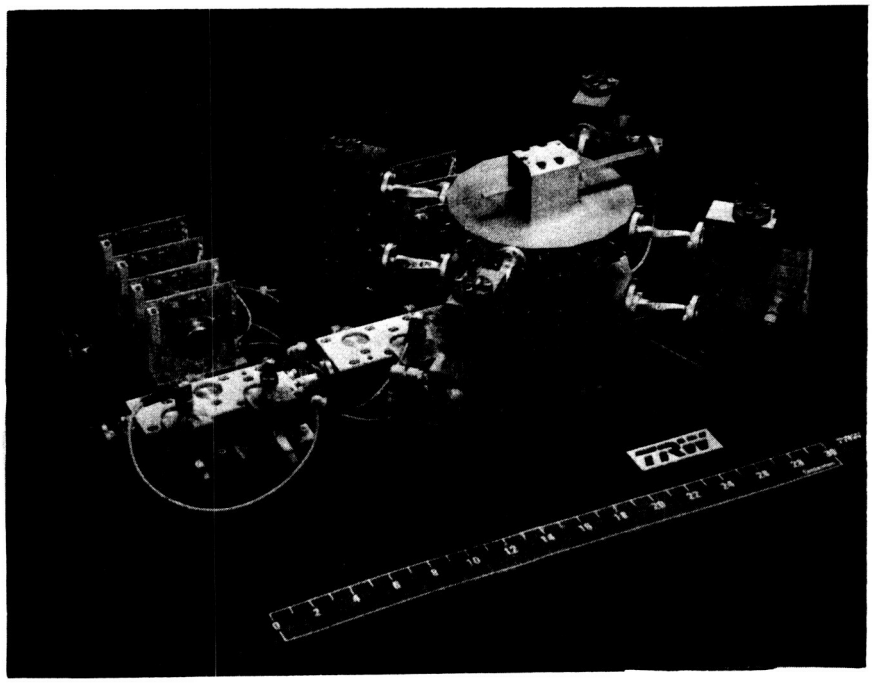

198358-84

Figure 5.9-2. V-band IMPATT amplifier.

6. CONCLUSIONS AND RECOMMENDATIONS

This final report details a program which was initiated due to the continuing demand for high data rate 60-GHz communications links. In general, the goal of the program was to investigate and develop a wideband power combining technique at 60 GHz which would be applicable to future requirements and demands. More specifically, the goals to meet were 2.5-GHz bandwidth centered at 60.25 GHz, at an output power of 1 W.

The program was based on the foundation that a nonresonant combining technique must be employed. Early in the program, the 90- and 180-degree hybrid coupler techniques of combining were eliminated due to the large number of coupler circuits required, thus introducing higher circuit losses.

The initial design approach used a single conical line divider/combiner network, combining from stable amplifier modules. This design resulted in relatively low isolation between the four output ports. In addition, the network generated high-order spatial modes which resulted in resonant type spikes in the insertion loss measurements. To improve the port-to-port isolation, a scheme using two back-to-back conical line networks was pursued. The necessary isolation between the four output ports was achieved using external ferrite components. This arrangement did develop the required port-to-port isolation, but it was also a moderately large and complex structure. To help simplify the structure we replaced the three-dimensional conical line combiner network with a two-dimensional assembly, the radial line combiner. The radial line combiner is the final evaluation stage of the V-band amplifier. Keeping in mind that this is a technology program, and allowing for possibilities of future improvements, we chose to develop a 16-port radial line divider/combiner as opposed to a four-port. To ensure adequate port-to-port isolation between output ports, the two-layered structure was employed using two identical radial line divider networks. Development, fabrication, assembly, and test of the power modules to be mounted onto the 16 radial ports of the divider/combiner would have been too large a task for this program; therefore, we limited the number of power modules to four. This left 12 unused ports which are terminated with matched loads. This construction has no practical application other than that of a proof of concept for the V-band two-layered radial line combining technique. Because only four of a possible 16 power modules were used, the amplifier output power should equal

that of only one of the power modules, assuming all four power modules are identical. An output power equal to that of one power module would indicate a 100 percent combining efficiency. Less power at the output would indicate the percent of combining efficiency for the divider/combiner networks. The delivered amplifier yielded approximately 70 percent combining efficiency.

Improvement of the combining efficiency for the radial line amplifier can be achieved by further matching both amplitude and phase of the four power modules placed around the divider/combiner networks. Figure 5.7-1 is a clear indication that four power modules are not exactly identical. Further matching of these power modules is probably the most significant method for improving the combiner efficiency. Minor improvements in combining efficiency can be achieved with improvements on the surface finish of the combiner network thus reducing ohmic circuit losses.

Clearly, this radial line combiner is a module assembly with 16 identical power module ports, which is amenable to mass production fabrication techniques. A single housing incorporating the two waveguide twists, two isolator junctions with their respective waveguide loads, and the single circulator junction is a strong possibility. This could reduce both size and weight of the overall amplifier. Future increases in output power can also be achieved by retrofitting 16 new identical power module amplifiers.

The radial line combiner presented here is an excellent structure for achieving a wide bandwidth, high power, millimeter-wave power combiner which otherwise would be very difficult to develop using resonant cavity combiners and/or hybrid coupler type systems.